Physics, Modeling and Design Implications of RF Correlated Noise in SiGe HBTs

by

Ziyan Xu

A dissertation submitted to the Graduate Faculty of
Auburn University
in partial fulfillment of the
requirements for the Degree of
Doctor of Philosophy

Auburn, Alabama
May 5, 2013

Keywords: SiGe HBT, RF noise, compact modeling, noise extraction, LNA

Copyright 2013 by Ziyan Xu

Approved by

Guofu Niu, Chair, Alumni Professor of Electrical and Computer Engineering
Fa Foster Dai, Professor of Electrical and Computer Engineering
Stuart Wentworth, Associate Professor of Electrical and Computer Engineering
Bogdan Wilamowski, Professor of Electrical and Computer Engineering

Abstract

Accurate noise compact modeling and efficient noise extraction techniques are required for RF circuit design. Understanding the impact of noise sources and the noise propagation is also necessary for device and circuit noise optimization. In this work, we discuss RF noise physics, modeling, extraction and circuit design implications. The related compact model parameters are determined based on the experimental results of various SiGe HBTs.

After a review of previous noise model and their implementation in compact models, we develop a much improved physics-based compact noise model for use with any existing compact models. We investigate the impact of CB SCR transit time effect on noise parameters of bipolar transistors, together with the noise transport in the neutral base. A model suitable for compact model implementation is developed. The resulting frequency dependence and correlation of terminal current noises can be generated from independent white noise sources, which is important as the current standard simulators are unable to handle correlated noise sources.

We present a new compact modeling approach to extraction of intrinsic transistor terminal current noises and terminal resistance thermal noise. The extraction method are based on the transfer function which can be calculated using ac small signal simulation results. Thus this method is independent of specific compact model and avoids tedious element by element de-embedding procedure.

The relevant importance of noise sources are evaluated in various noise representations and proved to be varying from one representation to another. It is even unfair to claim the noise source's dominance within one single representation as it depends on each noise power spectre density and noise parameter. The base resistances are identified to be the most important elements of the extrinsic network that determine the intrinsic terminal noise current propagation towards the external

terminals. Such propagation increases the NF_{min} due to intrinsic noise currents considerably, making it much higher than the NF_{min} due to R_b's thermal noise. R_b's role as an impedance element can be much more important than its role as a thermal noise source for practical SiGe HBTs. Analytical expression are derived to demonstrate that the well known effect of noise correlation is shown to be highly dependent on R_b. Consequently, R_b reduction should continue for NF_{min} improvement despite a nearly negligible NF_{min} due to R_b's thermal noise.

Impact of correlated RF noise on LNA design is also examined. The useful simultaneous noise and impedance matching conditionally holds based on the simplified analytical derivation results. Simulation results show that noise matching requires a considerably larger transistor and power consumption in the presence of intrinsic terminal current noise correlation. The actual noise figure of LNA designed using SPICE model are found to be overall comparable to that of the correlated model designed LNA, which is due to the small noise conductance tolerating significant noise mismatch.

Acknowledgments

My deepest gratitude goes first and foremost to my major professor, Dr. Guofu Niu, for his encouragement and guidance all along the way. Dr. Niu is not only an inspiring mentor but also an outstanding role model.

I would like to thank the other members of my committee, Dr. Fa Dai, Dr. Stuart Wentworth and Dr. Bogdan Wilamowski. They never turned down my request and alway cooperate in a timely manner. Their constant help is an important factor to my academic growth. I would like also to thank my university reader, Dr. Xiao Qin. His participation helped to make sure my PhD study had a smooth ending.

Many thanks also go to Kejun Xia and Pei Shen. Collaborations with them on the noise study were pleasant and memorable.

I would like to thank my parents and families for their self-less support, understanding and love, which make me feel secure and confident. At last, I would like to thank my best friend and husband. To meet him is the best thing that ever happened to me; to marry him is the most correct decision that I have ever made.

Table of Contents

Abstract ii

Acknowledgments iv

List of Figures viii

List of Tables xv

1 Introduction 1

1.1 RF Noise 3

1.1.1 Thermal Noise 4

1.1.2 Terminal Current Noise 5

1.2 Noise Characterization 6

1.2.1 Noise Representations of Two Port Network 6

1.2.2 Noise figure and Noise Parameter 11

1.3 SiGe HBTs Noise Performance 15

2 Noise Compact Modeling and Implementation 19

2.1 van Vliet's model 19

2.2 CB SCR Effect 23

2.3 A survey of previous noise compact modeling methods 24

2.3.1 Noise compact model of Mextram group 24

2.3.2 Noise compact model of HICUM group 26

2.3.3 Noise transit time modeling approach 27

2.3.4 New method with RC delayed noise current 28

2.4 Noise source model 28

2.4.1 Consider CB SCR transit time alone 31

2.4.2 Intrinsic Base and CB SCR 38

2.4.3 General Compact Modeling Implementation 42
2.5 Conclusion 47
3 Compact Model Based Noise Extraction 49
3.1 Extraction Method 51
3.1.1 Basic Idea 51
3.1.2 Extraction procedure 53
3.2 Verification using synthesized data 55
3.3 Experimental Extraction 58
3.3.1 Model parameter determination 59
3.3.2 Frequency dependent extraction results 61
3.3.3 Bias dependent extraction results 63
3.4 Conclusion 64
4 Noise Source Importance Evaluation 66
4.1 Equivalent circuit simplification 68
4.2 Analytical derivations 72
4.2.1 Z-Noise Representation 72
4.2.2 Y-Noise representation 75
4.2.3 Chain Noise Representation 78
4.3 Noise Parameter Implications 79
4.3.1 Analytical Models of Noise Parameters 79
4.3.2 Model comparison with measurement 88
4.3.3 Simulation Results 89
4.4 Conclusions 93
5 Impact on Low Noise Amplifier Design 94
5.1 Analytical derivation of LNA noise figure 94
5.2 Simultaneous noise and impedance matching 97
5.3 Simulation Results based on a Cascade LNA 98

5.4 Conclusion . . . 102

Bibliography . . . 103

Appendices . . . 107

A Noise Representation Transformation . . . 108

B Derivation of Noise Parameters . . . 112

C Matlab Code for Intrinsic Noise Extraction . . . 114

D Verilog-A Code for Compact Noise Model Implementation . . . 121

E Derivation of relation between T_Y^{int} and T_Y . . . 122

List of Figures

1.1 Energy band diagram of a graded-base SiGe HBT [1] 2

1.2 Summary of SiGe BiCMOS technology from IBM. This chart is copied from [2]. . . . 3

1.3 Shockley's impedance field method. 4

1.4 RF noise sources of a transistor. 4

1.5 A simplified example of transistor as a noisy two port. 7

1.6 Y representation of a linear noisy two-port network. 7

1.7 Chain representation of a linear noisy two-port network. 8

1.8 Z representation of a linear noisy two-port network. 9

1.9 H representation of a linear noisy two-port network. 10

1.10 Illustration of the definition of Noise figure for an amplifier. 12

1.11 Asymmetric paraboloid of noise figure in the three-dimensional co-ordinate system. . . 14

1.12 Illustration of noise parameters of a two-port network. 15

1.13 NF_{min} versus frequency for SiGe HBTs from four SiGe BiCMOS technologies, including three high-performance variants at the 0.5-, 0.18-, and 0.13- μm nodes as well as a slightly higher breakdown voltage variant at the 0.18- μm node. This figure is copied from [3] 17

1.14 NF_{min} versus J_c at 10 GHz for 250 GHz SiGe HBT with $A_E = 0.094 \times 9.62 \mu m^2$. Measured data are shown by symbols. This figure is copied from [4]. 17

1.15 NF_{min} versus J_c at 25 GHz for 250 GHz SiGe HBT with $A_E = 0.094 \times 9.62 \mu m^2$. Measured data are shown by symbols. This figure is copied from [4]. 18

2.1 Comparison of noise parameters simulated for an IBM SiGe HBT using design kit with measurement from 2 to 26 GHz. Inside the design kit, HICUM model is used. . . 20

2.2 Y-parameter modeling result using equivalent circuit with NQS input. $\mu_0 = 270 cm^2/(V \cdot s)$, electron life time= $1.54x10^{-7}$ s, $T = 300$ K, $d_B = 45$ nm, $V_{BE} = 0.8$ V. $f_T = 184$ GHz for $\eta = 5$. $f_T = 83$ GHz for $\eta = 0$ (copied from [5]). 23

2.3 Network representation of the charge partitioning model. 25

2.4 Illustration the terminal noise currents. i_{b0} is from emitter hole velocity fluctuation. i_{b1} and i_{c1} are from base electron velocity fluctuation. i_{c1} becomes i_{c2} through CB SCR transport, which also produces i_{b2} 29

2.5 Calculated noise current spectral density normalized by $2qI_C$ vs frequency. $A_E = 0.8 \times 20 \mu m^2$. $I_C = 3.55$ mA. $f_T = 15$ GHz. τ_c is set to $0.7\tau_f$, τ_b is set to $0.2\tau_f$ and $\eta = 3$. 30

2.6 Calculated correlation normalized by $2qI_C$ vs frequency. $A_E = 0.8 \times 20 \mu m^2$. $I_C = 3.55$ mA. $f_T = 15$ GHz. τ_c is set to $0.7\tau_f$, τ_b is set to $0.2\tau_f$ and $\eta = 3$. 31

2.7 Equivalent circuit of proposed compact noise modeling implementation. 34

2.8 Verilog-A sample code of proposed noise model. 35

2.9 Comparison of measured and simulated noise parameters vs frequency. 37

2.10 Comparison of measured and simulated noise parameters vs I_C at 5 GHz. 38

2.11 Comparison of measured and simulated noise parameters vs I_C at 10 GHz. 39

2.12 Calculation results of PSDs of intrinsic i_c, i_b and their correlation with different τ_b, τ_c and η combinations. 41

2.13 Normalized correlation with different τ_b, τ_c and η combinations. 42

2.14 Equivalent circuit for Verilog-A implementation of the completely physics based version of the proposed model. 43

2.15 Comparison of measured and simulated noise parameters vs frequency. 46

2.16 Comparison of measured and simulated noise parameters vs I_C at 5 GHz. 46

2.17 Comparison of measured and simulated noise parameters vs I_C at 10 GHz. 47

2.18 Comparison of measurement and simulated noise parameters by making $\tau_b = \tau_f$. . . . 48

3.1 Illustration of noise extraction method based on small-signal equivalent circuit. 50

3.2 Illustration of noise extraction method based on lumped four-port network. 50

3.3 Illustration of transfer of internal terminal noise currents i_{bi} and i_{ci}, various resistance thermal noise i_{rk} to external terminal noise currents i_{bx} and i_{cx} with ac shorted base-emitter and collector-emitter voltages. 51

3.4 Sample Verilog-A code of nodes setup in VBIC model and symbols with external nodes displayed in schematic. 54

3.5 Illustration of simulating transfer functions $NT_{icx,ci}$ and $NT_{ibx,ci}$ by ac small signal analysis. 55

3.6 Screen shot of ADS simulation schematic. 56

3.7 Intrinsic noise extraction flow. . . . 57

3.8 Comparison of $S_{i_c i_c^*}$, $S_{i_b i_b^*}$ and $S_{i_c i_b^*}$ as a function of frequency. . . . 58

3.9 Comparison of the extracted $S_{i_{c_i} i_{c_i}^*}$, $S_{i_{b_i} i_{b_i}^*}$ and $S_{i_{b_i} i_{b_i}^*}$ with their input values as a function of frequency. . . . 59

3.10 Comparison of Y-parameters from simulation and measurement as a function of frequency at $I_C = 3.97$ mA. . . . 60

3.11 Comparison of noise parameters as a function of frequency from measurement and simulations with thermal noises plus correlated intrinsic current noises and thermal noises plus uncorrelated intrinsic current noises. . . . 61

3.12 Comparison of $S_{i_{cx} i_{cx}^*}$, $S_{i_{bx} i_{bx}^*}$ and $S_{i_{cx} i_{bx}^*}$ as a function of frequency from measurement and simulations with thermal noises plus correlated intrinsic noises, the correlated intrinsic noises alone and the thermal noises alone. . . . 62

3.13 Comparison of extracted $S_{i_{ci} i_{ci}^*}$, $S_{i_{bi} i_{bi}^*}$ and $S_{i_{ci} i_{bi}^*}$ as a function of frequency from measurement with different values of base resistance and simulations with and without correlation. . . . 63

3.14 Comparison of extracted $S_{i_{ci} i_{ci}^*}$, $S_{i_{bi} i_{bi}^*}$ and $S_{i_{ci} i_{bi}^*}$ as a function of frequency from measurement with two different values of effect base resistances and simulations with and without correlation. . . . 64

3.15 Comparison of extracted $S_{i_{ci} i_{ci}^*}$, $S_{i_{bi} i_{bi}^*}$ and $S_{i_{ci} i_{bi}^*}$ as a function of I_C from measurement with different values of base resistance and simulations with and without correlation. . . . 65

4.1 NF_{min} obtained from measurement and NF_{min} obtained from simulations with different noise sources turned on. . . . 67

4.2 $S_{i_c i_c^*}$ obtained from measurement and $S_{i_c i_c^*}$ obtained from simulations with different noise sources turned on. 68

4.3 Illustration of the full model and simplified model of the device. 69

4.4 Simulated Y_{11} and Y_{21} using the simplified model for intrinsic transistor plus R_b and using the complete HICUM model 70

4.5 Simulated noise transfer functions as a function of frequency at $I_C = 3.97$ mA with no extrinsic network element, with all extrinsic network elements, with only R_b and with only R_e. 71

4.6 The elements of $C_{i_{cm},i_{bm}}$ obtained with $[NT_{ibc}]$ simulated using complete extrinsic network compared with the elements of $C_{i_{cm},i_{bm}}$ obtained with $[NT_{ibc}]$ simulated using only a lumped R_b in the extrinsic network. 72

4.7 Illustration of Z presentation in the cases of the intrinsic device alone and the intrinsic device plus R_b. 73

4.8 The correlation matrix of Z-noise representation with $R_b = 0$, noiseless R_b and thermal noisy R_b. 74

4.9 Illustration of Y presentation in the cases of the intrinsic device alone and the intrinsic device plus R_b 76

4.10 Correlation matrix of Y representation from calculations. 78

4.11 Correlation matrix of chain noise representation from calculation with $R_b = 0\Omega$, thermal noiseless R_b and thermal noisy R_b. 80

4.12 Equivalent small-signal circuit with source noise v_s, device thermal noise v_b and current noise i_b and i_c. 81

4.13 Equivalent small-signal circuit with source noise v_s, device thermal noise v_b and current noise i_b and i_c. Emitter resistance is neglected. 82

4.14 Comparison of NF_{min} calculated from analytical equations and measurement. 88

4.15 Comparison of NF_{min} from 50 GHz SiGe HBT as a function of frequency from simulations with correlated intrinsic terminal current noises due to CB SCR plus thermal noises, correlated intrinsic terminal current noises alone and thermal noises alone. . . . 90

4.16 Simulated noise parameters using zero R_b, noiseless R_b and noisy R_b as a function of frequency at 3.97 mA; both uncorrelated SPICE model and new correlated model are included for comparison. 91

4.17 Simulated noise parameters using zero R_b, noiseless R_b and noisy R_b as a function of I_C at 10 GHz; both uncorrelated SPICE model and new correlated model are included for comparison. 92

5.1 Simplified equivalent circuit for a transistor with an emitter inductor L_e and a base inductor L_b. 95

5.2 Simplified equivalent circuit for a "noisy" transistor with an emitter inductor L_e and a base inductor L_b. The transistor has noise sources including the terminal noise current i_c and i_b and the thermal noise v_b of base resistance R_b. Power Source has a noise source v_s. 96

5.3 Modeled and measured noise parameters versus J_C at 5 GHz. 99

5.4 Schematic of the SiGe HBT cascode LNA used. 100

5.5 The noise matching source impedance of design using the correlated noise model versus J_c at 5 GHz and 10 GHz. 101

5.6 Emitter length (L_E) for R_{opt}=50 Ω and I_C versus J_C at 5 GHz. 101

5.7 NF_{LNA} and $NF_{min,LNA}$ of designs using SPICE and new noise models versus J_C at 5 GHz. 102

List of Tables

1.1 Transformation matrices to calculate noise representations 11

2.1 Noise currents of different mechanisms 30

2.2 Noise Model Parameters 45

Chapter 1

Introduction

Noise is a term describing any existing interference in a certain environment. It is therefore most of the time distressing and complicated. In electrical circuit and communication system, noise is anything but the desired signal. We can easily cite examples of this kind of noise from daily life. It could be the snow flake in the image when we watch TV; it could be the cacophony when we listen to the radio or make a cell phone call; or it could be the humming sound from the transformer device in your house.

Physically, noise presents in the form of the spontaneous fluctuations in current, voltage and even temperature in the electronic device, circuits and system. It sets the lower limits to the measurement accuracy and the strength of signal that can be processed correctly. By effective shielding methods, noise impact from outside environment and interconnection parasitics may be reduced. The main noise contribution then comes from the device employed in the system. This noise current or voltage detected at device terminals is the sum of the propagation of carrier current density fluctuations due to velocity fluctuations or carrier number fluctuations during carrier thermal motion. Carrier number fluctuations may be reduced by reducing introduced traps and defects with more mature process. However, the velocity fluctuations inherent in carrier random thermal motion can not be reduced even with perfect fabrication. Therefore, low-noise devices are always sought for low-noise RF application with higher frequency request.

A good candidate for low-noise operation is Silicon-Germanium (SiGe) heterojunction bipolar transistor(HBT). After being studied and developed for several decades, SiGe technology has become practical reality. The heart of SiGe technology is the SiGe HBT, which is the first practical bandgap engineering device realized in silicon and can be integrated with the modern

CMOS technology. By seamlessly introducing the graded Ge layer into the base of bipolar transistor (BJT), SiGe HBT technology exceeds the conventional Si BJT in both DC, RF and noise performance[6][7]. Fig. 1.1 shows that the graded-Ge induces an extra drift field in the neutral base. The smaller base bandgap increases the electron injection at emitter-base junction, and therefore the collector current density and current gain. The induced drift field also accelerates minority carrier transportation, yielding a decreased base transit time and higher cut-off frequency. This, together with its low noise feature, is why SiGe HBTs have been widely used in commercial and military wireless communication application. Fig. 1.2 is a SiGe BiCMOS chart of IBM showing the evolution of performance and minimum lithographic feature size over years from 0.5 μm technology to 0.13 μm technology [2]. The DOTFIVE project, uniting eleven of the best academic and institutes partners in Europe, has also demonstrated the realization of SiGe HBTs operating at a maximum frequency close to 0.5 THz (500 GHz) at room temperature [8].

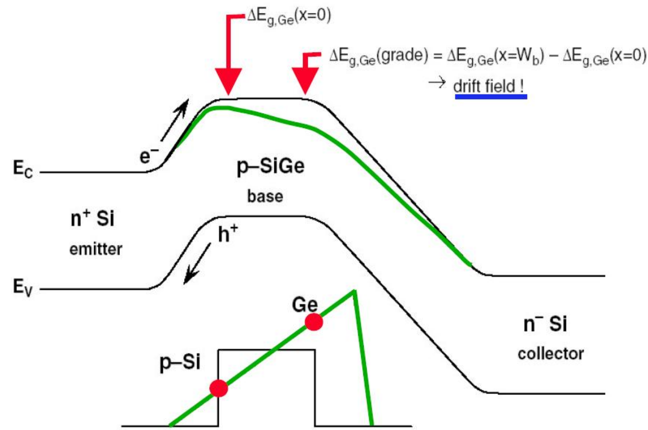

Figure 1.1: Energy band diagram of a graded-base SiGe HBT [1]

.

In this chapter, We first briefly introduce the main RF noise sources in SiGe HBTs and definitions of different noise representations as well as noise parameters. We will focus on the basic idea and method of noise study and give a general overview of status of the reported the RF noise performance of SiGe HBTs.

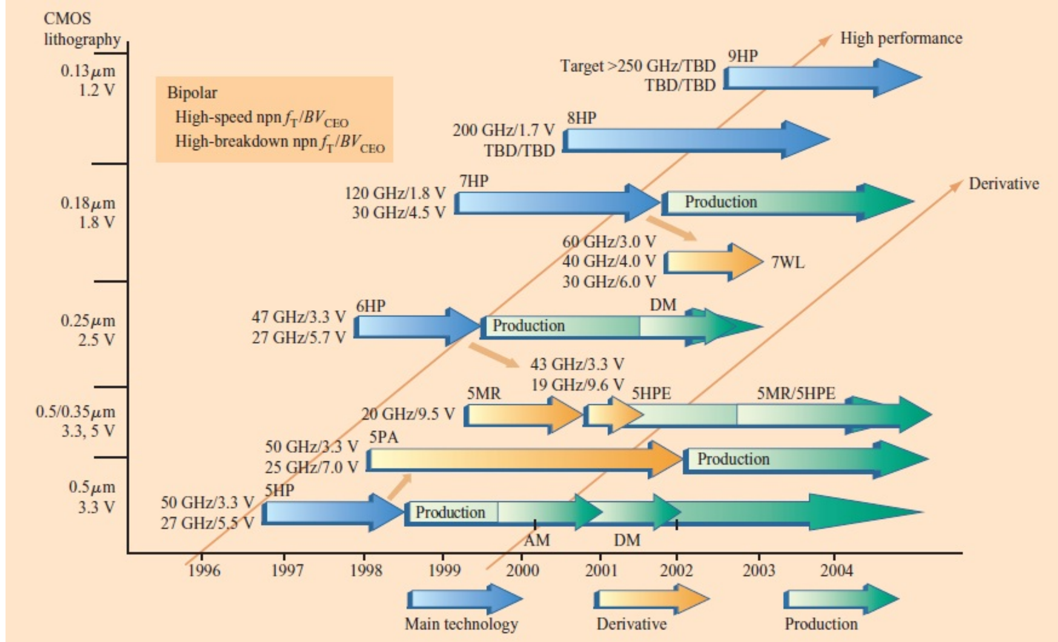

Figure 1.2: Summary of SiGe BiCMOS technology from IBM. This chart is copied from [2].

1.1 RF Noise

The operation of semiconductor devices is based on the carrier transportation. Under the action of external forces and the interaction with the lattice perturbations or other carriers, electrons and holes undergo a kind of Brownian motion whereby the velocity of each carrier exhibits large fluctuations [9]. The single particle fluctuation is large, while the collective fluctuations are small. From a device and circuit standpoint, the small collective fluctuation, however, propagates to the external device terminal and produces spontaneous fluctuations in current and voltage.

Fig. 1.3 illustrates Shockley's impedance field method [10]. Current density fluctuation $\delta I_{n/p}(r)$ caused by velocity fluctuation at origin r. Current density fluctuation propagates towards the contact $r_{contact}$ through the impedance factor $Z_{n/p}(r, r_{contact})$ during thermal motion and results in noise voltage fluctuation $V(r_{contact})$ at the contact.

From the equivalent circuit and compact modeling stand point, the velocity fluctuation caused by majority carrier thermal motion can be equivalently expressed by the thermal noises of resistors, while the velocity fluctuation caused by minority carrier thermal motion can be equivalent

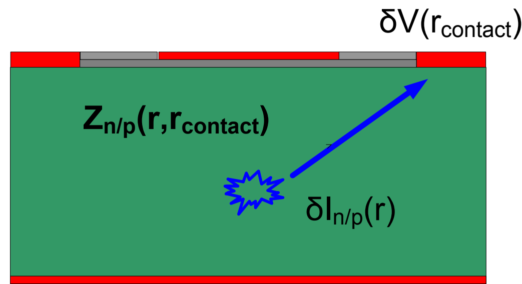

Figure 1.3: Shockley's impedance field method.

expressed by the intrinsic terminal current noises, which are the most important two kinds of noises in RF range. Fig. 1.4 illustrates the thermal noise sources of the base resistance, emitter resistance and collector resistance respectively as well as the terminal current noises of base and collector current.

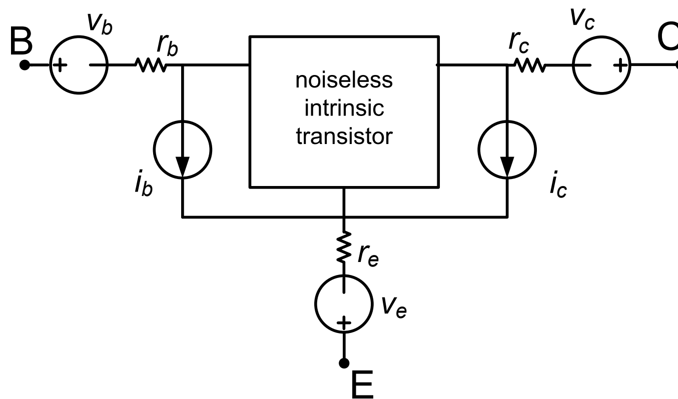

Figure 1.4: RF noise sources of a transistor.

1.1.1 Thermal Noise

The thermal noise of resistances describe by the Nyquist theorem is caused by random motion of the majority carriers and observed in thermal equilibrium, meaning regardless of applied

external bias [11]. The thermal noise can be regarded as a diffusion noise or velocity fluctuation noise [12]. The power spectral density (PSD) of thermal noise voltage is usually given by

$$S_{v_r,v_r^*} = 4KTR, \tag{1.1}$$

and that of thermal noise current is

$$S_{i_r,i_r^*} = \frac{4KT}{R}. \tag{1.2}$$

K is the Boltzmann constant and T is temperature in Kelvin. R represents the thermal resistance. Strictly speaking, the resistances are bias temperature dependant. The thermal noise is nearly constant at RF range, but not necessarily "white" due to carrier thermal motion nature [13] [14].

1.1.2 Terminal Current Noise

Traditionally, base and collector current noises are treated "shot" like, which means the carriers overcoming the junction potential barrier flow in a completely independent manner. The PSDs of shot noise are

$$S_{i_b,i_b^*} = 2qI_B, \tag{1.3}$$

and

$$S_{i_c,i_c^*} = 2qI_C. \tag{1.4}$$

I_B and I_C are base and collector DC current. Specifically, in a bipolar transistor, the base current shot noise $2qI_B$ results from the flow of base majority holes across the emitter-base junction potential barrier. The reason that I_B appears in the base shot noise is that the amount of hole current overcoming the EB junction barrier is determined by the minority hole current in the emitter, I_B. Similarly, the collector current shot noise results from the flow of electrons over the collector-base junction potential barrier, and has a spectral density of $2qI_C$. However, it is generally believed that the emitter-base junction is the origin of both base and collector noise [15]. Historically, the concept of shot noise originated from the random noise in a vacuum thermionic diode and the shot noise of transistors is of diffusion noise type. The transition of carriers across the CB junction, which is usually reverse-biased for low-noise amplification, however, is a drift process. Therefore,

a dc current passing through such a junction alone does not have intrinsic shot noise. The collector current shows shot noise only because the electron current is transported from the EB junction and injected into the CB junction.

The above two views may lead to the same collector current noise, but different base current noise and base collector current noise correlation at higher frequency [16]. Practically, the uncorrelated "shot" like $2qI$ noise model cannot successfully predict the device noise behavior at high frequency. Increasing interest to higher frequency application urges that the correlation of base and collector noise current has to be considered. The concept of noise transport is well accepted and the noise transit time as a signature of noise correlation is implemented in different approach [16] [17] . We will focus on the base and collector terminal current noise modeling in Chapter 2.

1.2 Noise Characterization

One important question is how to examine and evaluate the noise in the device. A useful way to analysis device noise is to use the two port network theory. The transistor can be classified as a twoport. As long as the device noise is much smaller in magnitude compared to the device external biases, the device noise can be treated linearly [18]. Therefore, we can treat the device noise problem as a linear noisy twoport problem.

1.2.1 Noise Representations of Two Port Network

A noisy two port network, can be equivalently described by a noiseless two port with two equivalent noise sources, regardless of the complicacy of the network topology. There are families of two-port representations, including impedance representations (Z representation), admittance representation (Y representations), Hybrid representation (H representation) and chain representation (ABCD representation). Each representation is corresponding to one noise representation. The expressions of each noise representation are related to the internal topology. The different two noise sources combinations and transfer function between different noise representations all lead to the different relative importance of noise sources.

Y representation

Fig. 1.5 shows an simplified example of transistor as a noisy two port. The upper case letters I and V indicate the Fourier transforms of the current and voltage, which are frequency dependent [18]. In this noisy two port, there are three original noise sources, the thermal noise voltage source v_b of base resistance r_b, the intrinsic terminal current noise sources i_{bi} and i_{ci}. This noisy

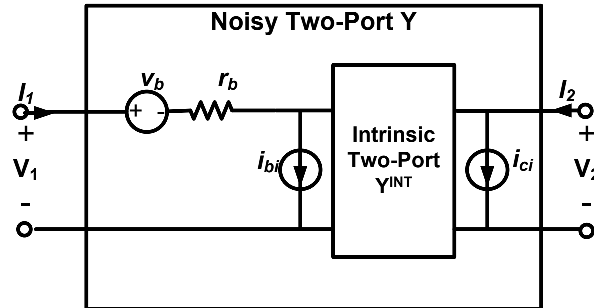

Figure 1.5: A simplified example of transistor as a noisy two port.

two port can be described by a noiseless two port with an equivalent current noise source i_1 at the input and an equivalent current noise source i_2 at the output port, as shown in Fig. 1.6. This is Y noise representation. i_1 and i_2 therefore consist of noise contribution from i_{bi}, i_{ci} and r_b. From the

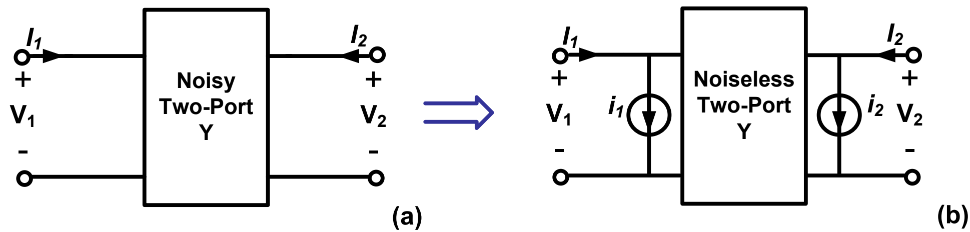

Figure 1.6: Y representation of a linear noisy two-port network.

intrinsic node, we have input current $I_1 - i_1$ and output current $I_2 - i_2$. Y representation $I - V$

relations including equivalent noise sources for Y representation are

$$\begin{pmatrix} I_1 - i_1 \\ I_2 - i_2 \end{pmatrix} = \begin{pmatrix} Y_{11} & Y_{12} \\ Y_{21} & Y_{22} \end{pmatrix} \cdot \begin{pmatrix} V_1 \\ V_2. \end{pmatrix} \tag{1.5}$$

The PSD's of i_1 and i_2 and their correlation are S_{i_2,i_2^*}, S_{i_1,i_1^*} and S_{i_2,i_1^*}. The chain noise matrix is defined as

$$C_Y = \begin{pmatrix} S_{i_1,i_1^*} & S_{i_1,i_2^*} \\ S_{i_2,i_1^*} & S_{i_2,i_2^*}. \end{pmatrix} \tag{1.6}$$

The Y noise representation are often used for modeling terminal current noise. (1.6) is also written as

$$C_Y = \begin{pmatrix} S_{i_{bx}i_{bx}^*} & S_{i_{bx}i_{cx}^*} \\ S_{i_{cx}i_{bx}^*} & S_{i_{cx}i_{cx}^*}. \end{pmatrix} \tag{1.7}$$

i_{bx} and i_{cx} here are the equivalent noise current sources instead of intrinsic noise origin.

ABCD representation

The chain noise representation, also referred as the general-circuit-parameter representation, describe the noise of two port network using an equivalent voltage noise source v_a and an equivalent current noise source i_a both at the input port, as shown in Fig. 1.7. The chain representation are most often used to calculate noise parameter. $I - V$ relations including equivalent noise sources

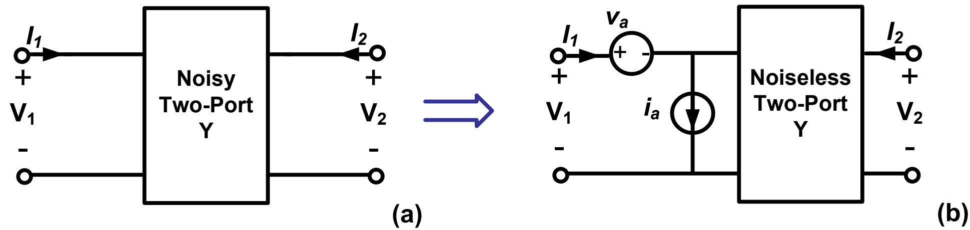

Figure 1.7: Chain representation of a linear noisy two-port network.

for the chain representation are

$$\begin{pmatrix} I_1 - i_a \\ I_2 \end{pmatrix} = \begin{pmatrix} Y_{11} & Y_{12} \\ Y_{21} & Y_{22} \end{pmatrix} \cdot \begin{pmatrix} V_1 - v_a \\ V_2. \end{pmatrix} \tag{1.8}$$

The PSDs of v_a and i_a and their correlation are S_{v_a,v_a^*}, S_{i_a,i_a^*} and S_{i_a,v_a^*} (S_{v_a,i_a^*}). The chain noise matrix is defined as

$$C_a = \begin{pmatrix} S_{i_a,i_a^*} & S_{i_a,v_a^*} \\ S_{v_a,i_a^*} & S_{v_a,v_a^*}. \end{pmatrix} \tag{1.9}$$

Z representation

The Z noise representation describes the noise of two port network using an equivalent voltage noise source v_1 at the input and an equivalent voltage noise source v_2 at the output port, as shown in Fig. 1.8. The Z noise representation is best used for de-embedding the noise of series parasitics. $I - V$ relations including equivalent noise sources for Z representation are

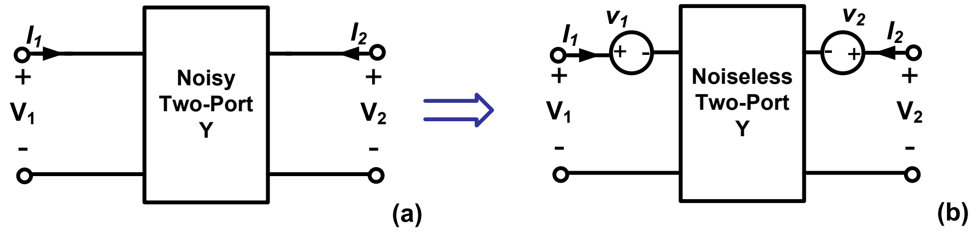

Figure 1.8: Z representation of a linear noisy two-port network.

$$\begin{pmatrix} I_1 \\ I_2 \end{pmatrix} = \begin{pmatrix} Y_{11} & Y_{12} \\ Y_{21} & Y_{22} \end{pmatrix} \cdot \begin{pmatrix} V_1 - v_1 \\ V_2 - v_2. \end{pmatrix} \tag{1.10}$$

The PSD's of v_1 and v_2 and their correlation are S_{v_2,v_2^*}, S_{v_1,v_1^*} and S_{v_2,v_1^*}. The chain noise matrix is defined as

$$C_Z = \begin{pmatrix} S_{v_1,v_1^*} & S_{v_1,v_2^*} \\ S_{v_2,v_1^*} & S_{v_2,v_2^*}. \end{pmatrix} \tag{1.11}$$

H representations

The H noise representation describes the noise of two port network using an equivalent voltage noise source v_h at the input and an equivalent current noise source i_h at the output port, as shown in Fig. 1.9. $I - V$ relations including equivalent noise sources for H representation are

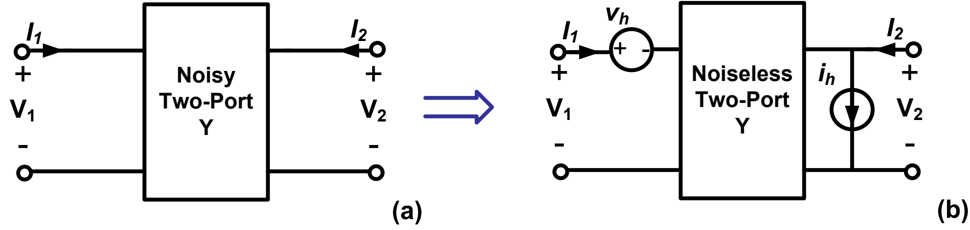

Figure 1.9: H representation of a linear noisy two-port network.

$$\begin{pmatrix} I_1 \\ I_2 - i_h \end{pmatrix} = \begin{pmatrix} Y_{11} & Y_{12} \\ Y_{21} & Y_{22} \end{pmatrix} \cdot \begin{pmatrix} V_1 - v_h \\ V_2. \end{pmatrix} \tag{1.12}$$

The PSD's of v_h and i_h and their correlation are S_{v_h,v_h^*}, S_{i_h,i_h^*} and S_{v_h,i_h^*}. The chain noise matrix is defined as

$$C_H = \begin{pmatrix} S_{v_h,v_h^*} & S_{v_h,i_h^*} \\ S_{i_h,v_h^*} & S_{i_h,i_h^*}. \end{pmatrix} \tag{1.13}$$

Transformation between different noise representations

The chain noise representation, Y noise representation, Z noise representation, and H noise representations can be transformed from one to the others. An example of transformation between

Table 1.1: Transformation matrices to calculate noise representations

	C_A	C_Y	C_Z	C_H
C'_A	$\begin{pmatrix} 1 & 0 \\ 0 & 1 \end{pmatrix}$	$\begin{pmatrix} 0 & A_{12} \\ 1 & A_{22} \end{pmatrix}$	$\begin{pmatrix} 1 & -A_{11} \\ 0 & -A_{21} \end{pmatrix}$	$\begin{pmatrix} 1 & A_{12} \\ 0 & A_{22} \end{pmatrix}$
C'_Y	$\begin{pmatrix} -Y_{11} & 1 \\ -Y_{21} & 0 \end{pmatrix}$	$\begin{pmatrix} 1 & 0 \\ 0 & 1 \end{pmatrix}$	$\begin{pmatrix} Y_{11} & Y_{12} \\ Y_{21} & Y_{22} \end{pmatrix}$	$\begin{pmatrix} -Y_{11} & 0 \\ -Y_{21} & 1 \end{pmatrix}$
C'_Z	$\begin{pmatrix} 1 & -Z_{11} \\ 0 & -Z_{21} \end{pmatrix}$	$\begin{pmatrix} Z_{11} & Z_{12} \\ Z_{21} & Z_{22} \end{pmatrix}$	$\begin{pmatrix} 1 & 0 \\ 0 & 1 \end{pmatrix}$	$\begin{pmatrix} 1 & -Z_{12} \\ 0 & -Z_{22} \end{pmatrix}$
C'_H	$\begin{pmatrix} 1 & -H_{11} \\ 0 & -H_{21} \end{pmatrix}$	$\begin{pmatrix} -H_{11} & 0 \\ -H_{21} & 1 \end{pmatrix}$	$\begin{pmatrix} 1 & -H_{12} \\ 0 & -H_{22} \end{pmatrix}$	$\begin{pmatrix} 1 & 0 \\ 0 & 1 \end{pmatrix}$

ABCD representation and other representations is shown in Appendix A. More generally, the transformation can be realized by the matrix operation

$$C' = T \cdot C \cdot T^{\dagger}, \tag{1.14}$$

where C is the original noise correlation matrix and C' is the resulting noise correlation matrix. T is the transformation matrix given in Table 1.1, and $T^{\dagger}$ is the transpose conjugate of T . The used two-port network parameters, Y-, Z-, H-, ABCD-, are summarized as in Table 1.1.

1.2.2 Noise figure and Noise Parameter

The figure of merit that describes the level of excess noise present in the system is noise factor, F. It is defined to be the signal-to-noise ratio (SNR) at the input divided by the the SNR at the output,

$$F = \frac{S_i/N_i}{S_o/N_o}, \tag{1.15}$$

with S_i being the input signal power, S_o being the output signal power, N_i being the input noise power and N_o being the output noise power. Noise figure is the noise factor in decibels,

$$NF = 10 \cdot \log(F). \tag{1.16}$$

The concept of noise figure is easy to understand when we consider an amplifier, as shown in Fig. 1.10. Both the signal and noise at the input are amplified by the gain G of the amplifier. If the

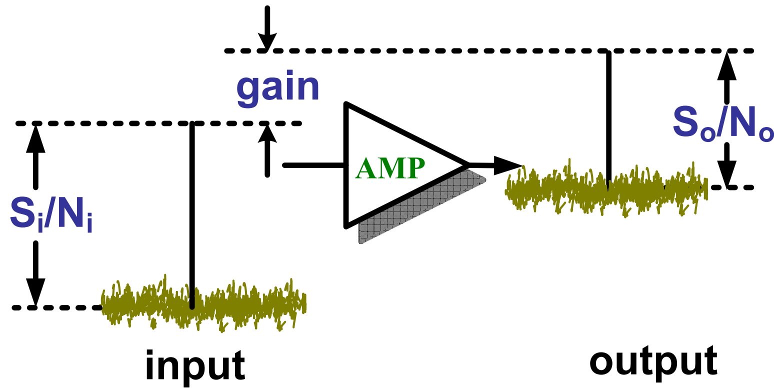

Figure 1.10: Illustration of the definition of Noise figure for an amplifier.

amplifier is perfect, the output noise is also equal to the input noise amplified by the amplifier's gain, resulting in the same SNR at both the input and output. However, the noise inherent the amplifier contributes additional noise at the output, so SNR at the output is smaller than that at the input, resulting in F being greater than one, or NF being greater than 0 dB. (1.15) can be rewritten as

$$\begin{aligned} F &= \frac{S_i}{S_o} \cdot \frac{N_o}{N_i} \\ &= \frac{1}{G} \cdot \frac{N_o}{N_i}. \end{aligned} \tag{1.17}$$

If the amplifier inherent noise is represented by equivalent noise sources at the input, as in the chain representation,

$$F = 1 + \frac{N_{amp,i}}{N_i}. \tag{1.18}$$

If the amplifier inherent noise is represented by equivalent noise sources at the output,

$$F = 1 + \frac{N_{amp,o}}{GN_i}. \tag{1.19}$$

Both $N_{amp,i}$ and $N_{amp,o}$ are dependent on the source impedance Z_S or source admittance Y_S.

The noise figure of a circuit is determined by the source termination and the noise properties of the circuit. The noise properties are usually expressed by noise parameters, including the minimum noise figure NF_{min}, the noise resistance R_n and the optimum source admittance Y_{opt}. $Y_{opt} = G_{opt} + jB_{opt}$. F related to noise parameters by

$$F = F_{min} + \frac{R_n}{G_S} \left| Y_S - Y_{opt} \right|^2, \tag{1.20}$$

where $Y_S = G_S + jB_S$ is the admittance of source. $NF_{min} = 10\log(F_{min})$. Or

$$F = F_{min} + \frac{G_n}{R_S} \left| Z_S - Z_{opt} \right|^2, \tag{1.21}$$

where $Z_S = G_S + jB_S = 1/Y_S$ and $Z_{opt} = R_{opt} + jX_{opt} = 1/Y_{opt}$.

Clearly, noise figure reaches it minimum, NF_{min}, when $Y_S = Y_{opt}$ ($Z_S = Z_{opt}$), i.e., at "noise matching", as shown in Fig. 1.11. Each set of four noise parameters define a noise surface which is an asymmetric paraboloid. Each NF, and the corresponding Y_S must be located on this noise surface. NF_{min} is the vertex of the paraboloid. R_n, determined by the curvature of the paraboloid, represents the sensitivity of NF deviation from NF_{min} to noise mismatch [19].

From linear noisy two-port theory, the noise parameter can be related to the noise correlation matrices [18]. The chain noise representation is most often used, as illustrated in Fig. 1.12

The relation between noise parameters and PSDs of chain representations are

$$R_n = \frac{S_{v_a,v_a*}}{4kT}, \tag{1.22}$$

$$G_{opt} = \sqrt{\frac{S_{i_a,i_a*}}{S_{v_a,v_a*}} - \left[\frac{\Im\left(S_{i_a,v_a*}\right)}{S_{v_a,v_a*}} \right]^2}, \tag{1.23}$$

$$B_{opt} = -\frac{\Im\left(S_{v_a,v_a*}\right)}{S_{v_a,v_a*}}, \tag{1.24}$$

$$R_n = \frac{S_{v_a,v_a*}}{4kT}, \tag{1.25}$$

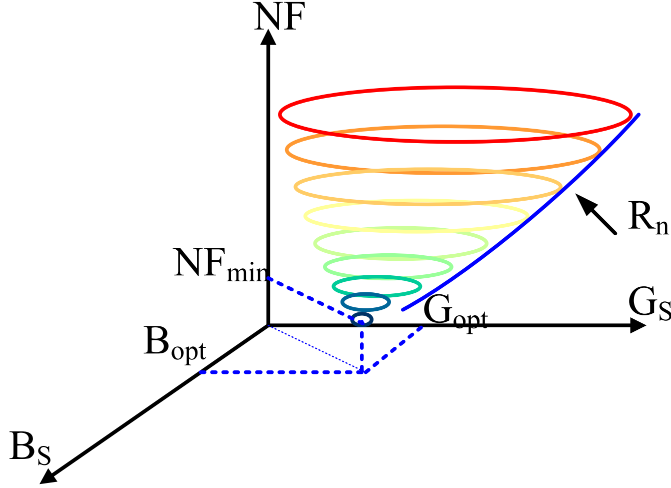

Figure 1.11: Asymmetric paraboloid of noise figure in the three-dimensional co-ordinate system.

$$F_{min} = 1 + \frac{\sqrt{S_{v_a,v_a*}S_{i_a,i_a*} - \left[\Im\left(S_{i_a,v_a*}\right)\right]^2} + \Re\left(S_{i_a,v_a*}\right)}{2kT}$$
$$= 1 + 2R_n\left(G_{opt} + \frac{\Re\left(S_{i_a,v_a*}\right)}{S_{v_a,v_a*}}\right), \tag{1.26}$$
$$NF_{min} = 10\log_{10} F_{min}.$$

T is noise temperature in Kelvin [20] and is conventionally taken to be room temperature, 290 K.

The chain noise representation correlation matrix can also be expressed using the noise parameters. As

$$S_{v_a,v_a*} = 4KTR_n, \tag{1.27}$$

$$S_{i_a,i_a*} = 4KTR_n\left|Y_{opt}\right|^2, \tag{1.28}$$

$$S_{i_a,v_a*} = 2KT\left(F_{min} - 1\right) - 4kKTR_nY_{opt}, \tag{1.29}$$

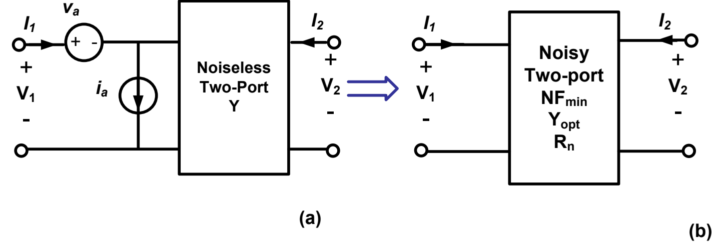

Figure 1.12: Illustration of noise parameters of a two-port network.

or

$$C_A = 4KT \begin{pmatrix} R_n & \frac{F_{min}-1}{2} - R_n Y_{opt}^* \\ \frac{F_{min}-1}{2} - R_n Y_{opt} & R_n \left| Y_{opt} \right|^2 \end{pmatrix} \tag{1.30}$$

The detailed derivation procedure can be found in Appendix B.

1.3 SiGe HBTs Noise Performance

When we consider the single transistor as a two-port network, the noise parameters and noise representation matrices describe the noise characteristics of the transistor itself. They are independent of the source and load termination. Among the noise parameters, NF_{min} is the most important one. Small NF_{min} is most desirable for device optimization when noise is regarded.

In [7] and [15], the analytical expression of NF_{min} is related to transistor transconductance g_m, current gain β, base resistance r_b and cut-off frequency f_T

$$NF_{min} = 1 + \frac{1}{\beta} + \sqrt{2g_m r_b}\sqrt{\frac{1}{\beta} + \left(\frac{f}{f_T}\right)^2}. \tag{1.31}$$

A few simplifications are employed in derivation. First, intrinsic base and collector terminal current noise are "shot" like, $2qI$, and assumed to be uncorrelated. Second, base resistance are lumped equivalent resistance providing thermal noise but does not impact on intrinsic terminal noise current propagation. Third, the circuit application requires $g_m r_b >> 1/2$. In the following chapters,

we will develop more accurate model with correlation and evaluate the base resistance impact on intrinsic noise propagation.

The simplicity of (1.31) here helps us to understand how the device noise performance is related to DC/AC characteristics. At a fixed bias, NF_{min} increases with frequency increasing. Increasing β, f_T and decreasing r_b will help to reduce NF_{min}. Thus the higher f_T, smaller r_b and comparable current gain make SiGe HBTs have a better noise feature when compared to the traditional Si BJTs, while the continued development in lithography and other innovations in advanced technology bring a persistent improvement in transistor noise performance. Below is shown a few examples of the reported NF_{min} of SiGe HBTs over the last decade. Fig. 1.13 shows NF_{min} versus frequency for a sampling of IBM high-performance HBTs at the 0.5-, 0.18-, and 0.13- μm nodes as well as a slightly higher breakdown voltage variant at the 0.18- μm node [3]. $NF_{min} < 1dB$ is realized in SiGe HBT of 0.13 μm technology below 20 GHz. Fig. 1.14 and Fig. 1.15 shows NF_{min} versus J_C at 10 GHz and 25 GHz of SiGe HBT from 0.13 μm SiGe-BiCMOS process featuring f_T = 250 GHz [21]. NF_{min} below 1 dB is achieved at 10 GHz.

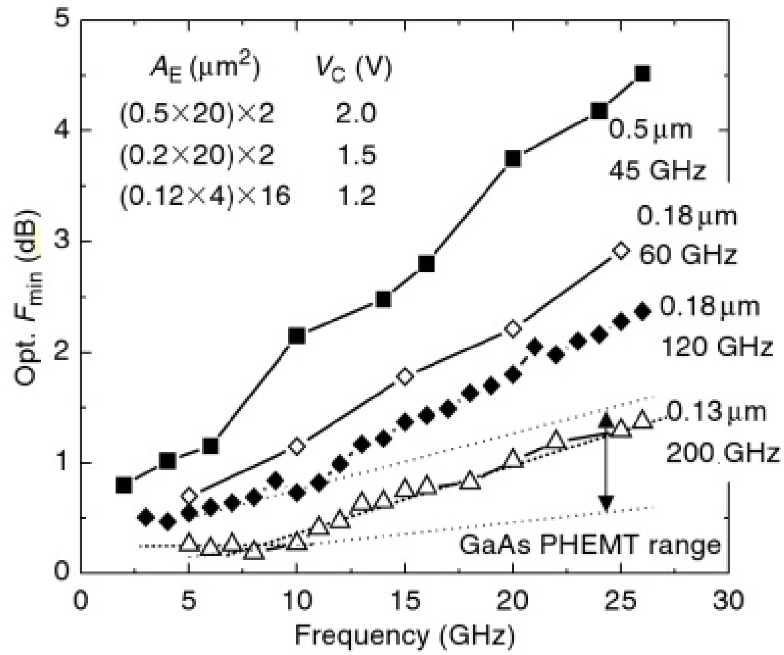

Figure 1.13: NF_{min} versus frequency for SiGe HBTs from four SiGe BiCMOS technologies, including three high-performance variants at the 0.5-, 0.18-, and 0.13- μm nodes as well as a slightly higher breakdown voltage variant at the 0.18- μm node. This figure is copied from [3] .

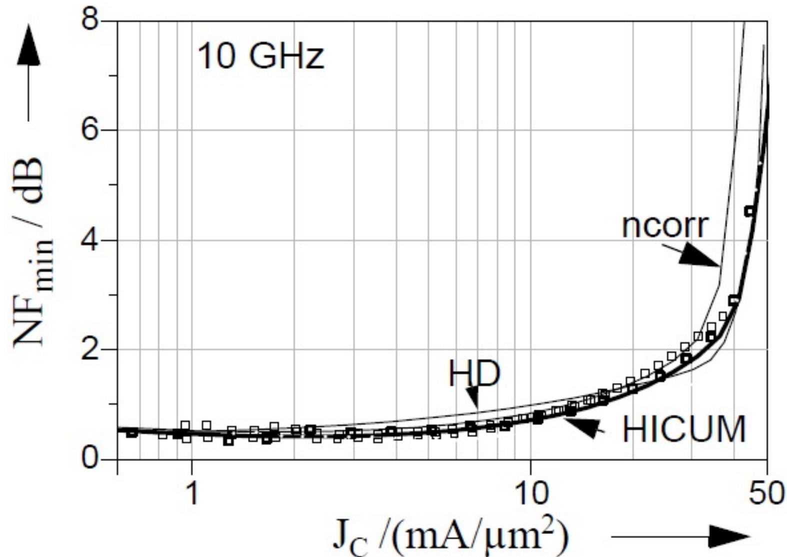

Figure 1.14: NF_{min} versus J_c at 10 GHz for 250 GHz SiGe HBT with $A_E = 0.094 \times 9.62 \mu m^2$. Measured data are shown by symbols. This figure is copied from [4].

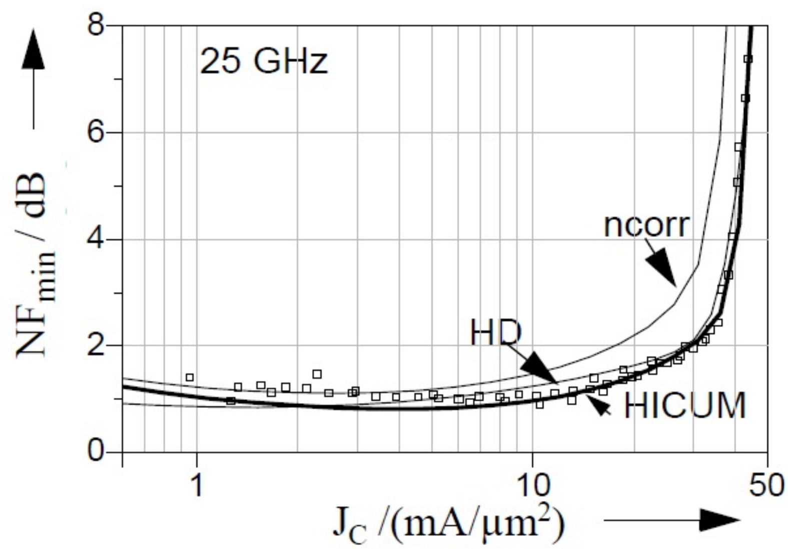

Figure 1.15: NF_{min} versus J_c at 25 GHz for 250 GHz SiGe HBT with $A_E = 0.094 \times 9.62\mu m^2$. Measured data are shown by symbols. This figure is copied from [4].

Chapter 2

Noise Compact Modeling and Implementation

Successful circuit design requires accurate compact transistor models that can faithfully and efficiently describe transistor electrical characteristics across a wide frequency, biasing and temperature range. Accurate noise compact model is in particular important for mixed-signal analog and RF circuit design, e.g., low noise amplifier (LNA) design. Currently the noise model in industry standard compact models is essentially the same as what was in early SPICE Gummel-Poon model. All terminal resistances have the usual $4kTR$ thermal noise. The base and collector currents show uncorrelated $2qI$ "shot" noises which are frequency independent.

Semiconductor technology development is driven by aiming at realizing larger systems and lower cost with scaling, specifically higher density, lower power and higher speed. Higher operation frequency is especially requested for RF application and overall challenges the conventional model accuracy at high frequency. Fig. 2.1 compares noise parameters simulated using IBM' s design kit which employs the HICUM transistor model with measurement for a SiGe HBT featuring peak f_T = 36 GHz from IBM 0.5/0.35 μm technology [22]. De-embedding was done by on-chip open and short structures. The model parameters have been extracted to reproduce well fitted DC current and S-parameters. The compact model, however, does not reproduce the noise parameters well. NF_{min} is severely overestimated above 5 GHz. The real part of Y_{opt} is poorly modeled as well. The imaginary part of Y_{opt} is well modeled. R_n is reasonably modeled, but increases with frequency and becomes higher than measurement above 10 GHz.

2.1 van Vliet's model

Many efforts have been made to improve high frequency compact noise modeling in HBTs. One popular approach is to develop the noise compact model based on van Vliet's pioneering

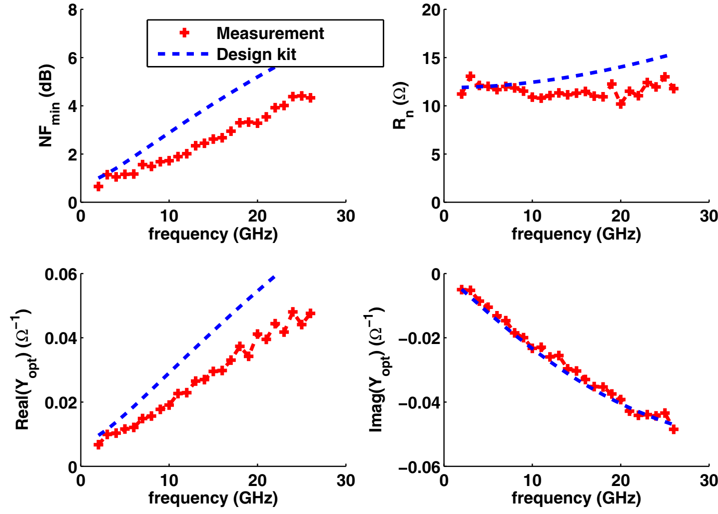

Figure 2.1: Comparison of noise parameters simulated for an IBM SiGe HBT using design kit with measurement from 2 to 26 GHz. Inside the design kit, HICUM model is used.

work. Van Vliet's model was derived about 4 decades ago [23] [12]. Device noise comes from the fluctuations of the number of particles due to generation and recombination processes and fluctuations due to thermal motion of carriers (thermal noise or diffusion noise). Impact of these fluctuations can be taken into account by adding stochastic noise to the continuity and current equations resulting in the Langevin equations of transport theory [11]. Van Vliet's model solves the Langevin equation of base minority carrier velocity fluctuation (and hence current density noise) propagation towards the two boundaries of the neutral base. In the 1-D condition, the Langevin equation based on Drift-Diffusion model for the base electron diffusion noise is

$$D_n \frac{\partial^2}{\partial x^2} \triangle n + \mu_n E \frac{\partial}{\partial_x} \triangle n - \frac{\triangle n}{\tau_c} - j\omega \triangle n + \xi(\omega) = 0. \tag{2.1}$$

E is the built-in electric field. μ_n is the electron high field mobility

$$\mu_n = \frac{\mu_{n0}}{\sqrt[\beta]{1 + \left(\frac{\mu_{n0} E}{v_{sat}}\right)^\beta}}, \tag{2.2}$$

where v_{sat} is saturation velocity, μ_{n0} is low field mobility and β is a constant specifying how abruptly the velocity goes into saturation. The noise source is

$$\xi(\omega) = \zeta(\omega) + \frac{1}{q}\frac{\partial}{\partial x}\gamma(\omega), \tag{2.3}$$

where $\zeta(\omega)$ is GR noise source and $\gamma(\omega)$ is diffusion noise source

$$\gamma(\omega) = 4q^2 D_n N(x). \tag{2.4}$$

$N(x)$ is the DC electron concentration. GR noise can be negligible at RF and only diffusion noise is considered. The boundary condition is

$$\triangle n|_{x=0} = 0, \triangle n|_{x=d_B} = 0. \tag{2.5}$$

We can use the Green function method to solve the Langevin equation [9]. van Vliet solved the 3-D Langevin equation for base electron noise using Green's function method. A unique feature of van Vliet's model is that the base and collector current noises, as well as their correlation, are explicitly expressed as a function of the *intrinsic* Y-parameters due to base minority carrier. In the derivation, the Y-parameters are expressed by Green's functions in linear fashion using the extended Green theorem. The PSDs of noise are initially quadratic in Green's functions. In order to make the connection between noise PSD and the Y-parameter, it is convenient to transform the noise PSD into a result whose main part is linear in the Green's functions. Finally the base electron noises are related to the Y-parameters of the base region [23] [5]. The original results are in common-base configuration but can be transformed into common-emitter configuration as

$$S^B_{i_b,i_b^*} = 4kT\Re\left(Y^B_{11}\right) - 2qI^B_B, \tag{2.6}$$

$$S^B_{i_c,i_c^*} = 2qI_C + 4kT\Re\left(Y^B_{22}\right), \tag{2.7}$$

$$S^B_{i_c,i_b^*} = 2kT\left(Y^B_{21} + Y^{B*}_{12}\right) - 2qI_C. \tag{2.8}$$

The superscript B refers to base. I^B_B is the DC neutral base recombination current, which is negligible in modern transistors. We emphasize that Y^B in van Vliet's derivation refers to the Y-parameters

of the intrinsic base region only and requires rigorous frequency domain solution, meaning the frequency dependence of $S^B_{i_b,i_b^*}$, $S^B_{i_c,i_c^*}$, and their correlation, are taken into account through the frequency dependence of the Y-parameters of base Y^B due to the base electron transport.

The frequency dependence of Y^B for the base was first examined by [24] using a 1D transistor structure.

$$Y^B_{11} = \frac{I_C}{V_T} j \frac{\omega}{\omega_{TB}} \left[1 - j \frac{\omega}{\omega_{TB}} \left\{ \frac{\eta \coth \frac{\eta}{2} + 1 + \eta}{\eta - 1 + \exp(-\eta)} - \frac{3\eta^2}{2(\eta - 1 + \exp(-\eta))^2} \right\} + ... \right] \tag{2.9}$$

$$\frac{1}{Y^B_{21}} = \frac{V_T}{I_C} \left[1 + j \frac{\omega}{\omega_{TB}} \left\{ \frac{\eta \coth \frac{\eta}{2} + 1 + \eta}{\eta - 1 + \exp(-\eta)} \right\} + ... \right] \tag{2.10}$$

where $V_T = KT/q$, η is a measure for electrical field (assuming $\eta = \triangle E_G/V_T$ for SiGe HBT) and $\omega_{TB} = 1/\tau_b$ with τ_b being base transit time. This result was given for drift transistor when it was developed. We are using it here for SiGe HBT as there is Ge induced electrical field in the base and we are using it for constant doping and linear Ge profile. This results can be approximately regarded as that the base minority carrier charge responds to the base emitter voltage with an input delay time, after which the collector current at the end of base region responds to the stored base minority carrier charge with output delay time. The input delay time represents the input non-quasistatic (NQS) effect and the output delay time represents the output excess phase delay. Results of Y^B are shown in Fig. 2.2[5]. With a larger η, Y^B has a stronger frequency dependence. The input NQS effect becomes stronger at a given frequency for a larger Ge gradient device, as shown by $\Re(Y_{11})$. In [25], van Vliet model is extended to include emitter minority carrier induced base noise. The PSDs of $S^{EB}_{i_b,i_b^*}$, $S^{EB}_{i_c,i_c^*}$ and their correlation can be obtained as

$$S^{EB}_{i_b,i_b^*} = 4kT\Re\left(Y^{EB}_{11}\right) - 2qI_B, \tag{2.11}$$

$$S^{EB}_{i_c,i_c^*} = 2qI_C + 4kT\Re\left(Y^{EB}_{22}\right), \tag{2.12}$$

$$S^{EB}_{i_c,i_b^*} = 2kT\left(Y^B_{21} + Y^{EB*}_{12}\right) - 2qI_C. \tag{2.13}$$

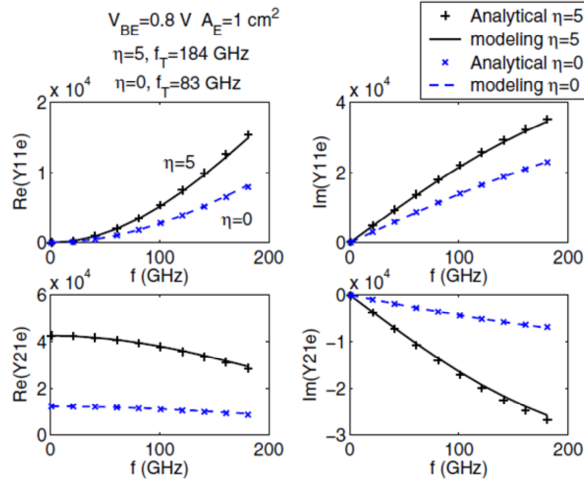

Figure 2.2: Y-parameter modeling result using equivalent circuit with NQS input. $\mu_0 = 270cm^2/(V \cdot s)$, electron life time= $1.54x10^{-7}$ s, $T = 300$ K, $d_B = 45$ nm, $V_{BE} = 0.8$ V. $f_T = 184$ GHz for $\eta = 5$. $f_T = 83$ GHz for $\eta = 0$ (copied from [5]).

where Y^{EB} represents Y-parameters of base and emitter region. I_B is mainly due to is the hole current at the emitter injection point, essentially the mount of base current due to the injection of base holes.

The intrinsic Y-parameters in a compact model do not have all the necessary frequency dependence required for van Vliet's model, as detailed in Section 2.3. Therefore directly implementing van Vliet's model into compact models may cause some issues.

2.2 CB SCR Effect

van Vliet model considers only the minority carrier transport in base but does not consider the transport effect in collector-base junction space charge region (CB SCR), which becomes important and even dominant in the aggressively scaled transistor. The collector current $2qI_C$ noise from the van Vliet model was derived as the minority electron current noise (for NPN) at the end or collector side of the neutral base. This electron noise current travels through the CB SCR, producing extra correlated terminal current noises [26], while Y-parameters have considerable contributions

from CB SCR transport. From a Y-parameter standpoint, CB SCR electron transport modifies transistor Y-parameter, and to first order, causes an extra diffusion capacitance component.

$$Y_{11} = Y_{11}^{B} + (1 - \lambda)Y_{21}^{B}, Y21 = \lambda Y_{21}^{B}, \tag{2.14}$$

where

$$\lambda = \frac{1 - exp\,(-2j\omega\tau_c)}{2j\omega\tau_c}, \tag{2.15}$$

τ_c the well known collector transit time corresponding to CB SCR transport. The drift of electrons across the CB SCR induces additional base hole current. The noise in the electron current exiting the neutral base gets transported across the CB SCR, and in the process, directly creates additional base hole current noise. Depending on HBT design, at higher frequencies this extra base hole current noise can be comparable to, or even dominate over the "regular' base current noise that is described by the van Vliet model. The van Vliet's model has been recently extended for modern SiGe HBTs, and included CB SCR effect [25]. However, like van Vliet model, the model requires accurate intrinsic transistor Y-parameters [25] [27]. As a result, empirical modifications have to be made to produce improved noise modeling result in [28] and [29].

2.3 A survey of previous noise compact modeling methods

Most popular noise compact modeling approach is implementing van Vliet's model into modern compact models. This approach is being explored in research versions of two industry standard compact models, namely Mextram and HICUM [28] [29]. Correlation between base and collector current noise are added. Note that in the official versions of HICUM and Mextram that are currently implemented in commercial simulators, including Cadence Spectre and Agilent ADS, the respective correlated noise implementations reported in [28] and [29] are not yet available.

2.3.1 Noise compact model of Mextram group

This model formulation is developed based on charge partitioning. In charge partitioning, a part of the total diffusion charge is partitioned between the emitter and the collector. Collector and

emitter currents are given by [30] [31]

$$I_E = I_{DC} + (1 - \alpha_{cp})\frac{d}{dt}Q_{tot}, \tag{2.16}$$

$$I_C = I_{DC} - \alpha_{cp}\frac{d}{dt}Q_{tot}, \tag{2.17}$$

Where I_{DC} is the DC emitter to collector transport current. The net build-up of charge is $I_E - I_C = dQ_{tot}/dt$. α_{cp} is the charge partitioning factor and has a value between 0 and 1. $1 - \alpha_{cp}$ means the fraction of charge reclaimed by the emitter, as illustrated in Fig. 2.3. The PSDs of base and

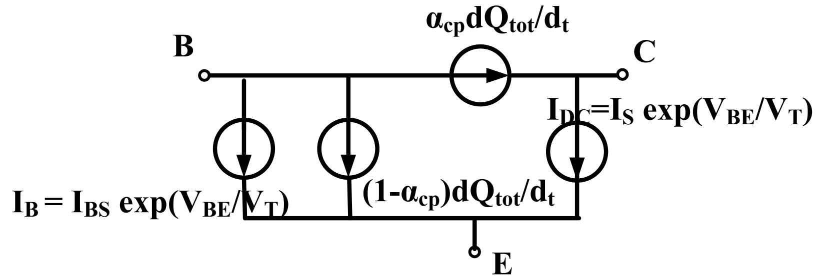

Figure 2.3: Network representation of the charge partitioning model.

collector intrinsic noise and their correlation are given as [28]:

$$S_{i_b,i_b^*} = 2qI_B, \tag{2.18}$$

$$S_{i_c,i_c^*} = 2qI_C, \tag{2.19}$$

$$S_{i_c,i_b^*} = 2qj\omega\alpha_{cp}Q_{tot}. \tag{2.20}$$

In this model formulation, van Vliet's model is brutally used, together with highly simplifying and inconsistent use of quasi-static Y-parameters where non-quasistatic Y-parameters are required. The step-by-step "derivation" of (2.18),(2.19) and (2.20) from van Vliet model, (2.6), (2.7) and (2.8) is given below. According to Fig. 2.3,

$$Y_{11} = \frac{I_B}{V_T} + j\omega C_{tot}, \tag{2.21}$$

where

$$C_{tot} = \frac{dQ_{tot}}{dV_{BE}}. \tag{2.22}$$

Both forward and reverse Early effect are neglected in I_B, I_C and Q_{tot}.

$$Y_{21} = \frac{I_C}{V_T} - j\omega\alpha_{CP}C_{tot}. \tag{2.23}$$

$S_{i_b,i_b^*} = 4KT\Re(Y_{11}) - 2qI_B$ with neglecting Early effect in I_B and exponential $I_B - V_{BE}$ relation. $\Re(Y_{11}) = \frac{dI_B}{dV_{BE}} = \frac{I_B}{V_T} = \frac{qI_B}{KT}$, which is alway giving frequency independent $S_{i_b,i_b^*} = 2qI_B$. $Y_{21} = \frac{dI_C}{dV_{BE}} - j\omega\alpha_{cp}C_{tot} = \frac{I_C}{V_T} - j\omega\alpha_{cp}C_{tot} = \frac{qI_C}{KT} - j\omega\alpha_{cp}C_{tot}$ gives

$$S_{i_c,i_b^*} = 2KTY_{21}^* - 2qI_C = j\omega\alpha_{cp}C_{tot} \cdot 2KT = j\omega\alpha_{cp}2qV_TC_{tot} \cdot . \tag{2.24}$$

Again $C_{tot} = \frac{dQ_{tot}}{dV_{BE}}$ and $Q_{tot} = Q_{tot,s}\exp\left(\frac{V_{BE}}{V_T}\right)$, so $C_{tot}V_T = Q_{tot}$ and $S_{i_c,i_b^*} = j\omega\alpha_{cp}Q_{tot}$ If normalized correlation $C = S_{i_c,i_b^*} / \sqrt{S_{i_c,i_c^*}S_{i_,i_b^*}}$ is calculated, one may find that $|C| > 1$ beyond some frequency point. For purpose of mathematical consistent in the model implementation, an extra term $2q(\omega\alpha_{cp}Q_{tot})^2/I_C$ is added to S_{i_b,i_b^*}. This extra term does not have a physical basis in this model, but we will show in the later section that "the extra term" becomes important at higher frequency and is essentially the key to improve the Mextram model fitting results. Again, Mextram noise model does not attempt to include CB SCR effect. In reality, Q_{tot} has all charges and α_{cp} is the equivalent to the ratio factor of τ_c / τ_f. Therefore Mextram model is equivalent to CB SCR alone model detailed in Section 2.4.1, but physical basis is wrong.

2.3.2 Noise compact model of HICUM group

The PSDs of base and collector of HICUM model are

$$S_{i_b,i_b^*} = 2qI_B\left[1 + 2\alpha_{qf}B_f\left(\omega\tau_f\right)^2\right], \tag{2.25}$$

$$S_{i_c,i_c^*} = 2qI_C, \tag{2.26}$$

$$S_{i_c,i_b^*} = -2qI_Cj\omega\tau_f\alpha_{it}. \tag{2.27}$$

τ_f is transit time, α_{qf} and α_{it} are the ratio of the minority charge and transfer current time delay with respect to the transit time. The model implementation is based on system theory of transfer of the noise signal in the linear network. The correlation is realized in the compact model using uncorrelated noise sources and dummy sources.

In this HICUM solution, a frequency dependent $\Re(Y_{11})$ is produced by adding non-quasi-static effect. That, however, has little effect on the overall transistor Y-parameters, as such frequency dependence is masked by the extra delays caused by parasitics, and is nearly impossible to extract from measured Y-parameters. In this model, the inherent correlation of base and collector current noise is still derived from noise transport in the neutral base.

2.3.3 Noise transit time modeling approach

Another recently reported approach is to develop an approximate compact model implementation of the noise transit time model [32], a small signal model that previously showed good results in some HBTs [17] [16] [33] [15].

The "noise transit time" τ_c in the original small signal models of [17] and [16] had a vague physical meaning, but was later found to be close to but not identical to the collector transit time τ_c in 2-D microscopic noise simulation of a SiGe HBT [33]. This is not a coincidence, and is instead due to the similarity between the "noise transit" concept and physical process of correlated noise generation induced by collector-base space charge region (CB SCR) transport [26] [25] [15] [34]. The PSDs are

$$S_{i_b,i_b^*} = 2q\left(I_b + |-e^{j\omega\tau}|^2 I_C\right), \tag{2.28}$$

$$S_{i_c,i_c^*} = 2qI_C, \tag{2.29}$$

$$S_{i_c,i_b^*} = 2qI_C\left(e^{j\omega\tau} - 1\right). \tag{2.30}$$

The compact model implementation of the noise transit time model in [32] has several problems. It relies on a specific large signal equivalent circuit formulation, and cannot be applied generally to an existing large signal compact model. In addition, the noise transit time, which

is responsible for generating noise correlation and frequency dependence, is set by a transcapacitance, and thus will affect both transistor y-parameters and noise parameters. This is undesired from a general compact modeling standpoint, as one typically would like to have the ability to separately adjust noise transit time to fit noise parameters without affecting y-parameters.

2.3.4 New method with RC delayed noise current

A new approach to implementing correlated terminal noises by placing an RC delayed noise current between the base and collector nodes has been recently developed [35]. The frequency dependence of the intrinsic noise sources due to the CB SCR transport effect has been modeled with an accuracy value up to the second order of ω. Another advantage of this model is its capability of implementing both the real and imaginary part of correlation. Overall, it gives the best fit to measurement data compared with the CB SCR model and SPICE model. A major drawback of this model is less flexibility for traditional transistor whose noise transport is still dominated by base transit time instead of CB SCR transit time.

2.4 Noise source model

Based on analysis of prior works detailed above, we would like to avoid all the unphysical results from trying to implement the van Vliet model in a large signal compact transistor model using the simplified intrinsic y-parameters available in the compact model. It is also clear that we need to account for the CB SCR transport effect and eventually keep the general applicability for those transistor less dominated by τ_c .

Fig. 2.4 illustrates the proposed model for including both minority carrier velocity fluctuation induced terminal current noises and additional noises from the CB SCR transport effect. i_{b0} is the base current noise resulting from velocity fluctuation of minority holes in the emitter. i_{b0} has a PSD of $2qI_B$ at low frequency. Velocity fluctuations of base minority electrons produce a base current noise i_{b1}, and an electron current noise at the end of the neutral base, i_{c1}. i_{b1} and i_{c1} are correlated as they both result from base electron velocity fluctuations. Here b_i, c_i, and e_i are the intrinsic base, collector and emitter nodes in the "parent" compact models, i.e., HICUM, Mextram,

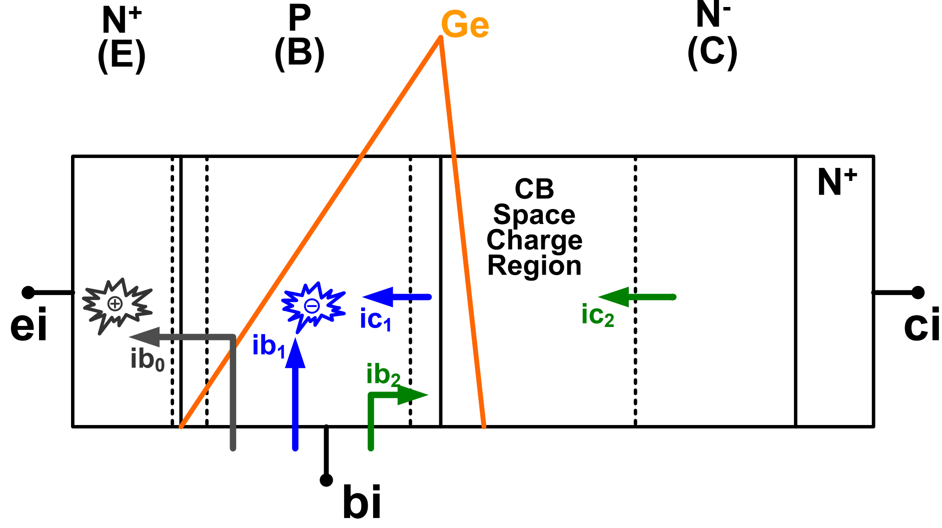

Figure 2.4: Illustration the terminal noise currents. i_{b0} is from emitter hole velocity fluctuation. i_{b1} and i_{c1} are from base electron velocity fluctuation. i_{c1} becomes i_{c2} through CB SCR transport, which also produces i_{b2} .

or VBIC [36]. Table. 2.1 summarize the specific models related to different noise currents. "Shot" like model, which is implemented in the standard SPICE simulators, takes frequency independent and uncorrelated noise sources i_{b0} and i_{c1} only into account. Intrinsic base model includes i_{b0}, i_{b1} and i_{c1}. Correlation comes from i_{b1} and i_{c1}. The research version of Mextram and HICUM models are good examples of noise compact model employing intrinsic base transport effect. CB SCR model considers the CB SCR transport effect besides the "Shot" like noise sources, therefore i_{c1} is "modified" by CB SCR region and becomes i_{c2} at the exit of CB SCR. Noise correlation comes from i_{c2} and the induced i_{b2}. The "consolidated" model includes the noise transport in both intrinsic base region and CB SCR. Base and collector noise current correlation comes from i_{c2} and the sum of i_{b1} and i_{b2}. Note that i_{b1} and i_{b2} are also correlated.

We bring forward and show the calculation results of different PSDs normalized by $2qI_C$ based on a 36 GHz SiGe HBTs in Fig. 2.5. The model equations used will be developed and fully detailed in the following Section 2.4.1 and Section 2.4.2. Device has $A_E = 0.8 \times 20\mu m^2$

Table 2.1: Noise currents of different mechanisms

Effect	i_b	i_c	Correlation
"Shot" like	i_{b0}	i_{c1}	None
Intrinsic Base	i_{b0}, i_{b1}	i_{c1}	$i_{b1}i_{c1}$
CB SCR	i_{b0}, i_{b2}	i_{c2}	$i_{b2}i_{c2}$
Intrinsic Base+CB SCR	i_{b0}, i_{b1}, i_{b2}	i_{c2}	$(i_{b1} + i_{b2})\, i_{c2}$

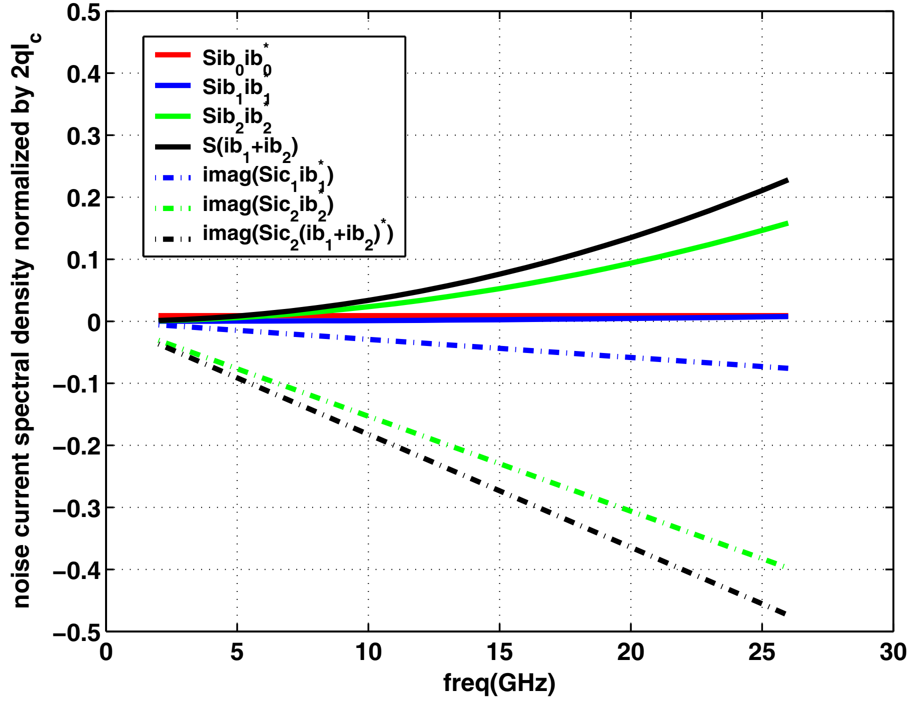

Figure 2.5: Calculated noise current spectral density normalized by $2qI_C$ vs frequency. $A_E = 0.8 \times 20\mu m^2$. $I_C = 3.55$ mA. $f_T = 15$ GHz. τ_c is set to $0.7\tau_f$, τ_b is set to $0.2\tau_f$ and $\eta = 3$.

and is biased at $I_C = 3.55$ mA with $f_T = 15$ GHz. τ_c is set to $0.7\tau_f$, τ_b is set to $0.2\tau_f$ and $\eta = 3$. Intuitively, the base noise current contribution for this device is less than the collector noise current and their correlation. Also, $S_{i_b i_b^*}$ is dominated by the contribution of $S_{i_{b_2} i_{b_2}^*}$. The imaginary part of$S_{i_{c_2} i_{b_{12}}^*}$ is dominated by the imaginary part of $S_{i_{c_2} i_{b_2}^*}$. CB SCR transport effect is more important than the noise transport in the neutral base. Fig. 2.6 shows that the real part of correlation is much smaller than the imaginary part.

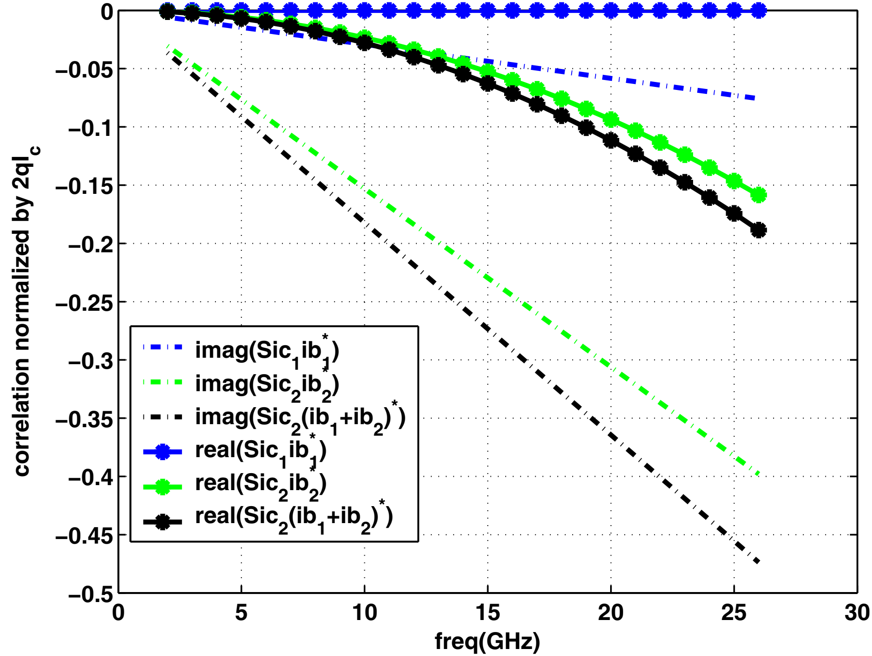

Figure 2.6: Calculated correlation normalized by $2qI_C$ vs frequency. $A_E = 0.8 \times 20\mu m^2$. $I_C = 3.55$ mA. $f_T = 15$ GHz. τ_c is set to $0.7\tau_f$, τ_b is set to $0.2\tau_f$ and $\eta = 3$.

2.4.1 Consider CB SCR transit time alone

With scaling and the introduction of graded SiGe HBTs, neutral base transit time has been decreasing constantly. In the same time, the collector-base junction space charge region (CB SCR) transit time does not decrease as much and becomes significant, which was not accounted for by the noise and Y-parameter expressions of van Vliet's. Recently, we have reexamined the microscopic noise transport in modern SiGe HBTs using van Vliet's approach, and extended that work by including the CB SCR transport effect [25] [26]. The resulting model, like van Vliet's, requires the use of strictly physically self consistent description of the frequency dependent y-parameters, and cannot be implemented in compact models required for IC design.

For now, we "neglect" the frequency dependence and correlation of noises resulting from base electrons, and include only the CB SCR transport effect. This at first was based on the consideration that the base cutoff frequency $1/2\pi\tau_b$ is much higher than f_T of modern device, and thus for typical RF applications operating below 20 GHz, the “low” frequency approximation should hold for van

Vliet's model, at least at low injection, , as i_{b1} is least important compared in i_{b0}, i_{b1} and i_{b2}. Both i_{b1} and i_{b0} are much less important than i_{b2} for the modern device. As shown below, this allows considerable simplification, and yields a set of noise equations suitable for all existing compact models with only a single CB SCR transit time parameter τ_c. In other words, any deviation of the base and collector current noises from the traditional independent shot noise model is a result of CB SCR electron transport effect, rather than frequency dependent base electron noise generation described by the van Vliet model.

Model Derivation and Description

First, let us consider the base and collector noise currents without CB SCR effect. One might understand them either from the viewpoint of shot noise producing passage of majority carriers through emitter-base junction potential barrier or the viewpoint of microscopic minority carrier velocity fluctuation and transport, which produce the traditional description:

$$S_{i_{b0}i_{b0}^*} = \langle i_{b1} i_{b1}^* \rangle / \triangle f = 2qI_B, \tag{2.31}$$

$$S_{i_{c1}i_{c1}^*} = \langle i_{c1} i_{c1}^* \rangle / \triangle f = 2qI_C, \tag{2.32}$$

$$S_{i_{c1}i_{b0}^*} = 0. \tag{2.33}$$

i_{b0} is the base noise current associated with hole injection into emitter (or emitter hole velocity fluctuation in microscopic view), and i_{c1} is the collector noise current associated with electron injection into base (or base electron velocity fluctuation). Due to the "low" frequency approximation we make, they are both frequency independent, and uncorrelated.

Transport of the i_{c1} noise current across the CB SCR induces an extra base current noise i_{b2}, which can be calculated from the difference between electron noise current at the exit of CB SCR, i_{c2}, and i_{c1}, as illustrated in Fig. 2.4. Following [37],

$$i_{c2} = i_{c1} \frac{1 - \exp(-2j\omega\tau_c)}{2j\omega\tau_c}. \tag{2.34}$$

where $\tau_c = W_c/(2v_{sat})$, the collector transit time.

To obtain expressions suitable for compact modeling, we then assume $\tau_c\omega \ll 1$, which is satisfied for typical applications. The exponential term in (2.34) can then be approximated with a Taylor series of order 2:

$$e^x \approx 1 + x + \frac{1}{2}x^2, \tag{2.35}$$

(2.34) can then be rewritten as

$$i_{c_2} \approx i_{c_1}(1 - j\omega\tau_c). \tag{2.36}$$

We then have

$$S_{i_{c_2}i_{c_2}{}^*} \approx 2qI_C(1 + (\omega\tau_c)^2) \approx 2qI_C. \tag{2.37}$$

i_{b2} then becomes

$$i_{b_2} = i_{c_1} - i_{c_2} = i_{c_1}(j\omega\tau_c), \tag{2.38}$$

and

$$S_{i_{b_2}i_{b_2}{}^*} = 2qI_C\omega^2{\tau_c}^2. \tag{2.39}$$

The correlation term is

$$S_{i_{c_2}i_{b_2}{}^*} = -j2qI_C\omega\tau_c. \tag{2.40}$$

We have neglected the real part of the correlation as it is proportional to $(\omega\tau_c)^2$, a second order term. The normalized correlation $C = S_{ic_2ib_2{}^*}/\sqrt{S_{ib_2ib_2{}^*}S_{ic_2ic_2{}^*}}$ is then negative imaginary unity, which allows a straightforward implementation into compact models.

Compact Modeling Implementation

Conventional noise computation implemented in all simulators are only able to handle uncorrelated noise sources. Therefore we need to implement the correlations from uncorrelated sources. Our implementation is similar to that of MOSFET correlated drain and gate noises in MOSFET recently presented in [38]. Instead of expressing everything in terms of the normalized correlation [38], here we directly implement the correlation between i_{b2} and i_{c2}. The equivalent circuit is

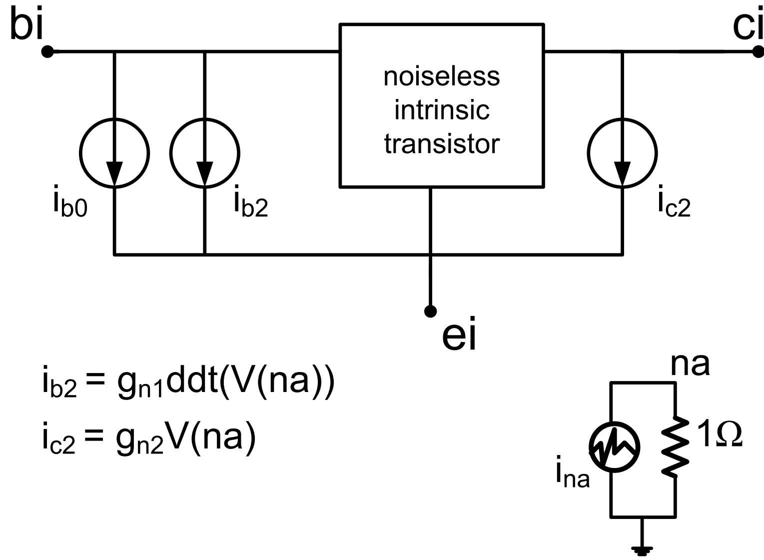

Figure 2.7: Equivalent circuit of proposed compact noise modeling implementation.

shown in Fig. 2.7. Note that i_{b0} is uncorrelated with i_{b2} and i_{c2}, and we no longer need i_{c1} in the equivalent circuit.

To generate the correlation between i_{b2} and i_{c2}, we make both current sources controlled by the voltage of the same dummy node, *na*. The dummy node is connected to ground by a 1Ω noise free resistor. A unity noise source current i_{na} is placed in parallel to the resistor to produce the dummy noise voltage.

i_{b2} and i_{c2} are generated from $V(na)$ as follows

$$i_{b2} = g_{n1}ddt(V(na)), \tag{2.41}$$

$$i_{c2} = g_{n2}V(na), \tag{2.42}$$

```
electrical  na;
branch(na)  b_na;
twoq = 2.0*'P_Q;
SIC2 = twoq*IC2;
SIB1 = twoq*IB1;
I(b_na)  <+  white_noise(1);
I(b_na)  <+  V(b_na);
gn1 = sqrt( SIC2)*Tc;
gn2 = sqrt(SIC2);
I(b,e) <+ white_noise(SIB1, "shot") + gn1*ddt(V(b_na));
I(c,e) <+ gn2*(V(b_na));
```

Figure 2.8: Verilog-A sample code of proposed noise model.

where g_{n1} and g_{n2} are coefficients that can be determined to reproduce (2.39), (2.37) and (2.40). The results are

$$g_{n1} = \sqrt{2qI_C}\tau_c, \tag{2.43}$$

$$g_{n2} = \sqrt{2qI_C}. \tag{2.44}$$

In frequency domain, the ddt operator becomes $j\omega$.

$$S_{i_{b_2}i_{b_2}^*} = (g_{n1}\omega)^2 \cdot S_{V_{na}} = 2qI_C\omega^2{\tau_c}^2, \tag{2.45}$$

$$S_{i_{c_2}i_{c_2}^*} = {g_{n2}}^2 \cdot S_{V_{na}} = 2qI_C, \tag{2.46}$$

$$S_{i_{c_2}i_{b_2}^*} = g_{n2} \cdot (-j\omega g_{n1}) = -j2qI_C\omega\tau_c. \tag{2.47}$$

This reproduces (2.39), (2.37) and (2.40). Fig. 2.8 shows a sample Verilog-A code.

The next question is how to determine τ_c. In typical compact models, the total transit time τ_f as a function of biasing current and voltage is available. Here we assume that τ_c is proportional to τ_f, $\tau_c = f_{g1}\tau_f$, with f_{g1} being a proportionality constant determined from fitting noise parameter versus frequency data. Strictly speaking, one should separately model τ_c, preferably from fitting noise data, which will necessitate additional model development.

Experimental Results

The proposed noise model is implemented using Verilog-A, and compared with noise measurements on a SiGe HBT technology optimized for wireless power applications [39]. A 0.8×20×3 μm^2 standard device with a 36 GHz peak f_T was measured. The HICUM model is used here, while the model can be implemented with any other compact models. Model parameters are extracted using standard procedures, including DC and Y-parameter fitting. Base resistance related model parameters (R_{bx} and R_{bi0}) need to be finely tuned against R_n at low frequency. Noise model parameter f_{g1} is extracted during optimization of noise parameter fitting at high frequency.

At RF, in addition to the transistor terminal current noise, there is terminal resistance thermal noise. To examine their relevant importance, we also run simulations with only resistance thermal noise turned on. Fig. 3.11 shows minimum noise figure NF_{min}, noise resistance R_n, real part of optimum generator admittance $\Re(Y_{opt})$, and imaginary part $\Im(Y_{opt})$ as a function of frequency. V_{CE}=3.3 V and I_C=3.55 mA. The traditional independent shot noise model, denoted as "SPICE noise model", is compared with the proposed model. In both models, the terminal resistance thermal noise is included.

For NF_{min}, the resistance noise contribution is negligibly small. However, it is a significant contributor to noise resistance R_n, primarily from the base resistances. Its impact on Y_{opt} is much smaller than the base and collector current noises.

NF_{min} increases monotonically with frequency, as expected, and R_n is almost independent of frequency. Compared with the traditional model, the new model significantly improves the overall noise parameter modeling accuracy for all of the four noise parameters. This also indicates the importance of CB SCR transit time effect on noise parameters. An exception is $\Im(Y_{opt})$, which is slightly worse. The extracted value of f_{g1} is 0.757, which indicates that τ_c dominates τ_f in this technology, which is also expected given the collector design for high breakdown voltage.

Using the same set of model parameters, noise parameters are simulated as a function of I_C at 5 and 10 GHz. V_{CE}=3.3 V. The results are shown in Fig. 2.10 and Fig. 4.17 for 5 and 10 GHz, respectively. The cutoff frequency f_T vs I_C is added in Fig. 2.10, and peak f_T happens when I_C

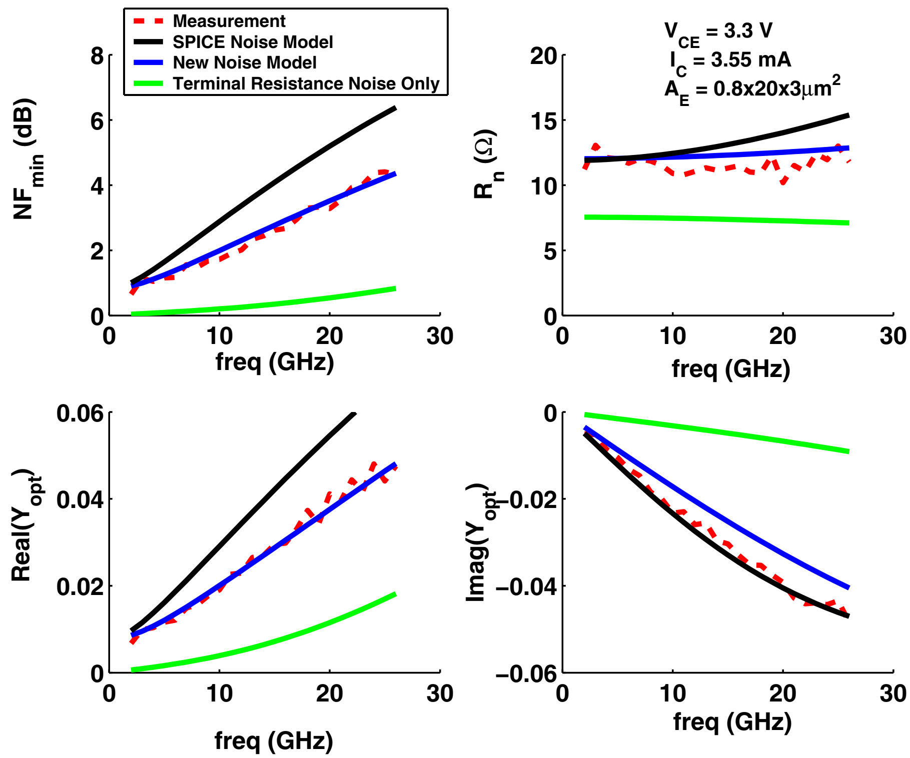

Figure 2.9: Comparison of measured and simulated noise parameters vs frequency.

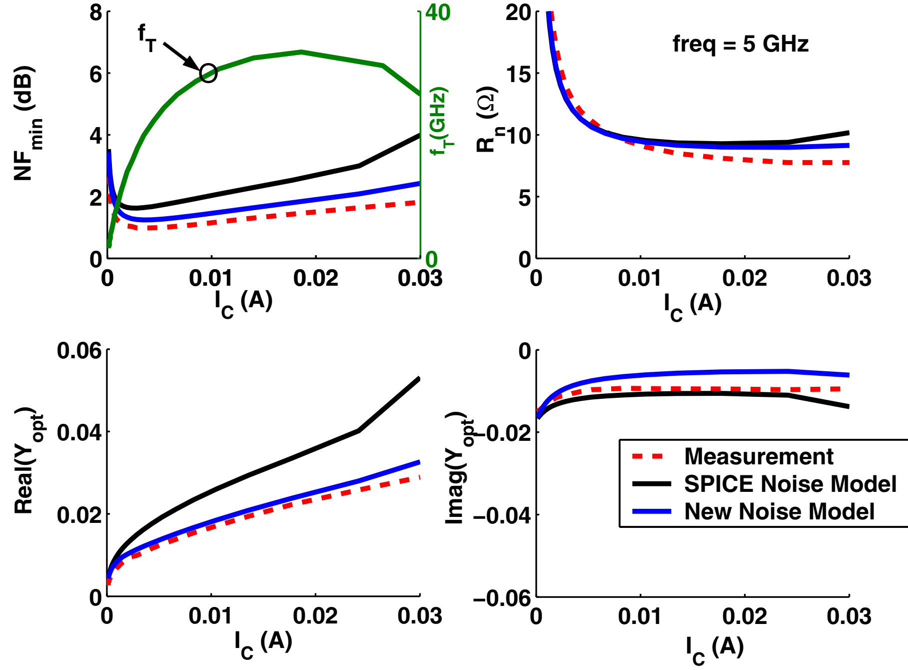

Figure 2.10: Comparison of measured and simulated noise parameters vs I_C at 5 GHz.

= 0.020 A. The f_{g1} determined from low injection is used as is for all biases. The discrepancy between model and data becomes larger at higher injection. This could be caused by the deviation of $S^*_{i_{c1}i_{c1}}$ from $2qI_C$ at high injection and/or the change of f_{g1}.

2.4.2 Intrinsic Base and CB SCR

Solving the microscopic transport equation in intrinsic base will obtain the current noise related to intrinsic Y-parameters [23]

$$S_{i_{b_1}i_{b_1}{}^*} = 4kT\,Re\,\{Y_{11,i}\}\,, \tag{2.48}$$

$$S_{i_{c_1}i_{c_1}{}^*} = 2qI_C + 4kT\,Re\,\{Y_{22,i}\} \approx 2qI_C, \tag{2.49}$$

$$S_{i_{c_1}i_{b_1}{}^*} = 2kT\,(Y_{21,i} + Y_{12,i} - g_m)\,. \tag{2.50}$$

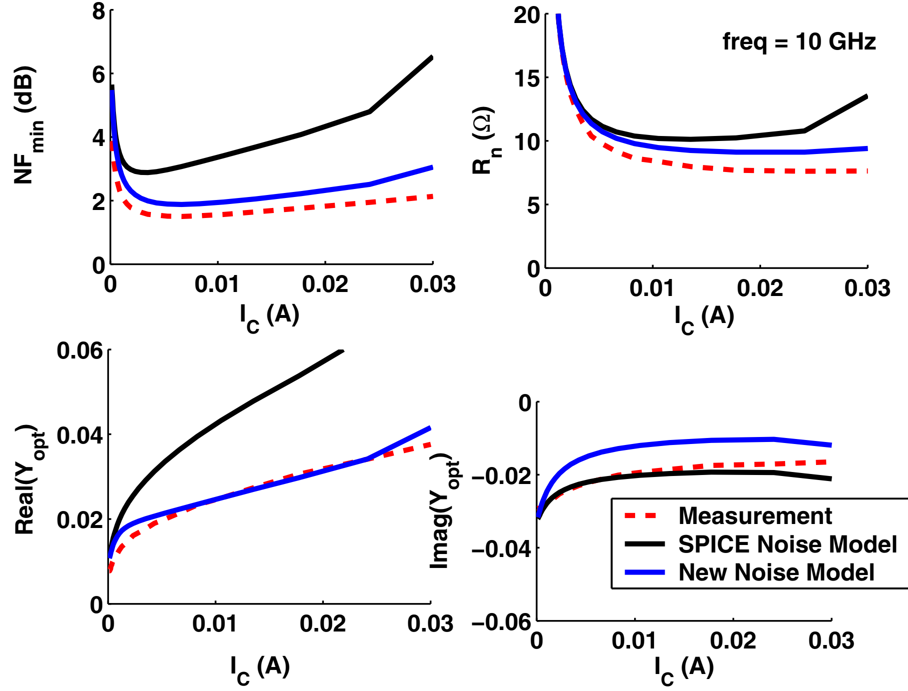

Figure 2.11: Comparison of measured and simulated noise parameters vs I_C at 10 GHz.

Approximation to first and second order expansion of Y-parameters under constant doping and uniform bandgap in base region in frequency domain will get

$$S_{i_{b_1} i_{b_1}{}^*} = 2qI_C \frac{1}{3} (\omega\tau_b)^2 , \tag{2.51}$$

$$S_{i_{c_1} i_{b_1}{}^*} = -j2qI_C \frac{1}{3} \omega\tau_b . \tag{2.52}$$

The expressions are easy for compact modeling implementation.

For SiGe HBTs, Ge ramp induces electric field and (2.51) and (2.52) will have to be modified by η, which is a measure for the electric field. For the constant doping and electrical field, η =

$\triangle E_g / V_T$ [24], and $\triangle E_g$ is the bandgap difference across the neutral base,

$$S_{i_{b_1} i_{b_1}^*} = 2qI_C \alpha_n (\omega \tau_b)^2 , \tag{2.53}$$

$$S_{i_{c_1} i_{c_1}^*} = 2qI_C, \tag{2.54}$$

$$S_{i_{c_1} i_{b_1}^*} = -j2qI_C \beta_n \omega \tau_b. \tag{2.55}$$

$$\alpha_n = 2A \tag{2.56}$$

$$\beta_n = A + B \tag{2.57}$$

$$A = \frac{3\eta^2}{2(\eta - 1 + \exp(-\eta))^2} - \frac{\eta + 3}{\eta - 1 + \exp(-\eta)} \tag{2.58}$$

$$B = \frac{\eta \coth\left(\frac{1}{2}\eta\right) + 1 + \eta}{\eta - 1 + \exp(-\eta)} - \frac{3\eta^2}{2(\eta - 1 + \exp(-\eta))^2} \tag{2.59}$$

We already have $S_{i_{c_2} i_{c_2}^*}$ (2.37) and we find $S_{i_{b_{12}} i_{b_{12}}^*}$ and $S_{i_{c_2} i_{b_{12}}^*}$:

$$S_{i_{b_{12}} i_{b_{12}}^*} = 2qI_C \left[\alpha_n (\omega \tau_b)^2 + (\omega \tau_c)^2\right] + 2qI_C \left(2\beta_n \omega^2 \tau_b \tau_c\right) \tag{2.60}$$

$$S_{i_{c_2} i_{b_{12}}^*} = -j2qI_C \omega (\tau_c + \beta_n \tau_b) - 2qI_C \omega^2 \tau_c \left(\frac{1}{3}\tau_c + \beta_n \tau_b\right) \tag{2.61}$$

Note that i_{b1} and i_{b2} are correlated by the minority carrier transport in the base region , so we denote $i_{b_{12}} = i_{b_1} + i_{b_2}$.

This model is well physics based and can cover:

1. Classic devices have τ_b effect only and $\eta = 0$ with uniform base doping. This is van Vliet model.

2. Classic devices have τ_b effect only and $\eta > 0$.

3. Devices have CB SCR effect only, i.e. τ_c only.

4. Devices have both intrinsic base and CB SCR effect. $\tau_b > 0$ and $\tau_c > 0$.

Fig. 2.13 shows model calculation results of (2.37) (2.60) and (2.61)with different τ_b, τ_c and η combinations. $I_C = 3.55$ mA, $I_B = 32\mu$A. $f_T = 1 / (2\pi (\tau_b + \tau_c))$. $\tau_F = 3$ ps.

1. $\tau_b = \tau_F$, $\tau_c = 0$ and $\eta = 0$.

2. $\tau_b = \tau_F$, $\tau_c = 0$ and $\eta = 4$.

3. $\tau_b = 0$, $\tau_c = \tau_F$ and $\eta = 0$.

4. $\tau_b = \tau_c = 0.5\tau_F$ and $\eta = 0$.

5. $\tau_b = \tau_c = 0.5\tau_F$ and $\eta = 4$.

$S_{i_c}i_c^*$ does not change. $\eta = 4$ leads to a stronger frequency dependence of $S_{i_b}i_b^*$ and $S_{i_c}i_b^*$. τ_c impact $S_{i_b}i_b^*$ and $S_{i_c}i_b^*$ more effectively than τ_b.

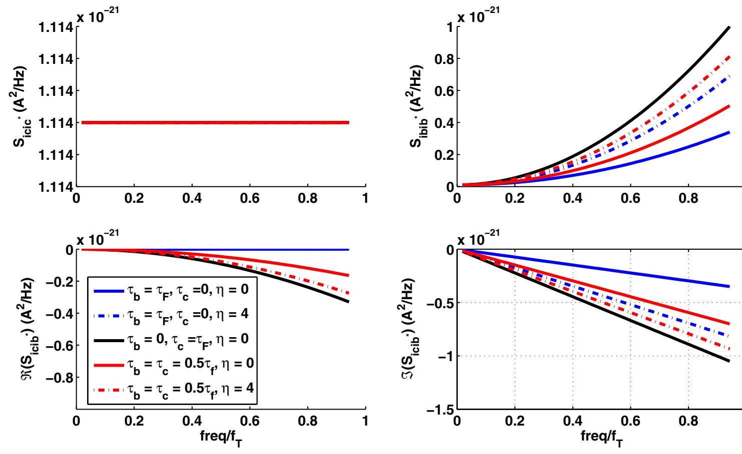

Figure 2.12: Calculation results of PSDs of intrinsic i_c, i_b and their correlation with different τ_b, τ_c and η combinations.

Fig. 2.13 shows normalized correlation results.

1. $\tau_b = \tau_F$, $\tau_c = 0$ and $\eta = 0$ leads to normalized correlation to the classical van Vliet model's value, $C = -j\ /\sqrt{3}$

2. $\eta = 4$ increases normalized correlation for both cases $\tau_{=}0$ and $\tau_c = 0.5\tau_F$.

3. $\tau_c = \tau_F$, $\tau_b = 0$ and $\eta = 0$ leads to normalized correlation around 1.

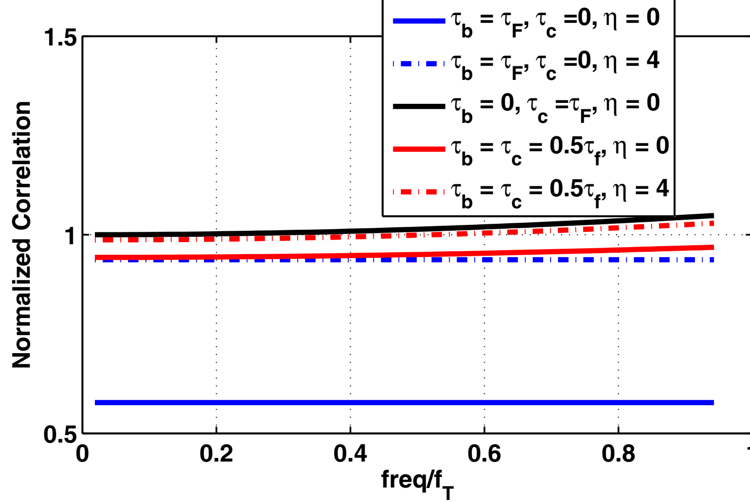

Figure 2.13: Normalized correlation with different τ_b, τ_c and η combinations.

2.4.3 General Compact Modeling Implementation

Next task is to generate the correlated i_{b12} and i_{c2} noises from uncorrelated white noise sources.

A close inspection of (2.37), (2.60) and (2.61) shows that:

1. $S_{i_{c_2} i_{c_2}^*}$ is dominated by a constant $2qI_C$ term, so long as $\omega^2\tau_c^2 \ll 1$, typically true. The negative sign of the second term is difficult to produce without involving additional low-pass filtering of basic white noise sources. From a modeling standpoint, if we "change" the second term to a positive number still proportional to $\omega^2\tau_c^2$, it can be then produced in Verilog-A with a *ddt* function. As long as the coefficient is small, which is the case in the proposed implementation below, it has negligible effect on final result. This is indeed verified to be the case. Having a *ddt* term in i_{c_2} helps generating a real part of the correlation that is proportional to ω^2.

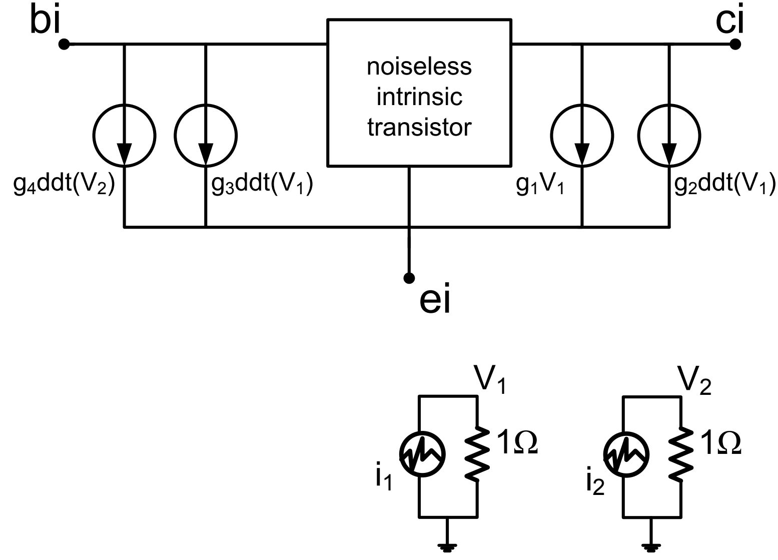

Figure 2.14: Equivalent circuit for Verilog-A implementation of the completely physics based version of the proposed model.

One way to model i_{c_2} is to use a unity voltage v_1 source as illustrated in Fig. 2.14. *ddt* becomes $j\omega$ in noise analysis:

$$i_{c_2} = g_1 v_1 + g_2 j\omega v_1, \tag{2.62}$$

$$S_{i_{c_2} i_{c_2}^*} = g_1^2 + g_2^2 \omega^2, \tag{2.63}$$

g_1 is then set to $\sqrt{2qI_C}$.

2. $\Re\left(S_{i_{c_2} i_{b_{12}}^*}\right) \propto \omega^2$, while $\Im\left(S_{i_{c_2} i_{b_{12}}^*}\right) \propto \omega$. This can be achieved if we have a $g_3 j\omega v_1$ term in $i_{b_{12}}$ to create the correlation:

$$i_{b_{12}} = g_3 j\omega v_1 + g_4 j\omega v_2, \tag{2.64}$$

where the other term, $g_4 v_2$, generates the part of $i_{b_{12}}$ uncorrelated with i_{c_2}, from v_2, another unity voltage noise source uncorrelated with v_1. We then have:

$$\Im\left(S_{i_{c_2} i^*_{b_{12}}}\right) = -g_1 g_3 \omega. \tag{2.65}$$

$$\Re\left(S_{i_{c_2} i^*_{b_{12}}}\right) = g_2 g_3 \omega^2, \tag{2.66}$$

$$S_{i_{b_{12}} i^*_{b_{12}}} = g_3^2 \omega^2 + g_4 \omega^2, \tag{2.67}$$

3. We can therefore determine g_3 from $\Im\left(S_{i_{c_2} i^*_{b_{12}}}\right)$ and previously determined g_1 according to (2.65).

4. We then determine g_2 from $\Re\left(S_{i_{c_2} i^*_{b_{12}}}\right)$ and previously determined g_3 according to (2.66).

5. We accept the g_2 determined above so long as $g_2^2\omega^2 \ll g_1^2$, that is, $g_2^2\omega^2 \ll 2qI_C$. This indeed turns out to be the case. Even in the extreme case of CB SCR effect dominating, the final $g_2^2\omega^2$ is $2qI_C \times \omega^2\tau_c^2/9$, which is a better approximation of $S_{i_{c2} i^*_{c2}}$ than previous compact model implementations. For instance, in [32], the approximation is $2qI_C(1 + \omega^2\tau_c^2)$.

6. We then determine g_4 from $S_{i_{b_{12}} i^*_{b_{12}}}$ and previously determined g_3.

Overall we have now completely reproduced $S_{i_{c_2} i^*_{c_2}}$, $S_{i_{b_{12}} i^*_{b_{12}}}$, $\Re\left(S_{i_{c_2} i^*_{b_{12}}}\right)$, $\Im\left(S_{i_{c_2} i^*_{b_{12}}}\right)$ using two uncorrelated unity voltage sources, with a negligible small error in $S_{i_{c_2} i^*_{c_2}}$.

The i_{b0} base current noise is uncorrelated with any others, and can be easily added as shot noise between bi and ei.

We are now able to evaluate the relative importance of each noise current by calculating their frequency dependence according the analytical expressions above. We assume τ_c and τ_b are proportional to τ_f here, τ_c and τ_b have different V_{CB} dependence though. f_{g1} and f_{g2} are proportionality constants. $\tau_c = f_{g1}\tau_f$ and $\tau_b = f_{g2}\tau_f$. η is again the Ge induced electric field constant. $\tau_c = 0.7\tau_f$, $\tau_b = 0.2\tau_f$ and $\eta = 3$, which are estimated from the same 36 GHz SiGe HBT having total transit time $\tau_f = 3.48ps$. Note that for different device from different technology and application, the ratios of τ_c/τ_f and τ_b/τ_f should be varied and carefully chosen.

Table 2.2: Noise Model Parameters

Model	f_{g1}	f_{g2}	η
Spice-like	0	0	0
Intrinsic Base	0	0.2	3
CB SCR	0.7	0	0
Intrinsic Base+CB SCR	0.7	0.2	3

We next examine the results of noise parameters. we are able to obtain the different models related to different physics effects from the same piece of Verilog-A code, by turning on or off the three parameter's value, The HICUM model will be used, while the model can be implemented with any other compact models. Four cases corresponding to Table 2.1 are present in Table 2.2. 1) Typical Spice model, $f_{g1} = 0$, $f_{g2} = 0$ and $\eta = 0$; 2) Only intrinsic base effect is considered, $f_{g1} = 0$, $f_{g2} = 0.2$ and $\eta = 3$; 3) Only CB SCR effect is considered,$f_{g1} = 0.7$, $f_{g2} = 0$ and $\eta = 0$; 4) both intrinsic base and CB SCR effect are considered, $f_{g1} = 0.7$, $f_{g2} = 0.2$ and $\eta = 3$. Physics wise, for a given base, varying η changes τ_b's value. However, for modeling, one may use η as an additional parameter to adjust correlation.

All the DC and AC model parameters are extracted using standard procedures. As we know, R_B affect noise characteristics significantly and is extracted from DC characteristics for this case.

Fig. 2.15 shows minimum noise figure NF_{min}, noise resistance R_n, real part of optimum generator admittance $\Re(Y_{opt})$, and imaginary part $\Im(Y_{opt})$ as a function of frequency. V_{CE}=3.3 V and I_C=3.55 mA. Using the same set of model parameters, noise parameters are also simulated as a function of I_C at 5 and 10 GHz. V_{CE}=3.3 V. The results are shown in Fig. 2.16 and Fig. 2.17.

The CB SCR models and the model including both CB SCR and intrinsic base transport effect give similar simulation results and are closer to the measurement data than the first two models which mainly exclude the CB SCR effect. This means that CB SCR dominates the total transit time for this technology and enough to be responsible for the noise modeling. As for other technology, such as a transistor of high performance, the results could be different.

A quick experiment by turning off the CB SCR effect, making $\tau_b = \tau_f$ and $\eta = 3$ against measurement in Fig. 2.18 shows an acceptable fitting results, which is obviously wrong as τ_c

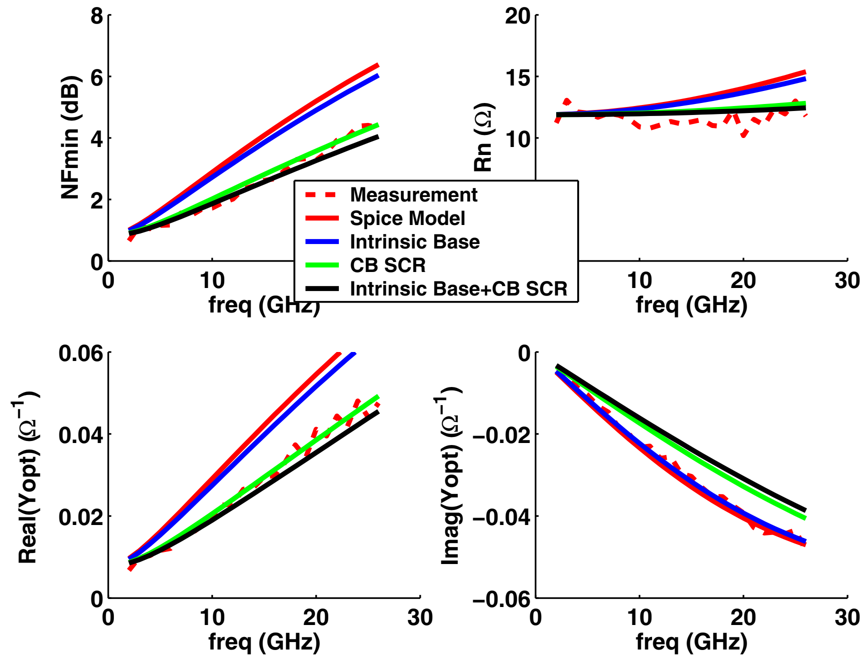

Figure 2.15: Comparison of measured and simulated noise parameters vs frequency.

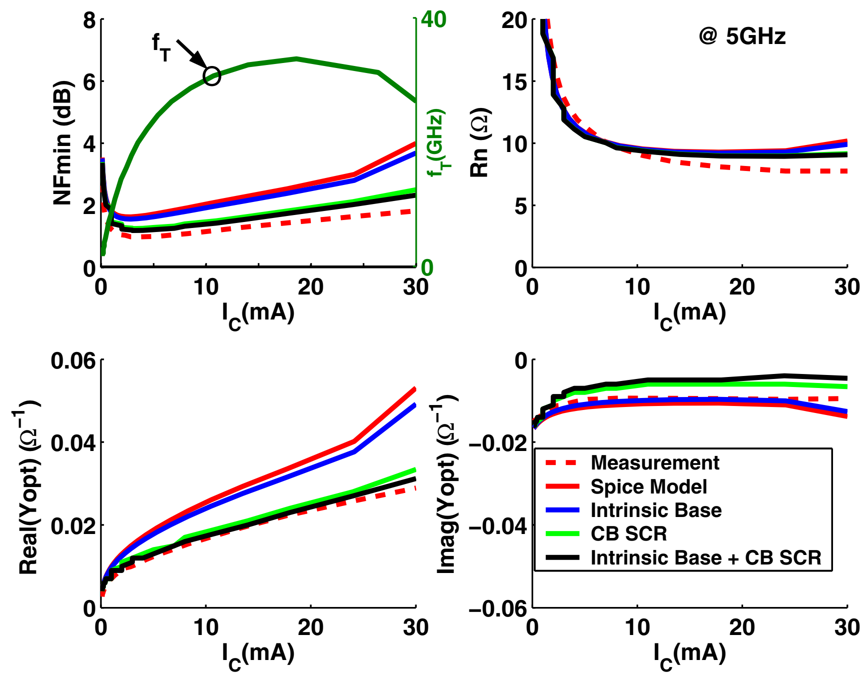

Figure 2.16: Comparison of measured and simulated noise parameters vs I_C at 5 GHz.

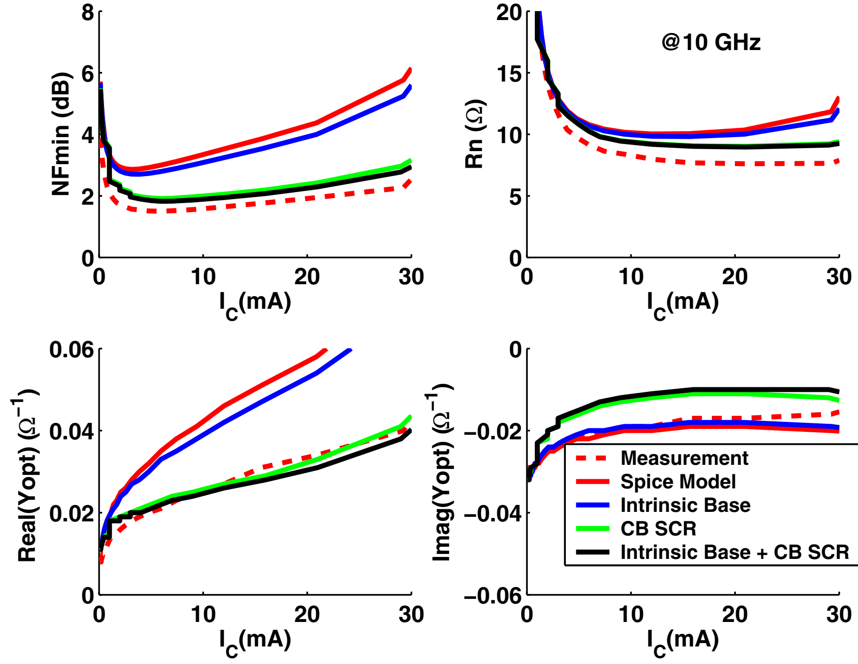

Figure 2.17: Comparison of measured and simulated noise parameters vs I_C at 10 GHz.

dominates τ_f in such power device. Thus the extraction of the noise model parameters f_{g1}, f_{g2} and η cannot totally rely on optimizer which may give multiple unreasonable solutions.

2.5 Conclusion

We have reviewed various noise models and developed a physics-based compact noise model for use with any existing compact transistor model, primarily HICUM, Mextram, and VBIC for SiGe HBTs, corresponding Verilog-A implementation compatible with all major circuit simulators. This model is able to be reduced to all extreme cases and therefore cover both conventional discrete transistors and modern advanced transistors. Comparison with noise measurement on a SiGe HBT technology shows that overall the noise modeling results are much improved.

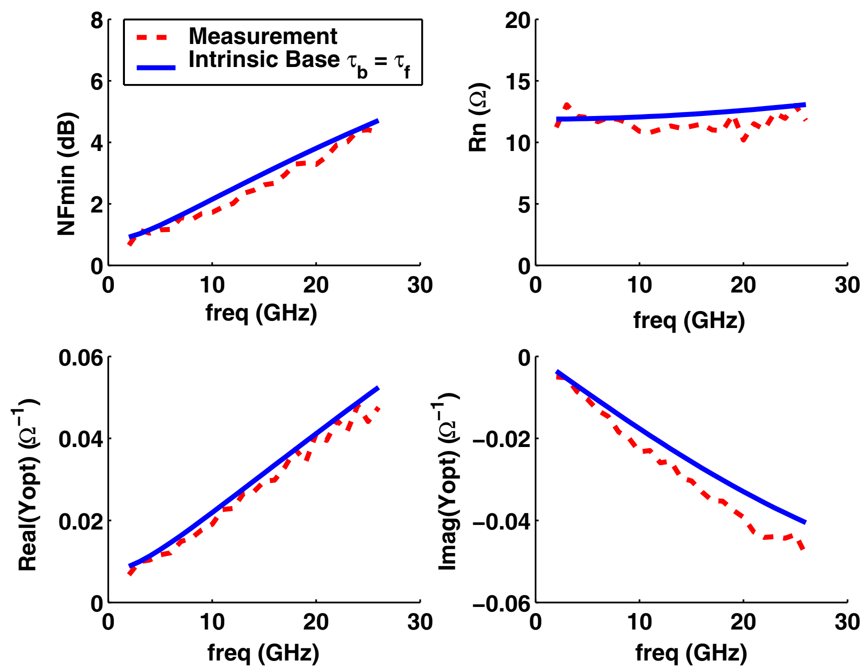

Figure 2.18: Comparison of measurement and simulated noise parameters by making $\tau_b = \tau_f$.

Chapter 3

Compact Model Based Noise Extraction

Of critical importance to developing better models for RF noise in terminal noise currents is to be able to experimentally extract them. There are two kinds of existing extraction methods. One is based on element by element de-embedding of passive parasitics through a series of two-port network operations on a simplified small signal equivalent circuit [40], as shown in Fig. 3.1. Enclosed in the dash box is the intrinsic transistor. Noise sources include thermal noise sources of r_{bi}, r_{bx}, r_e and r_c, and the intrinsic noise sources of terminal current i_b and i_c. The other one is based on a lumped 4-port network modeling of parasitic elements [41][42], as shown in Fig. 3.2. $i_{N,e1}$, $i_{N,e2}$, $i_{N,i1}$ and $i_{N,i2}$ are noise current sources at port 1-4, respectively. $i_{N,int1}$ and $i_{N,int2}$ are the noise current sources of the intrinsic two-port system. The 4-port noise current sources and the correlation matrix can be written as

$$SY_4 = \begin{pmatrix} SY_{n,ee} & SY_{n,ei} \\ SY_{n,ie} & SY_{n,ii} \end{pmatrix} = 4KT Real \begin{pmatrix} Y_{ee} & Y_{ei} \\ Y_{ie} & Y_{ii} \end{pmatrix}. \tag{3.1}$$

Y_{ee}, Y_{ei}, Y_{ie} and Y_{ii} are four 2×2 matrices, which can be obtained from 4-port I-V relations. One can calculate the intrinsic noise correlation matrix as

$$SY_{n,int} = {Y_T}^{-1} \left(SY_{n,total} - SY_{n,ee}\right) Y_T^{*-1} - SY_{n,ii} + {Y_T}^{-1} SY_{n,ei} + SY_{n,ei} Y_T^{*-1}, \tag{3.2}$$

where $Y_T = Y_{ei} \left(Y^{INT} + Y_{ii}\right)^{-1}$. This method requires additional de-embedding structures.

These methods, however, are difficult to implement for extracting noise sources from measured noise parameters and a transistor compact model. Even if one goes through the lengthy process of analytically formulating all of the parasitic elements from linearization of the large signal equivalent circuit, these approaches are highly inefficient and error prone, due to the large

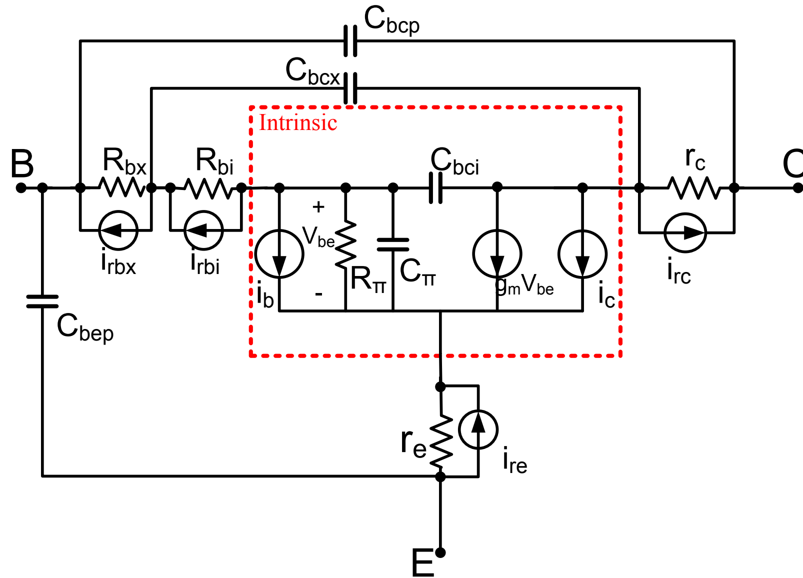

Figure 3.1: Illustration of noise extraction method based on small-signal equivalent circuit.

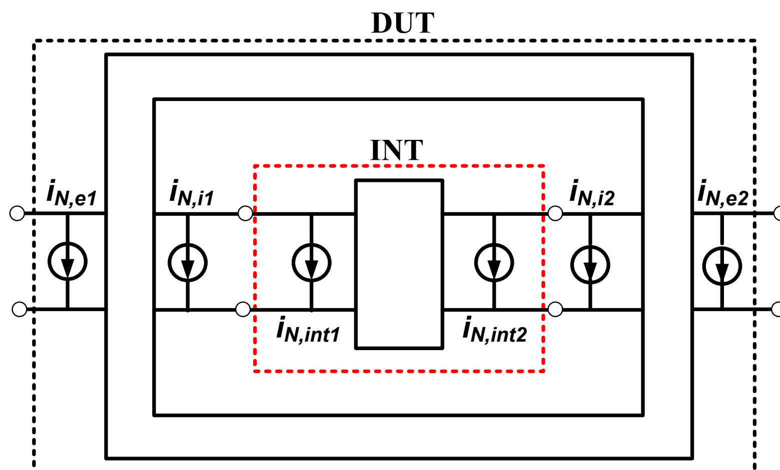

Figure 3.2: Illustration of noise extraction method based on lumped four-port network.

number of circuit elements involved and much more complex small signal elements. These extraction methods cannot possibly handle complex controlled sources, which certainly exists in all compact models, for instance, in the delicate epi-layer models. Furthermore, extraction procedure is model specific due to its analytical nature.

In this chapter, we present a general purpose method of extracting RF noise in SiGe HBT base and collector currents using the very same compact models used for RFIC design. It is shown that the fittings of Y-parameter, noise parameters and the external terminal noise currents are all needed to meaningfully extract base resistances and intrinsic terminal noise currents experimentally.

3.1 Extraction Method

3.1.1 Basic Idea

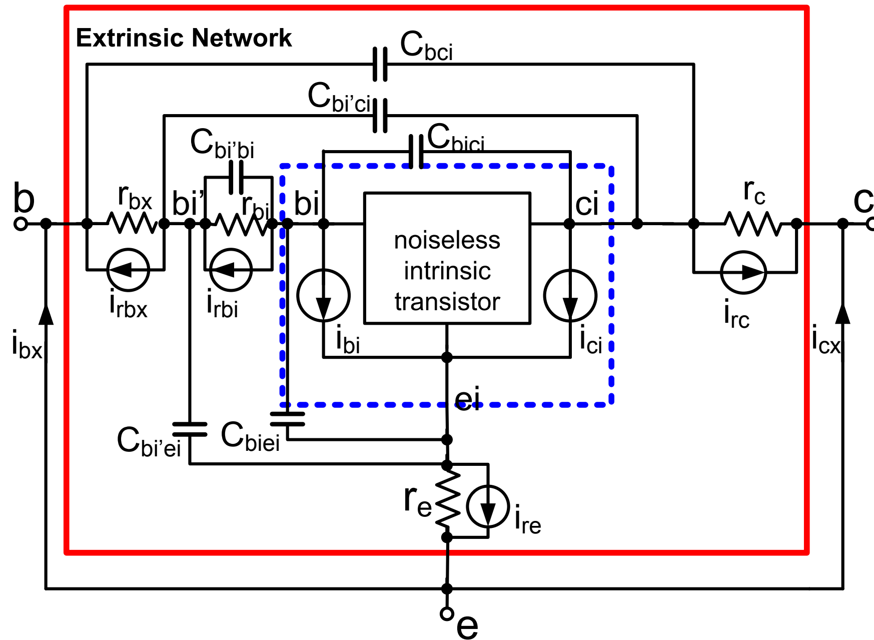

Figure 3.3: Illustration of transfer of internal terminal noise currents i_{bi} and i_{ci}, various resistance thermal noise i_{rk} to external terminal noise currents i_{bx} and i_{cx} with ac shorted base-emitter and collector-emitter voltages.

Our basic idea is to utilize ac small signal analysis in circuit simulation to find out the response currents under short circuit boundary conditions placed at the external transistor terminals when

we place an ac current excitation at all noise sources, including the intrinsic base and collector terminals and the terminals across each resistance, as illustrated in Fig. 3.3.

1. i_{ci} and i_{bi} are the intrinsic terminal noise currents. The positive directions are from ci to ei and bi to ei.

2. i_{cx} and i_{bx} are the response noise currents, which are the equivalent input and output noise currents using admittance representation for the whole transistor [43] [7]. The positive directions are from e to c and from e to b. Short circuit are imposed at two ports.

3. each resistor r_k has a thermal noise current excitation i_{rk} , $S_{i_{rk}i^*_{rk}} = 4kT/r_k$ with $k = bi$ (intrinsic base), bx (extrinsic base), e (emitter) and c (collector).

Only a few selected parasitic elements are shown in the extrinsic network for illustration. However, we emphasize that complete intrinsic and extrinsic networks as defined by the compact model are used in actual extraction.

In matrix form, we can write $\begin{pmatrix} i_{cx} \\ i_{bx} \end{pmatrix}$ as sum of $\begin{pmatrix} i_{cm} \\ i_{bm} \end{pmatrix}$, contribution from i_{ci} and i_{bi}, and contribution from i_{rk}, $k = bx, bi, e$ and c as follows.

$$\begin{pmatrix} i_{cx} \\ i_{bx} \end{pmatrix} = \begin{pmatrix} i_{cm} \\ i_{bm} \end{pmatrix} + \sum_k [NT_{rk}] i_{rk}, \tag{3.3}$$

where

$$\begin{pmatrix} i_{cm} \\ i_{bm} \end{pmatrix} = [NT_{ibc}] \times \begin{pmatrix} i_{ci} \\ i_{bi} \end{pmatrix}, \tag{3.4}$$

$[NT_{ibc}]$ is a 2×2 transfer function matrix describing transfer of i_{ci} and i_{bi} towards i_{cx} and i_{bx}. $[NT_{rk}]$ is 2×1 transfer function matrix for propagation of i_{rk} towards i_{cx} and i_{bx}. Observe that all of the i_{rk} are uncorrelated with each other, and uncorrelated with i_{bi} and i_{ci}. According to standard two port noise admittance representation [7][18][43], we denote the correlation matrix of two noise

currents i_1 and i_2 as

$$C_{i_1,i_2} = \begin{pmatrix} S_{i_1 i_1^*} & S_{i_1 i_2^*} \\ S_{i_2 i_1^*} & S_{i_2 i_2^*} \end{pmatrix} = \begin{pmatrix} i_1 \\ i_2 \end{pmatrix} \begin{pmatrix} i_1{}^* & i_2{}^* \end{pmatrix} / \triangle f, \tag{3.5}$$

where $S_{i_x i_y^*} = i_x i_y^* / \triangle f$. $C_{i_{cx},i_{bx}}$ denotes correlation matrix of i_{cx} and i_{bx}; $C_{i_{ci},i_{bi}}$ denotes correlation matrix of i_{ci} and i_{bi}; $C_{i_{cm},i_{bm}}$ denotes correlation matrix of i_{cm} and i_{bm}. Using (3.3)(3.4)(3.5), $C_{i_{cx},i_{bx}}$ can be written as

$$C_{i_{cx},i_{bx}} = C_{i_{cm},i_{bm}} + \sum_k [NT_{rk}] \times S_{i_{rk} i_{rk}^*} \times [NT_{rk}]^\dagger, \tag{3.6}$$

$$C_{i_{cm},i_{cm}} = [NT_{ibc}] \times C_{i_{ci},i_{bi}} \times [NT_{ibc}]^\dagger. \tag{3.7}$$

$\sum_k [NT_{rk}] \times S_{i_{rk} i_{rk}^*} \times [NT_{rk}]^\dagger$ represents the contributions of all resistance thermal noises to $C_{i_{cx},i_{bx}}$. $C_{i_{ci},i_{bi}}$ is then related to $C_{i_{cm},i_{bm}}$ by:

$$C_{i_{ci},i_{bi}} = [NT_{ibc}]^{-1} \times C_{i_{cm},i_{bm}} \times ([NT_{ibc}]^\dagger)^{-1}, \tag{3.8}$$

$$C_{i_{cm},i_{bm}} = C_{i_{cx},i_{bx}} - \sum_k [NT_{rk}] \times S_{i_{rk} i_{rk}^*} \times [NT_{rk}]^\dagger. \tag{3.9}$$

3.1.2 Extraction procedure

To extract $C_{i_{ci},i_{bi}}$ from noise parameters, we need to:

1. calculate $C_{i_{cx},i_{bx}}$ from minimum noise figure NF_{min}, noise resistance R_n, optimum generator admittance Y_{opt} and Y-parameters [18] [40] [43]. Correlation matrix is first obtained from noise parameters , and Y representation matrix is then obtained using matrix transformation as shown in Chapter 1.

$$C_{i_{cx},i_{bx}} = T_{A2Y} \times \left[4kT \begin{pmatrix} R_n & \frac{F_{min}-1}{2} - R_n Y_{opt}^* \\ \frac{F_{min}-1}{2} - R_n Y_{opt} & R_n \left| Y_{opt} \right|^2 \end{pmatrix} \right] \times T_{A2Y}^\dagger. \tag{3.10}$$

$$T_{A2Y} = \begin{pmatrix} -Y_{21} & 0 \\ -Y_{11} & 1 \end{pmatrix}; F_{min} = 10^{\frac{NF_{min}}{10}}.$$

T here is noise temperature 290 K, which is not same as the T in $4kTr_k$.

2. simulate $\sum_k [NT_{rk}] \times S_{i_{rk} i_{rk}^*} \times [NT_{rk}]^\dagger$, the total contribution of terminal resistance thermal noise to $C_{i_{cx}, i_{bx}}$. Summation can be simply achieved in a single simulation by turning on all thermal noise sources (i_{rk}) and turning off i_{ci} and i_{bi}.

3. simulate $[NT_{ibc}]$ by placing ac current excitations at the current noise locations and observing i_{cx} and i_{bx}. All the nodes of interest in the large signal equivalent circuit can be made externally visible and accessible in circuit simulation by using Verilog-A [44]. Fig. 3.4 shows a sample code of nodes setup in VBIC model [36] Verilog-A code and symbols with external nodes displayed in schematic.

```
module      vbic(c,b,e,s,dt,cx,ci,bx,bi,ei,si,bp);
inout       e,s,c,b,cx,ci,bx,bi,ei,si,bp;             // external nodes
electrical  c,b,e,s;                                  // old external nodes
electrical  dt;                                       // electrothermal node
electrical  cx,ci,bx,bi,ei,bp,si,xf1,xf2;             // internal nodes
```

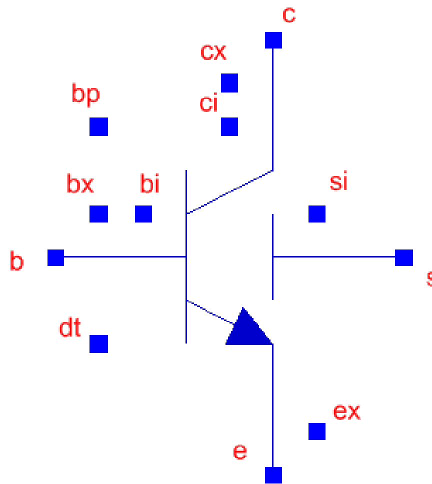

Figure 3.4: Sample Verilog-A code of nodes setup in VBIC model and symbols with external nodes displayed in schematic.

Fig. 3.6 shows an example of simulating $NT_{ibx,ci}$ and $NT_{icx,ci}$. An ac current excitation $i_{ci,ac}$ is placed between ci and ei. cx and bx are both ac shorted to ex. Two elements of $[NT_{ibc}]$, $NT_{ibx,ci}$ and $NT_{icx,ci}$ are then evaluated according to their definitions:

$$NT_{icx,ci} \triangleq \frac{i_{cx,ac}}{i_{ci,ac}}\bigg|_{i_{bi,ac}=0}, NT_{ibx,ci} \triangleq \frac{i_{bx,ac}}{i_{ci,ac}}\bigg|_{i_{bi,ac}=0}, \tag{3.11}$$

Similarly, the other two ($NT_{ibx,bi}$ and $NT_{icx,bi}$) can be obtained by placing an excitation current source between the intrinsic bi and ei nodes. A screen shot of ADS simulation schematic is also shown in Fig. 3.6.

The extraction flow is summarized in Fig. 3.7.

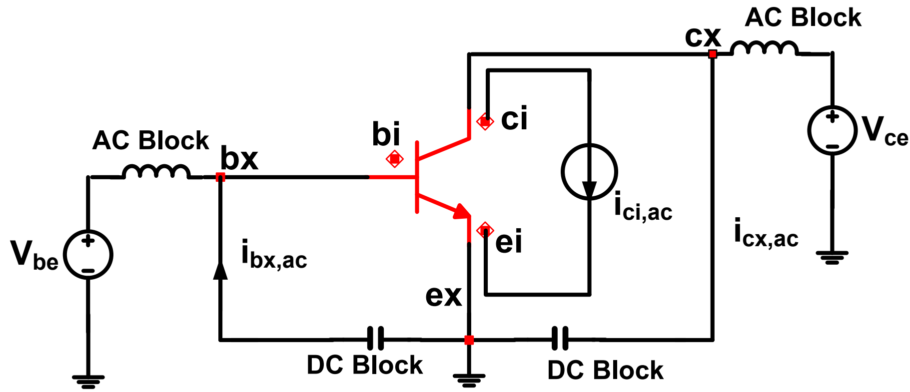

Figure 3.5: Illustration of simulating transfer functions $NT_{icx,ci}$ and $NT_{ibx,ci}$ by ac small signal analysis.

3.2 Verification using synthesized data

To verify the proposed intrinsic noise source extraction method, we take our CB SCR noise model [34] and implement it in the VBIC compact model using Verilog-A [44]. We then run ADS simulation to generate noise parameters, and use them in place of measured noise parameters to

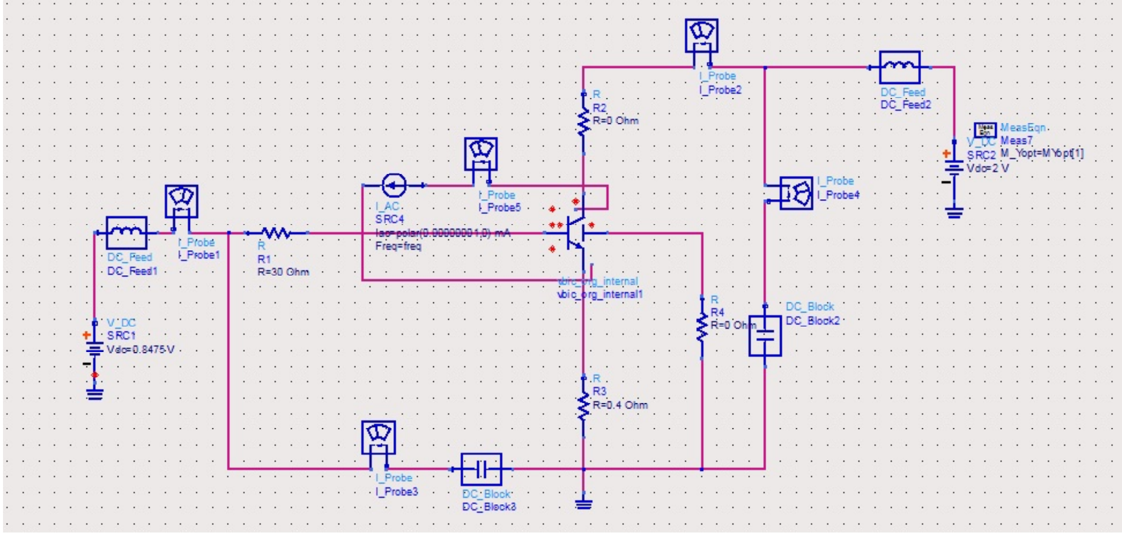

Figure 3.6: Screen shot of ADS simulation schematic.

extract i_{ci} and i_{bi}, which are represented by their correlation matrix consisting of $S_{i_{bi}i^*_{bi}}$, $S_{i_{ci}i^*_{ci}}$ and $S_{i_{ci}i^*_{bi}}$.

A comparison with the model equations of i_{ci} and i_{bi} implemented in our Verilog-A code immediately tells us if the extraction method works or not. Since everything is done in simulation, resistance noise is precisely known, a working extraction should produce the same i_{ci} and i_{bi} used in the model.

The extraction steps are:

1. Calculate correlation matrix of i_{cx} and i_{bx}, $C_{i_{cx},i_{bx}}$, $S_{i_{bx}i^*_{bx}}$, $S_{i_{cx}i^*_{cx}}$, $S_{i_{cx}i^*_{bx}}$ and $S_{i_{bx}i^*_{cx}}$ from noise parameters NF_{min}, R_n and Y_{opt}. The matrix is obtained from ac analysis using simulator, e.g. Agilent ADS [45].

2. Calculate $S_{i_{rk}i^*_{rk}} = 4KT \ /r_k$ from the compact model equation for thermal noise for all resistances.

3. Calculate (3.9) by subtracting $\sum\limits_{k=bx,bi,e,c,s} [NT_{rk}]\, i_{rk}$ from $C_{i_{cx},i_{bx}}$.

4. Simulate the transfer function matrix $[NT_{ibc}]$ and $[NT_{rk}]$ by placing an ac current excitation at the noise source location and observing the responses in i_{cx} and i_{bx}.

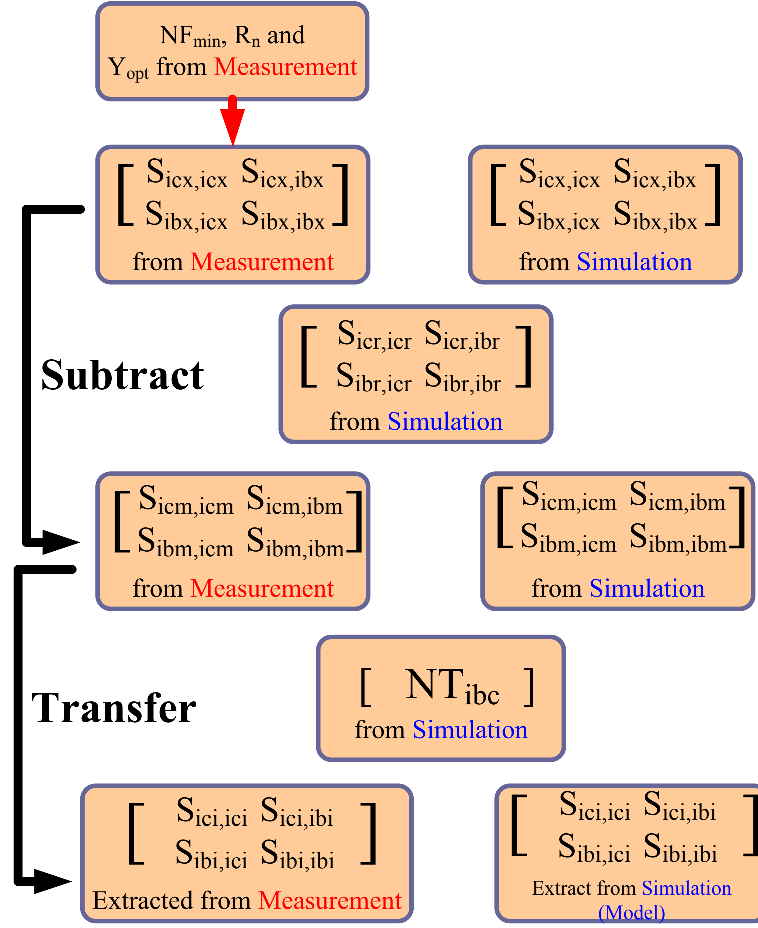

Figure 3.7: Intrinsic noise extraction flow.

Below we show simulations for a SiGe HBT from a 0.18μm BiCMOS technology [46]. The device has an emitter size of 0.48 × 20 × 1 μm^2 and peak f_T of 55 GHz. Most of design kit model parameters are kept as it is, except for R_{bx} and R_{bi}, which are finely tuned to fit experimental noise data, as detailed below. For this device, the extracted f_{g1} is 0.51, R_{bx} is 9.2 Ω and R_{bi} is 22.5 Ω. Next section details how to determine their values.

A set of frequency swept data at I_C = 3.97 mA is chosen as an example. Fig. 3.8 shows $S_{i_c i_c^*}$, $S_{i_c i_b^*}$ and $S_{i_b i_b^*}$ from different extraction steps. The PSD values of $S_{i_{bm} i_{bm}^*}$, $S_{i_{cm} i_{cm}^*}$ and $S_{i_{cm} i_{bm}^*}$ are much smaller than $S_{i_{bx} i_{bx}^*}$, $S_{i_{cx} i_{cx}^*}$ and $S_{i_{cx} i_{bx}^*}$ for the technology used. $S_{i_{bx,r} i_{bx,r}^*}$, $S_{i_{cx,r} i_{cx,r}^*}$ and $S_{i_{cx,r} i_{bx,r}^*}$ are

thermal noise contributions, which are dominated by base resistance thermal noise contributions $S_{i_{bx,Rb}i^*_{bx,Rb}}$, $S_{i_{cx,Rb}i^*_{cx,Rb}}$ and $S_{i_{cx,Rb}i^*_{bx,Rb}}$. Furthermore, for the SiGe HBT technology used, base resistance thermal noise contributes significantly to i_{cx} and i_{bx}, making intrinsic noise source extraction more difficult, as detailed below.

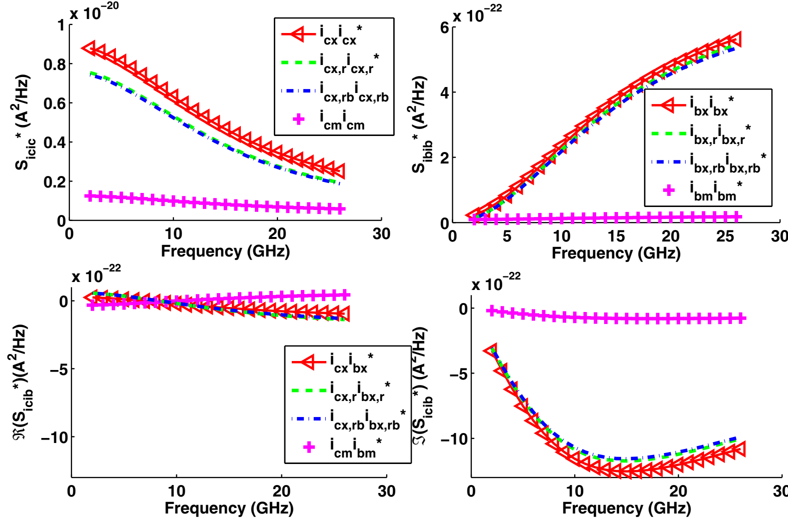

Figure 3.8: Comparison of $S_{i_ci_c^*}$, $S_{i_bi_b^*}$ and $S_{i_ci_b^*}$ as a function of frequency.

Fig. 3.9 shows the extracted intrinsic noise from simulation compared with their "input" values calculated using (2.37), (2.39) and (2.40). The uncorrelated $2qI_C$ and $2qI_B$ are also included as reference. A perfect reproduction of i_{ci} and i_{bi} is observed, proving the correctness of the extraction method.

3.3 Experimental Extraction

We now extract the intrinsic terminal current noises from noise measurements on the same SiGe HBT. VBIC compact model [36] is used. Ideally, we expect the extraction method can be directly applied to experimental data after obtaining good dc/ac fitting. However, experimental extraction is much more complicated as shown below.

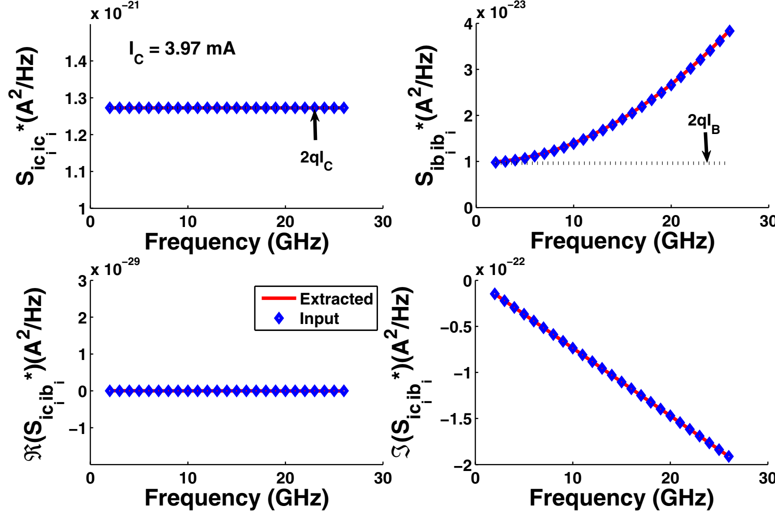

Figure 3.9: Comparison of the extracted $S_{i_{c_i}i^*_{c_i}}$, $S_{i_{b_i}i^*_{b_i}}$ and $S_{i_{b_i}i^*_{b_i}}$ with their input values as a function of frequency.

3.3.1 Model parameter determination

We start from compact model parameter extraction by fitting dc I–V data and ac Y-parameters. Using R_b from fitting dc $I-V$ data and ac Y-parameters alone, however, often results in unsatisfactory noise parameter fitting as well as unphysical $C_{i_{ci},i_{bi}}$, because noise parameters and $C_{i_{ci},i_{bi}}$ extraction results were found to be much more sensitive to R_b than Y-parameters. The extrinsic base resistance R_{bx} and the intrinsic R_{bi} can be approximately lumped into a single R_b for the device used, as shown below. Fig. 3.10 shows the simulation results of Y-parameters at $I_C = 3.97$ mA, using $R_b = 29\ \Omega$ and $31\ \Omega$. They both give good Y-parameter fitting. In fact, other R_b values close to $30\ \Omega$ will also give similarly good Y-parameter fitting.

We clearly do not want to apply the whole noise extraction procedure with every R_b value and then determine which R_b is correct for noise extraction. Therefore we extract R_b by fitting noise parameters and the noise correlation matrix of i_{cx} and i_{bx} together using a correlated noise model. The simplified version of correlated noise model that neglects the neutral base transit time effect as detailed in Chapter 2 is used here for its acceptable accuracy for the device used, meaning only frequency independent base plus CB SCR transport effect is considered.

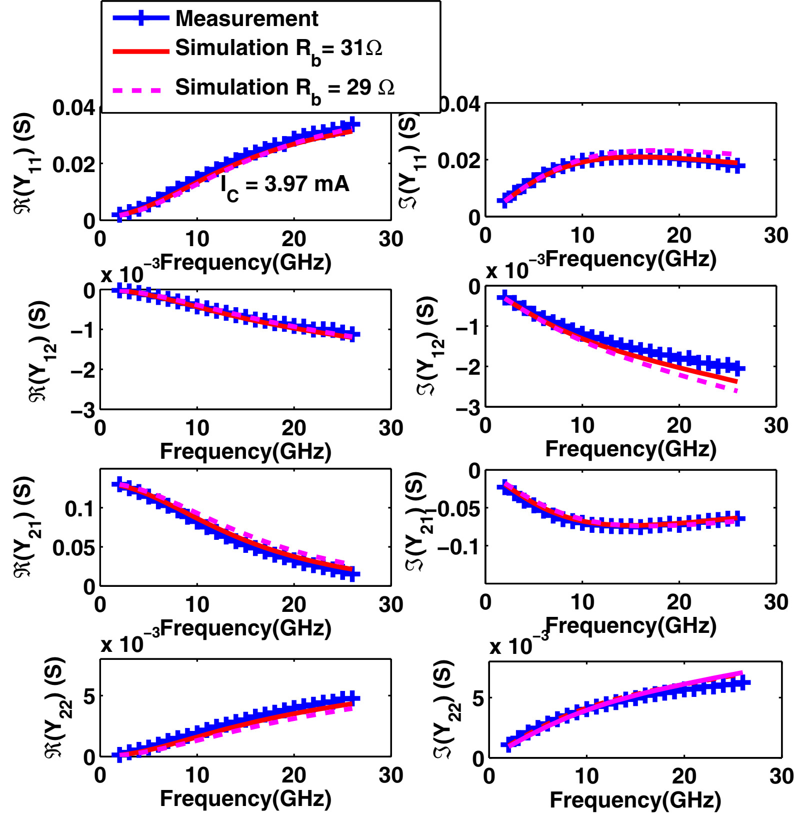

Figure 3.10: Comparison of Y-parameters from simulation and measurement as a function of frequency at I_C = 3.97 mA.

Fig. 3.11 compares noise parameter measurement with simulations obtained using two different intrinsic terminal noise current models, the uncorrelated SPICE model and CB SCR model. Base resistance values and noise model parameters τ_c using CB SCR model are both optimized to get the best fitting. Simulated noise parameters are clearly better using CB SCR model than SPICE model.

Fig. 3.12 shows $S_{i_{cx}i_{cx}^*}$, $S_{i_{bx}i_{bx}^*}$ and $S_{i_{cx}i_{bx}^*}$, including those calculated from measured noise parameters using (3.10) and those optimized simulation results using CB SCR model. $S_{i_{cx}i_{cx}^*}$, $S_{i_{bx}i_{bx}^*}$ and $S_{i_{cx}i_{bx}^*}$ from thermal noise alone are also included. $S_{i_{cx}i_{cx}^*}$ and $S_{i_{bx}i_{bx}^*}$ are dominated by thermal noise. This, however, does not mean NF_{min} is dominated by thermal noise, as we will show below. Together with the noise parameters fitting, R_b is extracted to be 31 Ω.

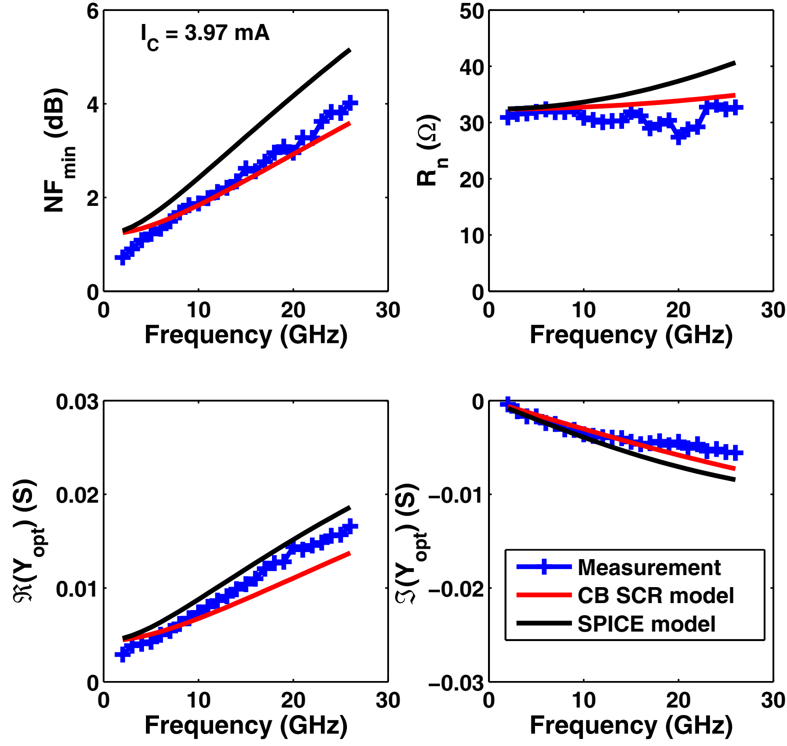

Figure 3.11: Comparison of noise parameters as a function of frequency from measurement and simulations with thermal noises plus correlated intrinsic current noises and thermal noises plus uncorrelated intrinsic current noises.

3.3.2 Frequency dependent extraction results

Fig. 3.14 compares the extracted $S_{i_{c_i} i^*_{c_i}}$, $S_{i_{b_i} i^*_{b_i}}$ and $S_{i_{c_i} i^*_{b_i}}$ as a function of frequency using R_b = 29 and 31 Ω. Modeling results using uncorrelated SPICE model and CB SCR model are both included for reference. Below 15 GHz, $S_{i_{ci} i^*_{ci}}$ extracted using R_b = 31 Ω is close to $2qI_C$. The real part of $S_{i_{ci} i_{bi*}}$ extracted using R_b = 29 Ω has a large positive value, which is contradictory to known physics that $S_{i_{ci} i_{bi*}}$ is dominated by the imaginary part [23][12][25]. The imaginary part of $S_{i_{ci} i_{bi*}}$ is negative and decreases linearly with frequency for both R_b values. Overall, the extracted $S_{i_{ci} i^*_{ci}}$, $S_{i_{bi} i^*_{bi}}$ and $S_{i_{ci} i^*_{bi}}$ are clearly different using two R_b values. R_b = 31 Ω gives more reasonable extraction results than R_b = 29 Ω below 15 GHz. Therefore, noise extraction is more sensitive to R_b than Y-parameters. The extraction of R_b needs to be included as part of the noise extraction. For

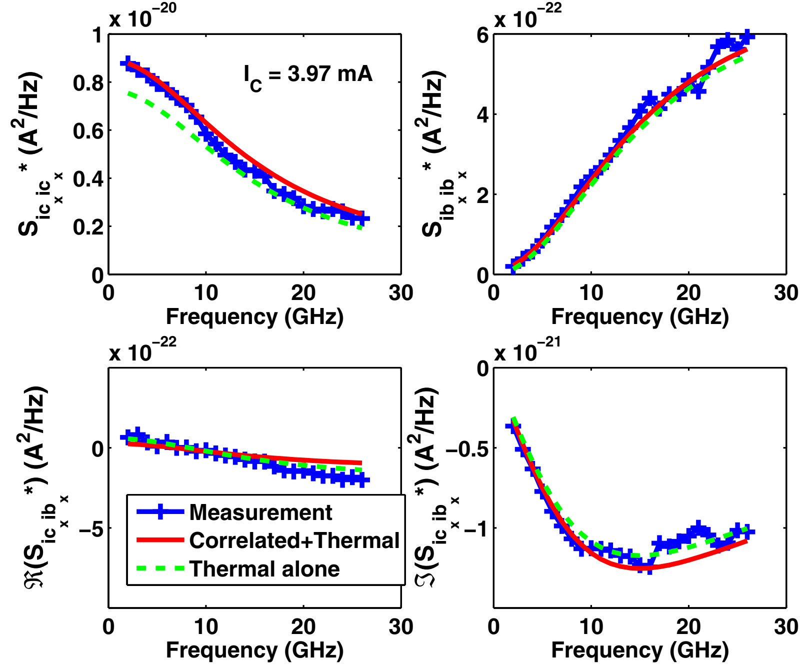

Figure 3.12: Comparison of $S_{i_{cx}i_{cx}^*}$, $S_{i_{bx}i_{bx}^*}$ and $S_{i_{cx}i_{bx}^*}$ as a function of frequency from measurement and simulations with thermal noises plus correlated intrinsic noises, the correlated intrinsic noises alone and the thermal noises alone.

similar reasons, we use a correlated intrinsic current noise model to help obtain more meaningful extraction results.

Fig. 3.14 shows the extracted $S_{i_{ci}i_{ci}^*}$, $S_{i_{bi}i_{bi}^*}$ and $S_{i_{ci}i_{bi}^*}$ as a function of frequency, together with the correlated model and simple shot noise model for i_{bi} and i_{ci}. Below 15 GHz, $S_{i_{ci}i_{ci}^*}$ is close to $2qI_C$. The imaginary part of $S_{i_{ci}i_{bi}^*}$ is negative and decreases linearly with frequency. The real part of $S_{i_{ci}i_{bi}^*}$ is positive and opposite to our model, (2.40). However, it is not important because its value is much less than the imaginary part of the correlation. $S_{i_{bi}i_{bi}^*}$ increases with frequency and is higher than $2qI_B$.

Above 15 GHz, the noise extraction results are noisy, in part because of the noise in the original noise parameter measurement, as illustrated by the zoom-in insert in Fig. 3.11.

Note that extraction was made with two sets of R_{bi} and R_{bx}. The sum of $R_{bi}+R_{bx}$ is the same. At this low I_C, the final extraction result is the practically the same, indicating that only the total value matters.

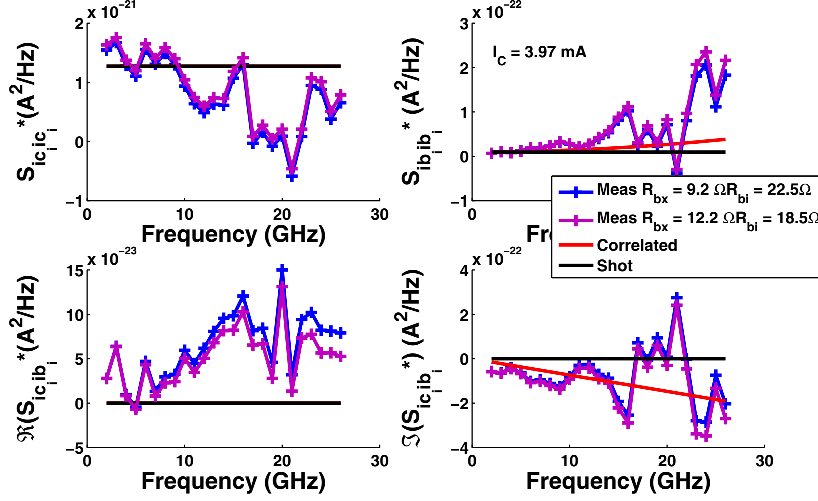

Figure 3.13: Comparison of extracted $S_{i_{ci}i_{ci}^*}$, $S_{i_{bi}i_{bi}^*}$ and $S_{i_{ci}i_{bi}^*}$ as a function of frequency from measurement with different values of base resistance and simulations with and without correlation.

Fig. 3.13 shows the extracted $S_{i_{ci}i_{ci}^*}$, $S_{i_{bi}i_{bi}^*}$ and $S_{i_{ci}i_{bi}^*}$ as a function of frequency, with two different effective R_b values. $R_b = 31\Omega$ is optimized with noise parameters after dc $I-V$ and ac Y-parameter fitting. $R_b = 29\Omega$ is determined only by dc $I-V$ and ac Y-parameter fitting. $R_b = 29\Omega$ leads to an unphysical extraction results even at low frequency, therefore R_b optimization with noise parameters are necessary for intrinsic noise extraction.

3.3.3 Bias dependent extraction results

Fig. 3.15 show the extracted $S_{i_{ci}i_{ci}^*}$, $S_{i_{bi}i_{bi}^*}$ and $S_{i_{ci}i_{bi}^*}$ as a function of I_C at 5 GHz. $S_{i_{bi}i_{bi}^*}$ and $S_{i_{ci}i_{bi}^*}$ are well fitted with the $R_{bi} = 22.5\Omega$ and $R_{bx} = 9.2\Omega$ except the highest bias point. Above 10 mA, the extracted $S_{i_{ci}i_{ci}^*}$ is clearly higher than model, i.e. $2qI_C$. One possible reason is $2qI_C$ does not describe the current dependence very well at higher current. This result is consistent with the result obtained from small-signal equivalent circuit based noise extraction in [40]. Another possible reason is that the current dependence of R_{beff} is not well modeled in VBIC.

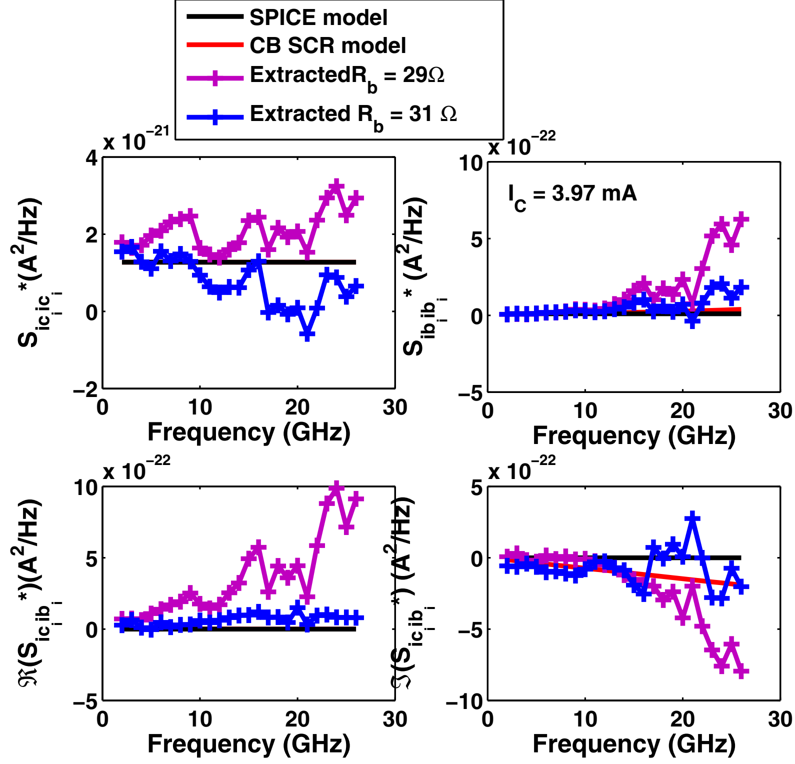

Figure 3.14: Comparison of extracted $S_{i_{ci}i_{ci}^*}$, $S_{i_{bi}i_{bi}^*}$ and $S_{i_{ci}i_{bi}^*}$ as a function of frequency from measurement with two different values of effect base resistances and simulations with and without correlation.

At higher I_C, the two sets of R_{bx} and R_{bi} lead to clearly different intrinsic noises, because $R_{bx} + R_{bi}/q_B$ are different. At lower I_C, q_B reduces to unity. Given that in this technology $S_{i_{cx}i_{cx}^*}$ is dominated by thermal noise, the current dependence of R_{beff} needs to be further investigated, possibly with a different model for its current dependence.

The same extraction method and procedure can be applied to any device. We have successfully done this on the 36 GHz SiGe HBT used in Chapter 2 as well.

3.4 Conclusion

We have developed a general purpose method of experimentally extracting base resistances and correlated RF noises in the intrinsic base and collector currents using the same compact model

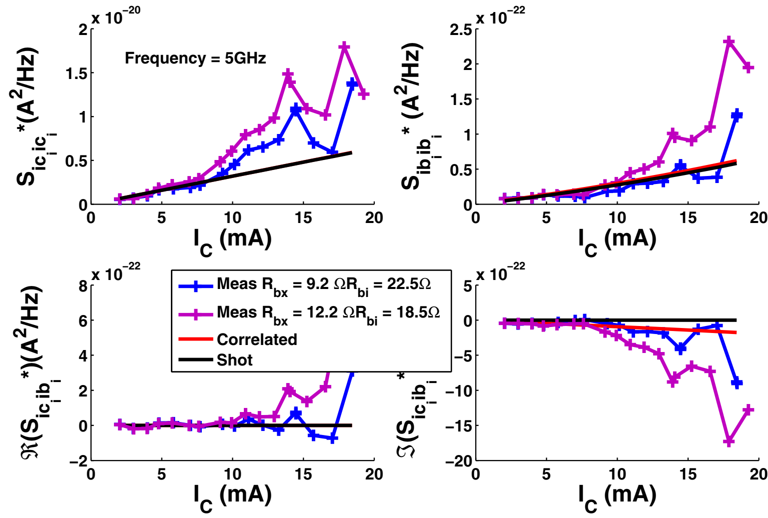

Figure 3.15: Comparison of extracted $S_{i_{ci}i_{ci}^*}$, $S_{i_{bi}i_{bi}^*}$ and $S_{i_{ci}i_{bi}^*}$ as a function of I_C from measurement with different values of base resistance and simulations with and without correlation.

used for RFIC design. The method is verified with synthetic data, and then applied to measurement data. Practical issues associated with removing thermal noise contributions are discussed, together with a method for compact noise model parameter extraction. Most meaningful extraction results are obtained with simultaneous fitting of Y-parameters, noise parameters and external terminal noise currents using a correlated noise model. The results also show that compact noise modeling accuracy and noise source extraction from noise parameter measurement both become more difficult at higher frequency or higher current.

Chapter 4

Noise Source Importance Evaluation

As we pointed out in the previous chapters, there are mainly two kinds of RF noise sources in bipolar transistors, i.e., the terminal resistance thermal noise and the correlated intrinsic terminal current noises. A logical question is which noise source is more important and in general how to evaluate their importance, as well as the importance of noise correlation.

Fig. 4.1 shows measured and simulated minimum noise figure (NF_{min}) versus frequency from 2 to 26 GHz of the same 0.35 μm technology SiGe HBT used for model development in Chapter 2 at I_C = 3.55 mA [22]. The emitter area is $0.8 \times 20 \times 3$ μm^2. Simulation is made using a modified version of the HICUM model that implements the collector base space charge region (CB SCR) transport noise model described in Chapter 2. NF_{min} is simulated with all the noise sources turned on, with only intrinsic current noise sources turned on, and with only thermal noise sources turned on to evaluate the relative importances of the two types of noise.

The NF_{min} due to thermal noises alone is very small and below 1 dB in the whole frequency range. The NF_{min} due to intrinsic current noises is dominant. The NF_{min} due to intrinsic noise from popular uncorrelated $2qI$ model is larger than that from correlated noise model, particularly at higher frequencies. It is generally believed that the intrinsic noise correlation is the key factor to reduce NF_{min} and many efforts have been made to model noise correlation [17][16][28][47][48][29][4][35]. However, we will show in the following that the intrinsic noise correlation itself is not able to reduce NF_{min}.

One may attempt to conclude from examining NF_{min} that intrinsic current noise is much more important than thermal noise. However, if we examine the power spectral density (PSD) of the external collector current noise under ac short circuit condition at both the base and collector for a common emitter configuration, $S_{i_c i_c^*}$, shown in Fig. 4.2 for the same device and biasing condition,

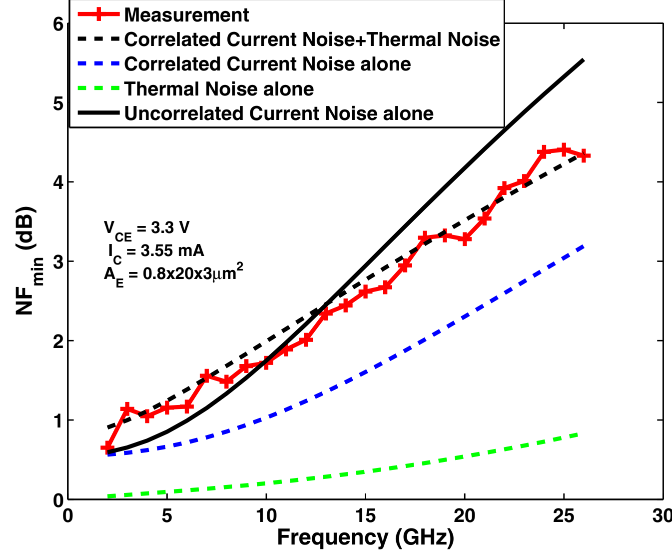

Figure 4.1: NF_{min} obtained from measurement and NF_{min} obtained from simulations with different noise sources turned on.

we come to a different conclusion. Note that here i_c refers to the external collector noise current obtained (i.e. i_{cx} in Fig. 3.3) instead of the intrinsic collector noise current. Thermal noise contribution dominates $S_{i_c i_c^*}$, which has the side effect of making extraction of intrinsic noise current from noise measurement difficult [49].

A logical and important question is which conclusion is correct, and how the relative importance of different noise source should be evaluated, which we address in this chapter. Instead of evaluating only NF_{min} or $S_{i_c i_c^*}$, we examine all noise parameters and all of the elements of the noise correlation matrices for all noise representations introduced in Chapter 1, including the Y representation, the Z representation and the chain (ABCD) representation.

To have a complete picture of the relevant importance of individual noise sources, we compare all elements of the noise correlation matrices for all representation calculated from turning on individual noise sources. Analytical expressions are derived to obtained better insight.

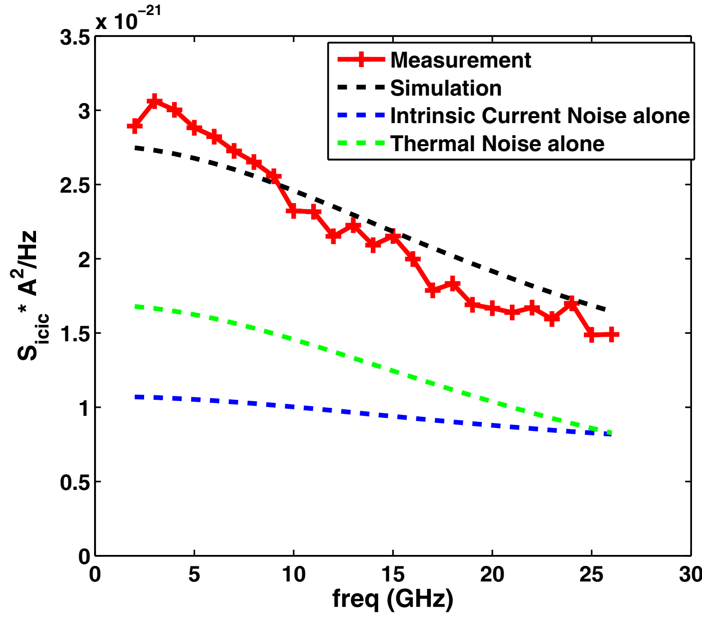

Figure 4.2: $S_{i_c i_c^*}$ obtained from measurement and $S_{i_c i_c^*}$ obtained from simulations with different noise sources turned on.

4.1 Equivalent circuit simplification

Our goal is to derive analytical expressions of noise correlation matrices in different representation, which can then be used to quantify relative importance of each noise source explicitly. The method is to relate the external correlation matrix of the noise representation to the intrinsic noise current correlation matrix that is made of $S_{i_{bi} i_{bi}^*}$, $S_{i_{ci} i_{ci}^*}$ and $S_{i_{ci} i_{bi}^*}$, PSDs of intrinsic noise current i_{ci}, i_{bi} and their correlation. This can be achieved through analytically combining linear noisy two-port networks, starting from the intrinsic transistor network.

Terminal resistances, the base resistance R_b in particular, have two roles in determining transistor noise parameters and the equivalent noise sources for any representation. They are impedance elements, and thermal noise sources at the same time. Fig. 4.3(a) illustrates a typical equivalent circuit for bipolar transistor. A few selected parasitic elements of extrinsic network are shown including the resistances which produce thermal noise. The real extrinsic circuit may be even more complex depending on the complexity of a specified compact model. Therefore, it is difficult and tedious to have all the extrinsic parasitics included for analytical derivation. We have

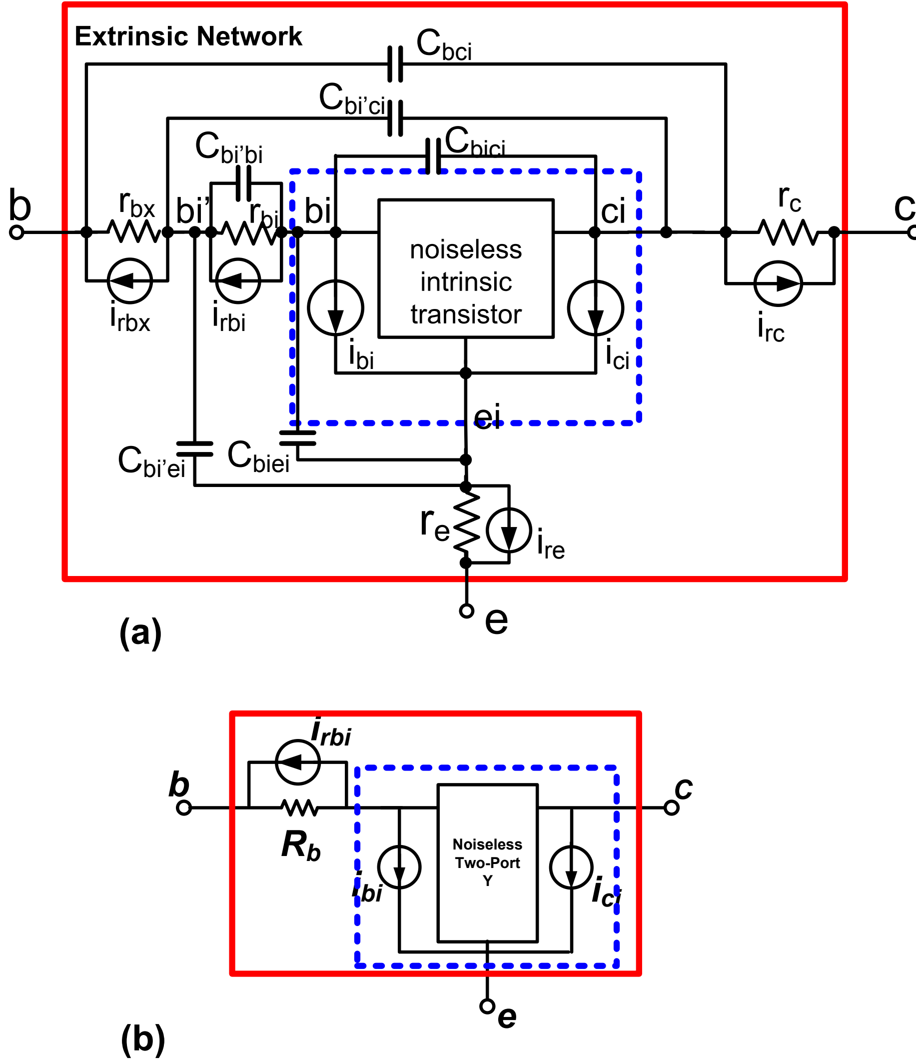

Figure 4.3: Illustration of the full model and simplified model of the device.

chosen to keep a single lumped R_b in the extrinsic network, as shown in Fig. 4.3(b). The justification is that collector resistances are less important and emitter resistance is of very small value for SiGe HBT. The capacitances are noiseless and do not have distinct impact on Y parameters except at very high frequencies. Based on this simplified two-port network, we derive below expressions of noise correlation matrices of the whole transistor for Z, Y and chain representations. To simplify derivation, the intrinsic base current noise source is placed between intrinsic base and emitter terminals [7].

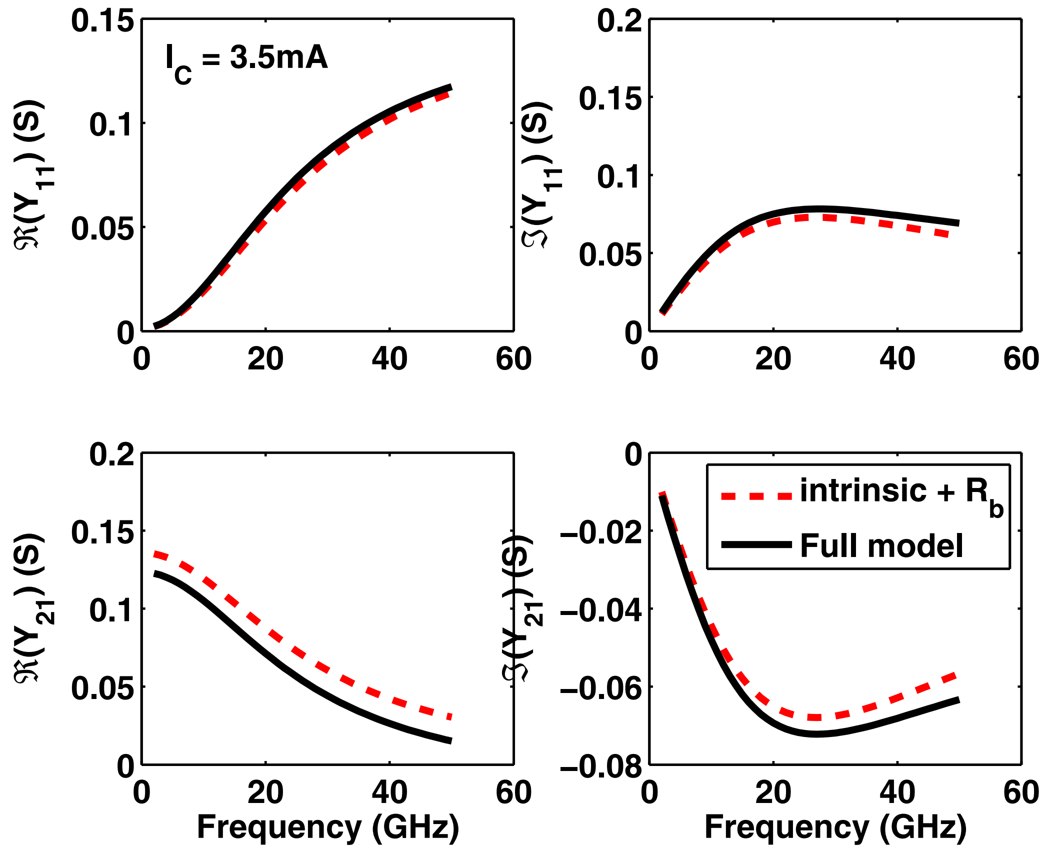

Figure 4.4: Simulated Y_{11} and Y_{21} using the simplified model for intrinsic transistor plus R_b and using the complete HICUM model .

Fig. 4.4 compares the Y_{11} and Y_{21} simulated using the full model, i.e. complete HICUM model, and the simplified model, i.e. only a lumped R_b is used in the extrinsic network. That is, all of the parasitics in extrinsic network are removed in the Verilog-A code of HICUM, except for R_b. The two simulation results are very close. Y_{11} and Y_{21} from the simplified model capture the frequency dependence of those from the full model very well, which justifies the model simplification for the HBT used. Y_{12} and Y_{22} of the device used are not shown here due to their extremely small magnitude.

Another evidence to prove that dominance of R_b among the extrinsic elements is to utilize the noise extraction method proposed in last chapter. To find out if there is one extrinsic element (or more) that dominates, we can keep extrinsic network elements individually and compare results

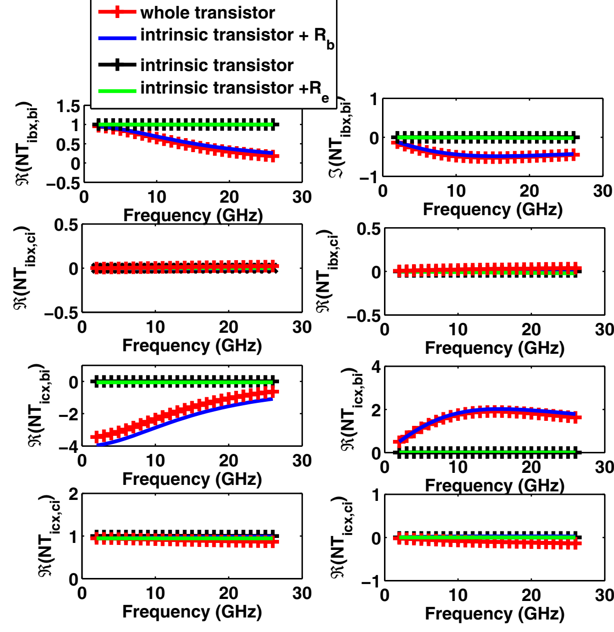

Figure 4.5: Simulated noise transfer functions as a function of frequency at $I_C = 3.97$ mA with no extrinsic network element, with all extrinsic network elements, with only R_b and with only R_e.

with keeping all of them. To insure it is completely clean intrinsic transistor before adding any parasitics, we can simulate its $C_{i_{cx},i_{bx}}$, the correlation matrix of PSDs of i_{cx} and i_{bx}, and see if it is identical to its $C_{i_{ci},i_{bi}}$, the correlation matrix of i_{ci} and i_{bi} from model calculation. The transfer functions in $[NT_{ibc}]$, defined in Chapter 3, are shown in Fig. 4.5. Examples with keeping R_e alone and R_b alone in the extrinsic network are included. With only a lumped $R_b = R_{bx} + R_{bi}$ in the extrinsic network, the transfer functions are nearly identical to those simulated with keeping all of the extrinsic network elements. The transfer functions simulated with only R_e in the extrinsic network are approximately same as the transfer functions with no extrinsic element.

To further confirm the dominance of R_b in determining the transfer function matrix $[NT_{ibc}]$, we compare $C_{i_{cm},i_{bm}}$, the correlation matrix of i_{cx} and i_{bx} due to i_{ci} and i_{bi}, obtained using (3.7), with $[NT_{ibc}]$ simulated using complete extrinsic network and with $[NT_{ibc}]$ simulated using only a lumped R_b in the extrinsic network, as shown in Fig. 4.6. The two $C_{i_{cm},i_{bm}}$ obtained are approximately identical. Therefore, R_b is the most dominant element in the extrinsic network in determining $[NT_{ibc}]$.

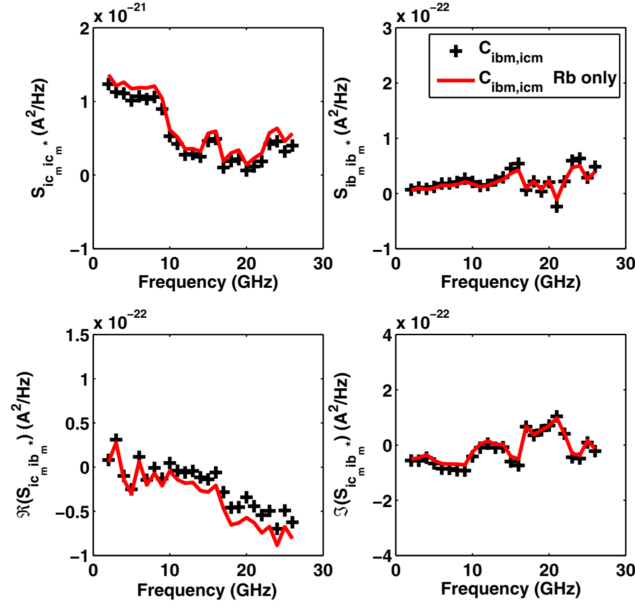

Figure 4.6: The elements of $C_{i_{cm},i_{bm}}$ obtained with $[NT_{ibc}]$ simulated using complete extrinsic network compared with the elements of $C_{i_{cm},i_{bm}}$ obtained with $[NT_{ibc}]$ simulated using only a lumped R_b in the extrinsic network.

4.2 Analytical derivations

In all derivations, we include R_b's contribution in two steps. In step 1, R_b only acts as an element of extrinsic network which modifies the propagation of i_{bi} and i_{ci}, and changes two-port parameters. In step 2, the thermal noise R_b is added.

4.2.1 Z-Noise Representation

Fig. 4.7(a) illustrates Z-noise representation. v_{1i} and v_{2i} are the equivalent input and output voltage noise sources for the intrinsic network. Fig. 4.7(b) and Fig. 4.7(c) show that adding R_b between external input terminal and v_{1i} is equivalent to adding R_b between external v_{1i} and the intrinsic base terminal. Therefore, v_{1i} is equal to v_1, $v_1 = v_{1i}$ and $v_2 = v_{2i}$. Adding the noiseless R_b does not affect v_1 and v_2 at all.

The two-port parameters, Z parameters, however, are affected. Here we denote the Z parameter matrix as T_Z rather than Z as it is going to be used to transform C_Y to C_Z, according to

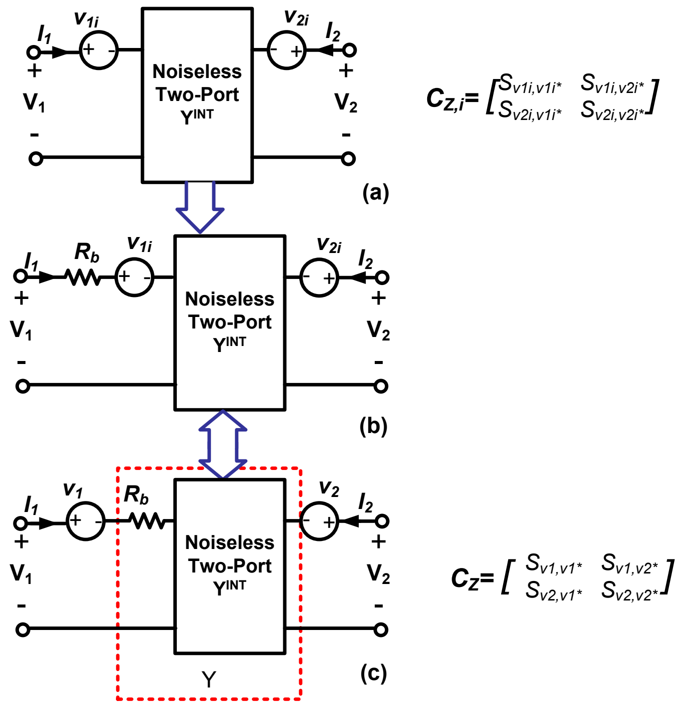

Figure 4.7: Illustration of Z presentation in the cases of the intrinsic device alone and the intrinsic device plus R_b.

Table 1.1. T_Z is different from T_Z^{int} due to R_b:

$$T_Z = \begin{pmatrix} Z_{11}^{int} + R_b & Z_{12}^{int} \\ Z_{21}^{int} & Z_{22}^{int} \end{pmatrix}, \tag{4.1}$$

and

$$T_Z^{int} = \begin{pmatrix} Z_{11}^{int} & Z_{12}^{int} \\ Z_{21}^{int} & Z_{22}^{int} \end{pmatrix}, \tag{4.2}$$

which is an excellent demonstration of R_b's impact as an impedance element.

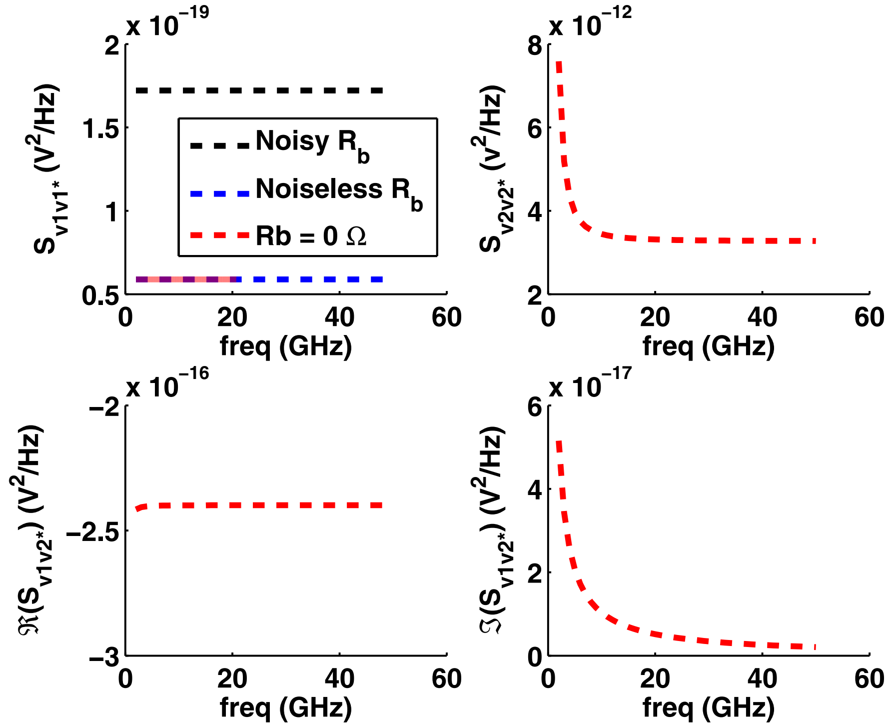

Figure 4.8: The correlation matrix of Z-noise representation with $R_b = 0$, noiseless R_b and thermal noisy R_b.

In general from two-port theory detailed in Chapter 1,

$$
\begin{aligned}
C_Z &= \begin{pmatrix} v_1 \\ v_2 \end{pmatrix} \begin{pmatrix} v_1 & v_2 \end{pmatrix}^* / \triangle f \\
&= T_Z^{int} \begin{pmatrix} i_1 \\ i_2 \end{pmatrix} \begin{pmatrix} i_1 & i_2 \end{pmatrix}^* / \triangle f T_Z^{int\dagger}
\end{aligned} \tag{4.3}
$$

The Z representation noise correlation matrix can be represented as

$$C_Z = C_Z^{int} = T_Z^{int} C_{Y,i} T_Z^{int\dagger}, \tag{4.4}$$

where

$$C_{Yi} = \begin{pmatrix} S_{ib_i ib_i^*} & S_{ib_i ic_i^*} \\ S_{ic_i ib_i^*} & S_{ic_i ic_i^*} \end{pmatrix}, \tag{4.5}$$

and

$$T_Z^{int} = \begin{pmatrix} \frac{Y_{22}^{int}}{\triangle Y^{int}} & -\frac{Y_{12}^{int}}{\triangle Y^{int}} \\ -\frac{Y_{21}^{int}}{\triangle Y^{int}} & \frac{Y_{22}^{int}}{\triangle Y^{int}} \end{pmatrix}, \triangle Y^{int} = Y_{11}^{int} Y_{22}^{int} - Y_{12}^{int} Y_{21}^{int}. \tag{4.6}$$

This is simply result of $Z = Y^{-1}$. C_Z can be related to C_{Yi} and the intrinsic Y^{int} as

$$S_{v_1 v_1^*} = \frac{1}{|\triangle Y^{int}|^2} \left(\left| Y_{22}^{int} \right|^2 S_{i_{bi} i_{bi}^*} - 2\Re \left(Y_{12}^{int} Y_{22i}^{int*} S_{i_{ci} i_{bi}^*} \right) + \left| Y_{12}^{int} \right|^2 S_{i_{ci} i_{ci}^*} \right), \tag{4.7}$$

$$S_{v_1 v_2^*} = \frac{1}{|\triangle Y^{int}|^2} \left(-Y_{22}^{int} Y_{21}^{int*} S_{i_{bi} i_{bi}^*} + Y_{12}^{int} Y_{21}^{int*} S_{i_{ci} i_{bi}^*} + Y_{22}^{int} Y_{11}^{int*} S_{i_{bi} i_{ci}^*} - Y_{12}^{int} Y_{11}^{int*} S_{i_{ci} i_{ci}^*} \right),$$

$$S_{v_2 v_2^*} = \frac{1}{|\triangle Y^{int}|^2} \left(\left| Y_{21}^{int} \right|^2 S_{i_{bi} i_{bi}^*} - 2\Re \left(Y_{11}^{int} Y_{21}^{int*} S_{i_{ci} i_{bi}^*} \right) + \left| Y_{11}^{int} \right|^2 S_{i_{ci} i_{ci}^*} \right).$$

The noiseless R_b gives the same C_Z as the intrinsic network only. Although thermal noiseless R_b has no impact on the correlation matrix of Z-noise representation, it still changes noise parameters through Y parameters, as detailed below. Thermal noise of R_b will only add a $4kTR_b$ term to $S_{v_1 v_1 *}$, as shown in Fig. 4.8. Therefore

$$C_Z(\text{noisy } R_b) = C_Z(\text{noiseless } R_b) + C_Z^{R_b} = \begin{pmatrix} S_{v_1 v_1^*} & S_{v_1 v_2^*} \\ S_{v_2 v_1^*} & S_{v_2 v_2^*} \end{pmatrix} + \begin{pmatrix} 4kTR_b & 0 \\ 0 & 0 \end{pmatrix}. \tag{4.8}$$

We then compare calculation results using (4.8) from three scenarios: 1. $R_b = 0\ \Omega$; 2. a noiseless $R_b = 6.8\ \Omega$, its experimentally extracted value; 3. a noisy $R_b = 6.8\ \Omega$. Fig. 4.8 shows results of comparison up to 50 GHz. The results with $R_b = 0\ \Omega$ and noiseless R_b show no difference. Overall $S_{v_1 v_1^*}$ is much smaller than $S_{v_2 v_2^*}$ and $S_{v_2 v_1^*}$, which are dominated by intrinsic current noise.

4.2.2 Y-Noise representation

We first examine how i_{ci} and i_{bi} propagate to external node by a thermal noiseless R_b under ac short circuit conditions at both the input and the output. The resulting currents at the collector and base are denoted as i_{cm} and i_{bm}. The correlation matrix is defined by

$$C_Y(\text{noiseless } R_b) = \begin{pmatrix} S_{i_{bm} i_{bm}^*} & S_{i_{bm} i_{cm}^*} \\ S_{i_{cm} i_{bm}^*} & S_{i_{cm} i_{cm}^*} \end{pmatrix}. \tag{4.9}$$

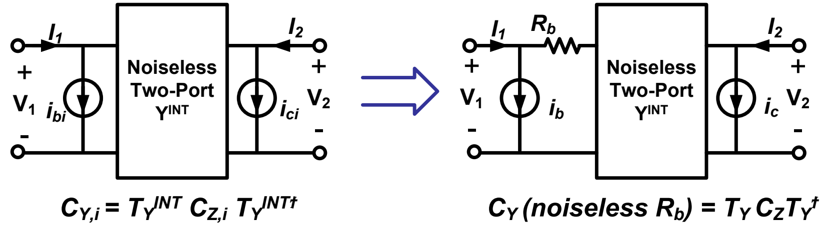

Figure 4.9: Illustration of Y presentation in the cases of the intrinsic device alone and the intrinsic device plus R_b

As shown in Fig. 4.9, noises of two port network in Z representation can be equivalently expressed by Y representation. The intrinsic Y representation noise correlation matrix $C_{Y,i}$ can be transformed from $C_{Z,i}$ multiplied by an transformation matrix T_Y^{int}, which is equal to the intrinsic Y parameter matrix.

$$C_{Y,i} = \begin{pmatrix} i_1 \\ i_2 \end{pmatrix} \begin{pmatrix} i_1 & i_2 \end{pmatrix}^* / \triangle f = T_Y^{int} \begin{pmatrix} v_1 \\ v_2 \end{pmatrix} \begin{pmatrix} v_1 & v_2 \end{pmatrix}^* / \triangle f T_Y^{int\dagger} = T_Y^{int} C_{Z,i} T_Y^{int\dagger},$$

where

$$T_Y^{int} = \begin{pmatrix} Y_{11}^{int} & Y_{12}^{int} \\ Y_{21}^{int} & Y_{22}^{int} \end{pmatrix}. \tag{4.10}$$

With the noiseless R_b,

$$C_Y(\text{noiseless } R_b) = T_Y C_Z(\text{noiseless } R_b) T_Y{}^{\dagger}, \tag{4.11}$$

where

$$T_Y = \begin{pmatrix} Y_{11} & Y_{12} \\ Y_{21} & Y_{22} \end{pmatrix} \tag{4.12}$$

$$= \frac{1}{1 + Y_{11}^{int} R_b} \begin{pmatrix} Y_{11}^{int} & Y_{12}^{int} \\ Y_{21}^{int} & Y_{22}^{int} + R_b \triangle Y^{int} \end{pmatrix}. \tag{4.13}$$

The detailed derivation of relation between T_Y^{int} and T_Y can be found in Appendix E. As $C_Z(\text{noiseless } R_b) = C_{Z,i}$, we can relate $C_Y(\text{noiseless } R_b)$ to $C_{Y,i}$ by matrix operation. Recall from Subsection 4.2.1,

$C_Z^{int} = T_Z^{int} C_{Y,i} T_Z^{int\dagger}$, we then have

$$C_Y(\text{noiseless } R_b) = T_Y T_Y^{int^{-1}} C_{Y,i} T_Y^{int^{\dagger^{-1}}} T_Y{}^{\dagger}. \tag{4.14}$$

We can now obtain the PSDs of external noise currents as

$$\begin{aligned} S_{i_{bm}i_{bm}^*} &= \frac{S_{i_{bi}i_{bi}^*}}{\left|1 + Y_{11}^{int} R_b\right|^2}, \\ S_{i_{cm}i_{cm}^*} &= S_{i_{ci}i_{ci}^*} + \frac{R_b^2 \left|Y_{21}^{int}\right|^2 S_{i_{bi}i_{bi}^*}}{\left|1 + Y_{11}^{int} R_b\right|^2} - \frac{2\Re\left(R_b Y_{21}^{int*} S_{i_{ci}i_{bi}^*}\right)}{\left(1 + R_b Y_{11}^{int*}\right)}, \\ S_{i_{cm}i_{bm}^*} &= -\frac{R_b Y_{21}^{int} S_{i_{bi}i_{bi}^*}}{\left|1 + Y_{11}^{int} R_b\right|^2} + \frac{S_{i_{ci}i_{bi}^*}}{\left(1 + R_b Y_{11}^{int*}\right)}. \end{aligned} \tag{4.15}$$

With an extremely small R_b, the external PSDs reduce to the intrinsic ones.

The contribution of R_b's thermal noise to i_b and i_c can be considered as $i_{b,Rb} = 4kTR_bY_{11}$ and $i_{c,Rb} = 4kTR_bY_{21}$ under ac short conditions. Y_{11} and Y_{21} can be related to Y_{11}^{int} and Y_{21}^{int} by (4.13). Therefore the contribution of R_b's thermal noise to total $S_{i_c i_c{}^*}$, $S_{i_b i_b{}^*}$ and $S_{i_c i_b^*}$ are

$$\begin{aligned} S_{i_{bRb}i_{bRb}^*} &= 4kTR_b \left|\frac{Y_{11}^{int}}{1 + Y_{11}^{int} R_b}\right|^2, \\ S_{i_{cRb}i_{cRb}^*} &= 4kTR_b \left|\frac{Y_{21}^{int}}{1 + Y_{11}^{int} R_b}\right|^2, \\ S_{i_{cRb}i_{bRb}^*} &= 4kTR_b \frac{Y_{21}^{int} Y_{11}^{int*}}{\left|1 + Y_{11}^{int} R_b\right|^2}. \end{aligned} \tag{4.16}$$

The values of $S_{i_{bRb}i_{bRb}^*}$, $S_{i_{cRb}i_{cRb}^*}$ and $S_{i_{cRb}i_{cRb}^*}$ increase with frequency and are related to f^2. As shown in [49], base resistance thermal noise dominates over the total thermal noise contributions and contributes significantly to i_c and i_b. Overall,

$$C_Y(\text{noisy } R_b) = C_Y(\text{noiseless } R_b) + C_Y^{R_b} = \begin{pmatrix} S_{i_{bm}i_{bm}^*} & S_{i_{bm}i_{cm}^*} \\ S_{i_{cm}i_{bm}^*} & S_{i_{cm}i_{cm}^*} \end{pmatrix} + \begin{pmatrix} S_{i_{b,Rb}i_{b,Rb}^*} & S_{i_{b,Rb}i_{c,Rb}^*} \\ S_{i_{c,Rb}i_{b,Rb}^*} & S_{i_{c,Rb}i_{c,Rb}^*} \end{pmatrix}. \tag{4.17}$$

Fig. 4.10 shows the calculation results using (4.15)-(4.17). $S_{i_c i_c^*}$, $S_{i_b i_b^*}$ and the imaginary part of $S_{i_c i_b^*}$ are dominated by thermal noise. The real part of $S_{i_c i_b^*}$ is less important because the value of correlation is dominated by its imaginary part.

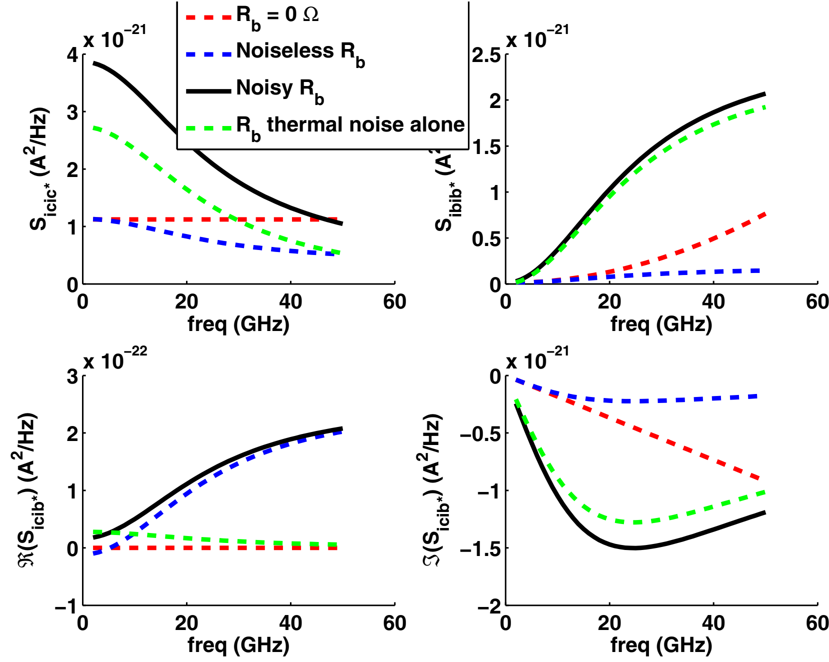

Figure 4.10: Correlation matrix of Y representation from calculations.

4.2.3 Chain Noise Representation

We now derive the chain noise representation matrix expressions, which directly relate to noise parameters. Recall from Chapter 1, the chain noise representation correlation matrix C_A can be transformed from C_Y multiplied by an transformation matrix T_A,

$$C_A = T_A C_Y T_A{}^{\dagger}, \tag{4.18}$$

where

$$T_A = \begin{pmatrix} 0 & A_{12} \\ 1 & A_{22} \end{pmatrix} = \begin{pmatrix} 0 & \frac{-1}{Y_{21}} \\ 1 & \frac{-Y_{11}}{Y_{21}} \end{pmatrix} = \begin{pmatrix} 0 & -\frac{1+Y_{11}^{int} R_b}{Y_{21}^{int}} \\ 1 & -\frac{Y_{11}^{int}}{Y_{21}^{int}} \end{pmatrix}. \tag{4.19}$$

The expressions of $S_{i_a i_a^*}$, $S_{v_a v_a^*}$ and their correlation can be obtained from (4.15)-(4.18). Without thermal noise,

$$S_{i_a i_a^*} = S_{i_{bi} i_{bi}^*} + \left| \frac{Y_{11}^{int}}{Y_{21}^{int}} \right|^2 S_{i_{ci} i_{ci}^*} - 2\Re \left(\frac{Y_{11}^{int}}{Y_{21}^{int}} S_{i_{ci} i_{bi}^*} \right), \tag{4.20}$$

$$S_{v_a v_a^*} = \frac{S_{i_{ci} i_{ci}^*}}{\left| Y_{21}^{int} \right|^2} + S_{i_{bi} i_{bi}^*} R_b^2 - 2\Re \left(\frac{R_b S_{i_{ci} i_{bi}^*}}{Y_{21}^{int}} \right) + \left(\left| Y_{11}^{int} R_b \right|^2 + 2\Re \left(Y_{11}^{int} R_b \right) \right) \frac{S_{i_{ci} i_{ci}}^*}{\left| Y_{21}^{int} \right|^2}$$
$$- 2\Re \left(\frac{R_b^2 Y_{11}^{int*}}{Y_{21}^{int}} S_{i_{ci} i_{bi}^*} \right),$$

$$S_{i_a v_a^*} = \frac{Y_{11}^{int}}{\left| Y_{21}^{int} \right|^2} S_{i_{ci} i_{ci}^*} - \frac{S_{i_{bi} i_{ci}^*}}{Y_{21}^{int*}} + R_b S_{i_{bi} i_{bi}^*} - 2\Re \left(\frac{R_b Y_{11}^{int}}{Y_{21}^{int}} S_{i_{ci} i_{bi}^*} \right) + \frac{R_b \left| Y_{11}^{int} \right|^2}{\left| Y_{21}^{int} \right|^2} S_{i_{ci} i_{ci}^*}.$$

Observe from (4.20) that a noiseless R_b changes not only the Y parameters but also introduces many terms to $S_{v_a v_a^*}$ and $S_{i_a v_a^*}$, although noiseless R_b has no impact on $S_{i_a i_a^*}$. The thermal noise of R_b adds only a $4kTR_b$ term to $S_{v_a v_a^*}$. That is

$$C_A(\text{noisy } R_b) = C_A(\text{noiseless } R_b) + C_A^{R_b} = \begin{pmatrix} S_{v_a v_a^*} & S_{v_a i_a^*} \\ S_{i_a v_a^*} & S_{i_a i_a^*} \end{pmatrix} + \begin{pmatrix} 4kTR_b & 0 \\ 0 & 0 \end{pmatrix}. \tag{4.21}$$

Fig. 4.11 shows the simulation results for all three scenarios for chain noise representation. It is clear that R_b has only changed $S_{v_a v_a^*}$ and $\Re(S_{v_a i_a^*})$, and thermal noise contribution shows up only in $S_{v_a v_a^*}$. Intrinsic current noise dominates $S_{i_a i_a^*}$ and $\Im(S_{v_a i_a^*})$

4.3 Noise Parameter Implications

4.3.1 Analytical Models of Noise Parameters

To obtain additional insight into device design and optimization for device noise performance, analytical expressions of noise parameters are desirable. The noise figure and noise parameters can always be related to the noise representations and small-signal parameters of the device. In this section, we derive the expressions of noise parameters based on the simplified small-signal equivalent circuit. We assume device is at room temperature and equal to noise temperature 290 K.

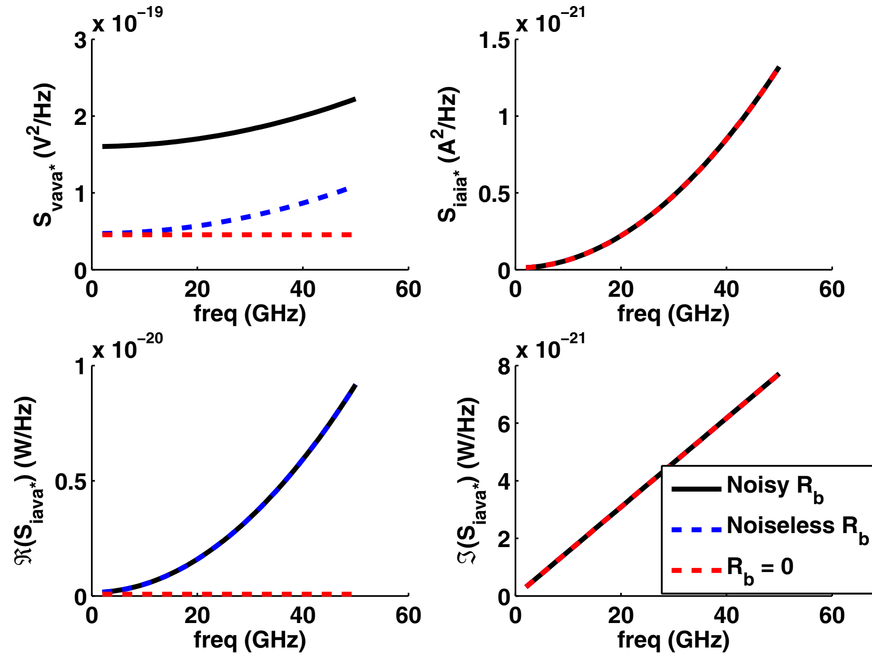

Figure 4.11: Correlation matrix of chain noise representation from calculation with $R_b = 0\Omega$, thermal noiseless R_b and thermal noisy R_b.

The simplified equivalent circuit is shown in Fig. 4.12. The intrinsic Y parameter can be obtained as,

$$\begin{aligned} Y_{11}^{INT} &= j\omega C_{be}; \\ Y_{21}^{INT} &= g_m; \\ Y_{12}^{INT} &= Y_{22}^{INT} = 0. \end{aligned} \tag{4.22}$$

Other assumption includes:

$$f_T = \frac{g_m}{2\pi C_{be}}. \tag{4.23}$$

The noise figure of the device can be defined as

$$F = 1 + \frac{Noise\ output\ due\ to\ device}{Noise\ output\ due\ to\ source}. \tag{4.24}$$

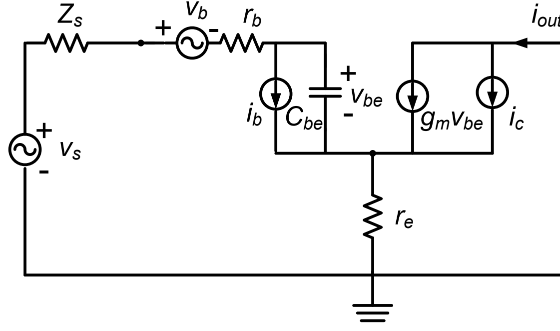

Figure 4.12: Equivalent small-signal circuit with source noise v_s, device thermal noise v_b and current noise i_b and i_c.

The transistor has noise sources including the terminal noise current i_c and i_b and the thermal noise v_b of base resistance r_b. Power Source has a noise source v_s. The source impedance is Z_S. Noise current i_c and i_b are correlated to each other, and thermal noise v_b is independent to i_c and i_b. Therefore, NF can be rewritten as

$$NF = 1 + \frac{< (i_{out,ic} + i_{out,ib}) \, , (i_{out,ic} + i_{out,ib})^* > + < i_{out,r_b}, i^*_{out,r_b} >}{< i_{out,R_s}, i^*_{out,R_s} >}. \tag{4.25}$$

$i_{out,ic}$, $i_{out,ib}$,i_{out,r_b} and i_{out,R_s} are output noise current respectively due to i_c, i_b, r_b and R_s (the real part of Z_S). They can be calculated by removing all the other noise sources.

$i_{out,ic}$

$$v_{be} \cdot j\omega C_{be} \cdot (Z_S + r_b) + v_{be} + (v_{be} \cdot j\omega C_{be} + g_m v_{be} + i_c) \, r_e = 0 \tag{4.26}$$

As r_e of device is small in the modern technology, we neglect r_e for now. The equivalent circuit is even simplified as in Fig. 4.13. Then

$$v_{be} = 0 \tag{4.27}$$

and

$$i_{out,ic} = i_c \tag{4.28}$$

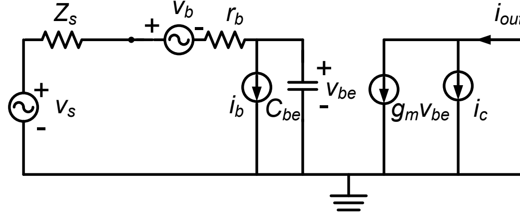

Figure 4.13: Equivalent small-signal circuit with source noise v_s, device thermal noise v_b and current noise i_b and i_c. Emitter resistance is neglected.

$i_{out,ib}$

$$(v_{be} \cdot j\omega C_{be} + i_b)(Z_S + r_b) + v_{be} = 0$$

$$v_{be} = -\frac{i_b (Z_S + r_b)}{j\omega C_{be}(Z_S + r_b) + 1} \tag{4.29}$$

and

$$i_{out,ib} = -\frac{g_m i_b (Z_S + r_b)}{j\omega C_{be}(Z_S + r_b) + 1}. \tag{4.30}$$

$< (i_{out,ic} + i_{out,ib}), (i_{out,ic} + i_{out,ib})^* >$

The output noise power produced by i_c and i_b is

$$(i_{out,ic} + i_{out,ib}), (i_{out,ic} + i_{out,ib})^*$$
$$= \left(i_c - \frac{g_m i_b (Z_S + r_b)}{j\omega C_{be}(Z_S + r_b) + 1} \right) \left(i_c - \frac{g_m i_b (Z_S + r_b)}{j\omega C_{be}(Z_S + r_b) + 1} \right)^* \tag{4.31}$$

As $Z_S = R_S + jX_S$, (4.31) can be written as

$$< (i_{out,ic} + i_{out,ib}), (i_{out,ic} + i_{out,ib})^* > = < i_c, i_c{}^* > + \frac{< i_b, i_b{}^* > g_m^2 |Z_S + r_b|^2}{1 + \omega^2 C_{be}^2 |Z_S + r_b|^2 - 2\omega C_{be} X_S}$$
$$- \frac{< i_c, i_b{}^* > g_m (Z_S + r_b)^* + < i_b, i_c{}^* > g_m (Z_S + r_b) + g_m j\omega C_{be} |Z_S + r_b|^2 (< i_c, i_b{}^* > - < i_b, i_c{}^* >)}{1 + \omega^2 C_{be}^2 |Z_S + r_b|^2 - 2\omega C_{be} X_S}$$

Let us define $< i_c, {i_b}^* >= (G_u + jB_u)\triangle f$ and $< i_b, {i_c}^* >= (G_u - jB_u)\triangle f$,

$< (i_{out,ic} + i_{out,ib}), (i_{out,ic} + i_{out,ib})^* >$

$$\begin{aligned} &=< i_c, {i_c}^* > + \frac{< i_b, {i_b}^* > g_m^2 \left| Z_S + r_b \right|^2}{1 + \omega^2 C_{be}^2 \left| Z_S + r_b \right|^2 - 2\omega C_{be} X_S} \\ &- \frac{2G_u \triangle f g_m \left(R_S + r_b \right) + 2B_u \triangle f g_m X_S - 2B_u \triangle f g_m \omega C_{be} \left| Z_S + r_b \right|^2}{1 + \omega^2 C_{be}^2 \left| Z_S + r_b \right|^2 - 2\omega C_{be} X_S} \end{aligned} \tag{4.32}$$

i_{out,r_b}

$$\begin{aligned} v_{be} \cdot j\omega C_{be} \left(Z_S + r_b \right) + v_{be} + v_b = 0 \\ v_{be} = -\frac{v_b}{j\omega C_{be} \left(Z_S + r_b \right) + 1} \end{aligned} \tag{4.33}$$

and

$$i_{out,r_b} = -\frac{g_m v_b}{j\omega C_{be} \left(Z_S + r_b \right) + 1} \tag{4.34}$$

$< i_{out,r_b}, {i_{out,r_b}}^* >$

The output noise power produced by r_b is

$$\begin{aligned} < i_{out,r_b}, {i_{out,r_b}}^* > &= \left(-\frac{g_m v_b}{j\omega C_{be} \left(Z_S + r_b \right) + 1} \right) \left(-\frac{g_m v_b}{j\omega C_{be} \left(Z_S + r_b \right) + 1} \right)^* \\ &= \frac{g_m^2 < v_b, {v_b}^* >}{1 + \omega^2 C_{be}^2 \left| Z_S + r_b \right|^2 - 2\omega C_{be} X_S} \end{aligned} \tag{4.35}$$

i_{out,R_S}

$$\begin{aligned} v_{be} \cdot j\omega C_{be} \left(Z_S + r_b \right) + v_{be} - v_S = 0 \\ v_{be} = \frac{v_S}{j\omega C_{be} \left(Z_S + r_b \right) + 1} \end{aligned} \tag{4.36}$$

and

$$i_{out,R_S} = \frac{g_m v_S}{j\omega C_{be} \left(Z_S + r_b \right) + 1} \tag{4.37}$$

$< i_{out,R_S}, i_{out,R_S}{}^* >$

The output noise power produced by R_S is

$$
\begin{aligned}
< i_{out,R_S}, i_{out,R_S}{}^* > &= \left(-\frac{g_m v_S}{j\omega C_{be}\left(Z_S + r_b\right) + 1}\right)\left(-\frac{g_m v_S}{j\omega C_{be}\left(Z_S + r_b\right) + 1}\right)^* \\
&= \frac{g_m^2 < v_S, v_S{}^* >}{1 + \omega^2 C_{be}^2 \left|Z_S + r_b\right|^2 - 2\omega C_{be} X_S}
\end{aligned} \tag{4.38}
$$

Noise figure

Substituting (4.32), (4.35) and (4.38) into (4.25) , we get

$$
\begin{aligned}
NF = 1 + \frac{r_b}{R_S} &+ \frac{S_{i_c i_c^*}\left(1 + \omega^2 C_{be}^2\left((R_S + r_b)^2 + X_S^2\right) - 2\omega C_{be} X_S\right)}{g_m^2 4KTR_S} \\
&+ \frac{S_{i_b i_b^*}\left((R_S + r_b)^2 + X_S^2\right)}{4KTR_S} - \frac{2G_u\left(R_S + r_b\right)}{g_m 4KTR_S} - \frac{2B_u X_S}{g_m 4KTR_S} + \frac{2B_u \omega C_{be}\left((R_S + r_b)^2 + X_S^2\right)}{g_m 4KTR_S}
\end{aligned} \tag{4.39}
$$

Therefore, the noise figure NF is related to the source impedance, the device small-signal equivalent circuit elements and the noise spectrum densities of internal terminal noise currents.

With $r_b = 0$

To find out the optimum X_S, X_{opt} to minimize the noise figure, we have

$$
\frac{\partial F}{\partial X_S} = 0 \tag{4.40}
$$

$$
X_S\left(S_{i_c i_c^*} + S_{i_b i_b^*}\left(\frac{\omega_T}{\omega}\right)^2 + 2B_u\frac{\omega_T}{\omega}\right) - \frac{1}{\omega C_{be}}\left(S_{i_c i_c^*} + B_u\frac{\omega_T}{\omega}\right) \tag{4.41}
$$

where $\omega_T = g_m / C_{be}$. Therefore, we obtain the expression of X_{opt},

$$
X_{opt} = \frac{\frac{1}{\omega C_{be}}\left(S_{i_c i_c^*} + B_u\frac{\omega_T}{\omega}\right)}{S_{i_c i_c^*} + S_{i_b i_b^*}\left(\frac{\omega_T}{\omega}\right)^2 + 2B_u\frac{\omega_T}{\omega}}. \tag{4.42}
$$

To find out the optimum R_S, similar to obtain X_{opt}, we have

$$
\frac{\partial F}{\partial R_S} = 0 \tag{4.43}
$$

$$S_{i_c i_c^*}\left(R_S^2-\left(X_S-\frac{1}{\omega C_{be}}\right)^2\right)+S_{i_b i_b^*}\left(R_S^2-X_S^2\right)\left(\frac{\omega_T}{\omega}\right)^2+2B_u\frac{\omega_T}{\omega}\left(R_S^2-X_S^2+\frac{X_S}{\omega C_{be}}\right)=0 \tag{4.44}$$

Substituting X_S with X_{opt} of (4.42), we obtain R_{opt},

$$R_{opt}^2=\frac{S_{i_c i_c^*}\left(\frac{1}{\omega C_{be}}\right)^2}{S_{i_c i_c^*}+S_{i_b i_b^*}\left(\frac{\omega_T}{\omega}\right)^2+2B_u\frac{\omega_T}{\omega}}-\left(\frac{\frac{1}{\omega C_{be}}\left(S_{i_c i_c^*}+B_u\frac{\omega_T}{\omega}\right)}{S_{i_c i_c^*}+S_{i_b i_b^*}\left(\frac{\omega_T}{\omega}\right)^2+2B_u\frac{\omega_T}{\omega}}\right)^2 \tag{4.45}$$

$$R_{opt}=\sqrt{\frac{S_{i_c i_c^*}\left(\frac{1}{\omega C_{be}}\right)^2}{S_{i_c i_c^*}+S_{i_b i_b^*}\left(\frac{\omega_T}{\omega}\right)^2+2B_u\frac{\omega_T}{\omega}}-\left(\frac{\frac{1}{\omega C_{be}}\left(S_{i_c i_c^*}+B_u\frac{\omega_T}{\omega}\right)}{S_{i_c i_c^*}+S_{i_b i_b^*}\left(\frac{\omega_T}{\omega}\right)^2+2B_u\frac{\omega_T}{\omega}}\right)^2} \tag{4.46}$$

Substituting (4.42) and (4.46) into (4.39) leads to an expression of NF_{min}:

$$NF_{min}=1-\frac{2G_u}{g_m 4KT}+\frac{\sqrt{S_{i_c i_c^*}S_{i_b i_b^*}-B_u^2}}{2KTg_m}. \tag{4.47}$$

As $|G_u| << |B_u|$, we assume $G_u=0$ here,

$$NF_{min}=1+\frac{\sqrt{S_{i_c i_c^*}S_{i_b i_b^*}-B_u^2}}{2KTg_m}. \tag{4.48}$$

With CB SCR model in Chapter 2,

$$S_{i_c i_c^*}=2qI_C, \tag{4.49}$$

$$S_{i_b i_b^*}=2qI_B+2qI_C(\omega\tau_c)^2, \tag{4.50}$$

$$G_u=0,\ B_u=-j2qI_C\omega\tau_c. \tag{4.51}$$

(4.47) is rewritten as

$$NF_{min}=1+\frac{q\sqrt{I_C I_B}}{KTg_m}. \tag{4.52}$$

It is clear to see that NF_{min} is independent of correlation between base and collector noise current and even independent of frequency. This is against existing understanding that noise correlation in general decreases NF_{min}, which also implies that the reduction of NF_{min} due to noise correlation

depends on r_b. With further simplification, $g_m = qI_C/KT$ and $\beta = I_C/I_B$,

$$NF_{min} = 1 + \sqrt{\frac{1}{\beta}}. \tag{4.53}$$

With thermal noiseless r_b

X_{opt} does not change compared to $r_b = 0$,

$$X_{opt} = \frac{\frac{1}{\omega C_{be}}\left(S_{i_c i_c^*} + B_u \frac{\omega_T}{\omega}\right)}{S_{i_c i_c^*} + S_{i_b i_b^*}\left(\frac{\omega_T}{\omega}\right)^2 + 2B_u \frac{\omega_T}{\omega}}. \tag{4.54}$$

R_{opt}

$$R_{opt}^2 = r_b^2 + \frac{\left(\frac{1}{\omega C_{be}}\right)^2\left(S_{i_c i_c^*} - 2G_u r_b g_m\right)}{S_{i_c i_c^*} + S_{i_b i_b^*}\left(\frac{\omega_T}{\omega}\right)^2 + 2B_u \frac{\omega_T}{\omega}} - \frac{\left(\frac{1}{\omega C_{be}}\right)^2\left(S_{i_c i_c^*} + B_u \frac{\omega_T}{\omega}\right)^2}{\left(S_{i_c i_c^*} + S_{i_b i_b^*}\left(\frac{\omega_T}{\omega}\right)^2 + 2B_u\left(\frac{\omega_T}{\omega}\right)\right)^2} \tag{4.55}$$

$$R_{opt} = \sqrt{r_b^2 + \frac{\left(\frac{1}{\omega C_{be}}\right)^2\left(S_{i_c i_c^*} - 2G_u r_b g_m\right)}{S_{i_c i_c^*} + S_{i_b i_b^*}\left(\frac{\omega_T}{\omega}\right)^2 + 2B_u \frac{\omega_T}{\omega}} - \frac{\left(\frac{1}{\omega C_{be}}\right)^2\left(S_{i_c i_c^*} + B_u \frac{\omega_T}{\omega}\right)^2}{\left(S_{i_c i_c^*} + S_{i_b i_b^*}\left(\frac{\omega_T}{\omega}\right)^2 + 2B_u\left(\frac{\omega_T}{\omega}\right)\right)^2}} \tag{4.56}$$

Substituting (4.54) and (4.56) into (4.39) and assuming $G_u = 0$, NF_{min} becomes

$$F_{min} = 1 + \frac{1}{2KT}\left(\frac{\omega}{\omega_T}\right)^2\left(R_{opt} + r_b\right)\cdot\left(S_{i_c i_c^*} + S_{i_b i_b^*}\left(\frac{\omega_T}{\omega}\right)^2 + 2B_u\frac{\omega_T}{\omega}\right). \tag{4.57}$$

Using the CB SCR transport model equations of (4.49),(4.50) and (4.51),

$$F_{min} = 1 + \left(\sqrt{g_m^2 r_b^2\left(\left(\frac{\omega}{\omega_T}\right)^2(1-\omega_T\tau_c)^2 + \frac{1}{\beta}\right)^2 + \frac{1}{\beta}} + g_m r_b\left(\left(\frac{\omega}{\omega_T}\right)^2(1-\omega_T\tau_c)^2 + \frac{1}{\beta}\right)\right). \tag{4.58}$$

$$F_{min} = 1 + \sqrt{g_m^2 r_b^2\left((1-\omega_T\tau_c)^2 + \frac{1}{\beta}\right)^2 + \frac{1}{\beta}} + g_m r_b\left(\left(\left(\frac{\omega}{\omega_T}\right)^2(1-\omega_T\tau_c)^2 + \frac{1}{\beta}\right)\right). \tag{4.59}$$

With r_b thermal noise

r_b does not impact on X_{opt}

$$X_{opt} = \frac{\frac{1}{\omega C_{be}} \left(S_{i_c i_c^*} + B_u \frac{\omega_T}{\omega} \right)}{S_{i_c i_c^*} + S_{i_b i_b^*} \left(\frac{\omega_T}{\omega} \right)^2 + 2B_u \frac{\omega_T}{\omega}}. \tag{4.60}$$

The thermal noise of r_b results in an additional term in R_{opt}^2

$$\begin{aligned} R_{opt}^2 = & \frac{4KTr_b \left(\frac{\omega_T}{\omega} \right)^2}{S_{i_c i_c^*} + S_{i_b i_b^*} \left(\frac{\omega_T}{\omega} \right)^2 + 2B_u \frac{\omega_T}{\omega}} + r_b^2 + \frac{\left(\frac{1}{\omega C_{be}} \right)^2 \left(S_{i_c i_c^*} - 2G_u r_b g_m \right)}{S_{i_c i_c^*} + S_{i_b i_b^*} \left(\frac{\omega_T}{\omega} \right)^2 + 2B_u \frac{\omega_T}{\omega}} \\ & - \frac{\left(\frac{1}{\omega C_{be}} \right)^2 \left(S_{i_c i_c^*} + B_u \frac{\omega_T}{\omega} \right)^2}{\left(S_{i_c i_c^*} + S_{i_b i_b^*} \left(\frac{\omega_T}{\omega} \right)^2 + 2B_u \left(\frac{\omega_T}{\omega} \right) \right)^2} \end{aligned} \tag{4.61}$$

$$R_{opt} = \frac{\sqrt{A}}{S_{i_c i_c^*} + S_{i_b i_b^*} \left(\frac{\omega_T}{\omega} \right)^2 + 2B_u \frac{\omega_T}{\omega}} \tag{4.62}$$

where

$$\begin{aligned} A = & r_b^2 \left(S_{i_c i_c^*} + S_{i_b i_b^*} \left(\frac{\omega_T}{\omega} \right)^2 + 2B_u \frac{\omega_T}{\omega} \right)^2 \\ & + \left(4KTr_b \left(\frac{\omega_T}{\omega} \right)^2 + S_{i_c i_c^*} \frac{1}{g_m^2} \left(\frac{\omega_T}{\omega} \right)^2 \right) \left(S_{i_c i_c^*} + S_{i_b i_b^*} \left(\frac{\omega_T}{\omega} \right)^2 + 2B_u \frac{\omega_T}{\omega} \right) \\ & - \frac{1}{g_m^2} \left(\frac{\omega_T}{\omega} \right)^2 \left(S_{i_c i_c^*} + B_u \frac{\omega_T}{\omega} \right)^2 \end{aligned} \tag{4.63}$$

Substituting (4.60) and (4.62) into (4.39) and assuming $G_u = 0$, the expression of NF_{min} is

$$F_{min} = 1 + \frac{r_b}{R_{opt}} + \frac{1}{2KT} \left(\frac{\omega}{\omega_T} \right)^2 \left(R_{opt} + r_b \right) \cdot \left(S_{i_c i_c^*} + S_{i_b i_b^*} \left(\frac{\omega_T}{\omega} \right)^2 + 2B_u \frac{\omega_T}{\omega} \right). \tag{4.64}$$

$$\begin{aligned} F_{min} = & 1 + \frac{r_b \left(S_{i_c i_c^*} + S_{i_b i_b^*} \left(\frac{\omega_T}{\omega}^2 \right) + 2B_u \frac{\omega_T}{\omega} \right)}{\sqrt{A}} \\ & + \frac{1}{2KT} \left(\frac{\omega}{\omega_T} \right)^2 \left(r_b \left(S_{i_c i_c^*} + S_{i_b i_b^*} \left(\frac{\omega_T}{\omega} \right)^2 + 2B_u \frac{\omega_T}{\omega} \right) + \sqrt{A} \right) \end{aligned} \tag{4.65}$$

Using the same transport model,

$$A = B * (2qI_C)^2 \tag{4.66}$$

where

$$\begin{aligned} B = & \left(\frac{1}{g_m}\right)^2 \left(\frac{\omega_T}{\omega}\right)^4 \frac{1}{\beta} \\ & + r_b \left((1-\omega_T\tau_c)^2 + \frac{1}{\beta}\left(\frac{\omega_T}{\omega}\right)^2\right) \cdot \\ & \left(\frac{2}{g_m}\left(\frac{\omega_T}{\omega}\right)^2 + r_b\left((1-\omega_T\tau_c)^2 + \frac{1}{\beta}\left(\frac{\omega_T}{\omega}\right)^2\right)\right) \end{aligned} \tag{4.67}$$

$$F_{min} = 1 + \frac{(1-\omega_T\tau_c)^2 + \frac{1}{\beta}\left(\frac{\omega_T}{\omega}\right)^2}{\sqrt{B}} \left(r_b + g_m\left(\frac{\omega}{\omega_T}\right)^2 \left(r_b\sqrt{B} + \frac{B}{(1-\omega_T\tau_c)^2 + \frac{1}{\beta}\left(\frac{\omega_T}{\omega}\right)^2}\right)\right) \tag{4.68}$$

4.3.2 Model comparison with measurement

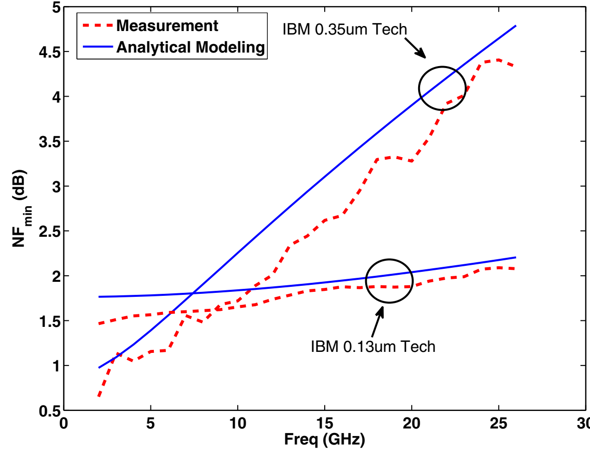

Figure 4.14: Comparison of NF_{min} calculated from analytical equations and measurement.

Fig. 4.14 compares analytical NF_{min} with measurement for two different technologies. The device from IBM 0.35 μm technology has a peak $f_T = 35$ GHz, $A_E = 0.8 \times 20 \times 3\mu m^2$ and total base resistance equal to 7 Ω. Device is biased at $I_C = 3.55$ mA and $f_T = 15$ GHz. $\tau_c = 0.75\tau_f$. The device from IBM 0.13 μm technology has a peak $f_T = 160$ GHz, $A_E = 0.12 \times 12\mu m^2$ and total

base resistance equal to 11 Ω. Device is biased at $I_C = 2.10$ mA and $f_T = 80$ GHz. $\tau_c = 0.4\tau_f$. For the device from IBM 0.35 μm technology, the calculated NF_{min} based on analytical model is at an average 0.3 dB higher than the measured NF_{min}; for the device from 0.13 μm technology, the calculated NF_{min} is at an average 0.15 dB higher than the measured NF_{min}. For both devices, the analytical model has captured the frequency dependence of NF_{min}.

We have established that the base resistances are the most important extrinsic circuit elements in determining the noise transfer functions for the propagation of the intrinsic terminal noise currents i_{ci} and i_{bi} towards the external terminals, and they can be approximately lumped into a single R_b for the device used. The best known role that R_b plays in the context of transistor noise discussion, however, is acting as a thermal noise source. One previously in general thinks of the intrinsic noise currents (i_{ci} and i_{bi}) and the resistor thermal noise current (i_{rb}) as independent noise sources. Comparison of (4.48) (4.57) and (4.65) shows that the correlation of i_c and i_b highly depends on the existence of R_b.

4.3.3 Simulation Results

A popular technique of comparing the relevant importance of noise sources is to turn on them individually and compare the noise parameters obtained with turning on them together. Modern simulators all support such comparison.

Fig. 4.15 shows the simulated NF_{min} at $I_C = 3.97$ mA in the situations of: 1) turning on thermal noise sources only (black), 2) turning on terminal current noise sources using CB SCR transport model only while keeping all the resistances noiseless (blue) and 3) turning on both thermal noise sources and terminal current noise sources (red). NF_{min} obtained with thermal noise only is clearly the smallest. The NF_{min} due to thermal noises is less than the NF_{min} due to intrinsic terminal current noises. In other words, R_b's impact on NF_{min} as thermal noise source is weak, although thermal noise contribution dominates $S_{i_{cx}i_{cx}^*}$ and $S_{i_{bx}i_{bx}^*}$ as shown in Fig 3.12. This is possible as NF_{min} is more directly related to the functions in the noise chain representation than in the admittance representation [43] [7][18].

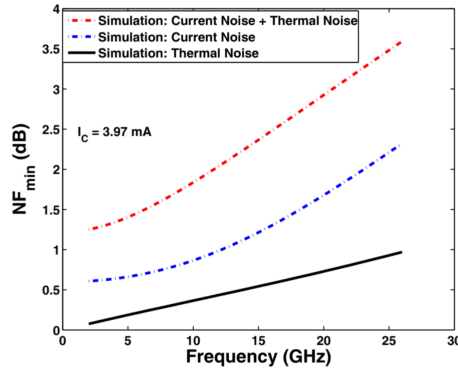

Figure 4.15: Comparison of NF_{min} from 50 GHz SiGe HBT as a function of frequency from simulations with correlated intrinsic terminal current noises due to CB SCR plus thermal noises, correlated intrinsic terminal current noises alone and thermal noises alone.

Next we examine R_b's impact as the dominant extrinsic circuit element on NF_{min}. We compare the simulation results using SPICE model and a more generic new model, which includes the noise transport in both intrinsic base and CB SCR and accurate to higher frequency than CB SCR transport model [35]. For both models, simulations are made with:

1. zero base resistances;
2. the base resistances as extracted experimentally, but with thermal noise turned off;
3. the base resistances as extracted experimentally, with thermal noise turned on.

The purpose is to distinguish R_b's two roles, as a thermal noise source, which is best known, and as the dominant extrinsic network element in determining propagation of i_{ci} and i_{bi} towards i_{cx} and i_{bx}.

Fig. 4.16 shows the noise parameters simulated at $I_C = 3.97$ mA from 2 to 50 GHz. For NF_{min}, the important findings include:

1. without R_b, NF_{min} from both uncorrelated and correlated model are much lower than with R_b. The difference is larger at higher frequency. Without R_b, the difference between using uncorrelated SPICE model and correlated new model can be barely observed at even

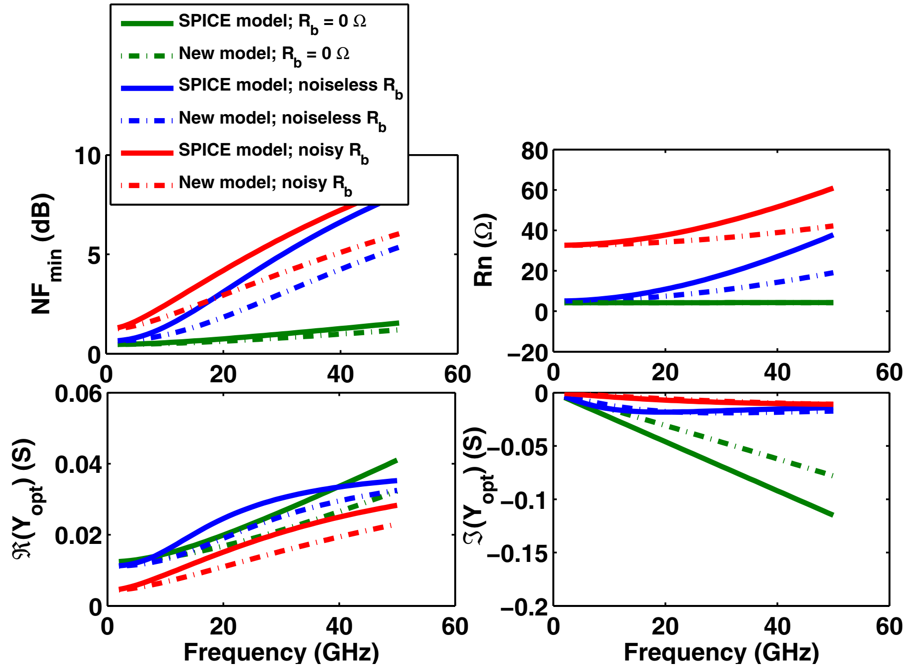

Figure 4.16: Simulated noise parameters using zero R_b, noiseless R_b and noisy R_b as a function of frequency at 3.97 mA; both uncorrelated SPICE model and new correlated model are included for comparison.

high frequency. So noise correlation does not fundamentally decrease NF_{min}, which was previously believed to be true [17][16] [28][47][48][34][35].

2. it is however true that noise correlation reduces NF_{min}, for the R_b value found in the actual device, whether R_b is noisy or noiseless. This means reduction of NF_{min} by correlation is R_b dependent, and thus will vary with technology.

3. NF_{min} increases considerably with noiseless R_b, for both uncorrelated and correlated i_{ci} and i_{bi}, although R_b as a noise source itself leads to small NF_{min}.

4. thermal noise of R_b further increases NF_{min}.

Therefore reduction of R_b should continue to be a priority in future technology development, not only for higher f_{max} and power gain, but also for lower NF_{min}, despite the fact that the NF_{min} due to R_b's thermal noise is already negligible.

R_n is very small without R_b and almost frequency independent with either model and thermal noise of R_b further increases R_n. Without R_b, the magnitude of $\Im(Y_{opt})$ is higher than $\Re(Y_{opt})$ at high frequency. With R_b, the magnitudes of $\Im(Y_{opt})$ from both two models decrease and become close to each other. Both magnitudes of $\Re(Y_{opt})$ and $\Im(Y_{opt})$ decrease after adding the thermal noise of R_b.

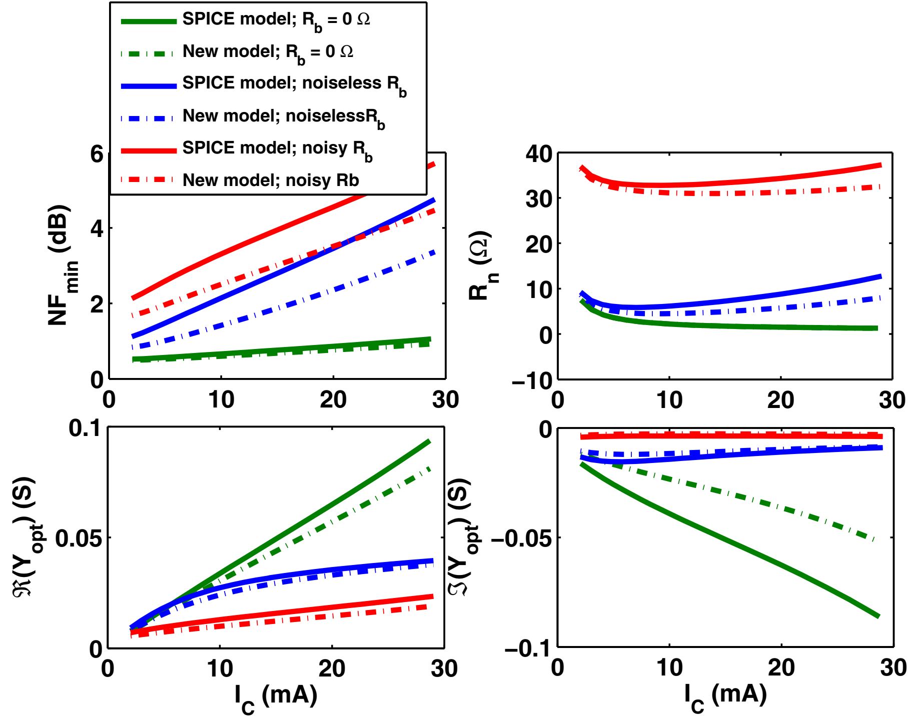

Figure 4.17: Simulated noise parameters using zero R_b, noiseless R_b and noisy R_b as a function of I_C at 10 GHz; both uncorrelated SPICE model and new correlated model are included for comparison.

Fig. 4.17 shows bias dependent noise parameter simulation results at 10 GHz. The major difference between different models emerges after adding noiseless R_b and the difference increases with increasing I_C. Noisy R_b further adds approximately 1 dB NF_{min}. Both magnitudes of $\Re(Y_{opt})$ and $\Im(Y_{opt})$ are higher without R_b, and the magnitudes of $\Re(Y_{opt})$ and $\Im(Y_{opt})$ from uncorrelated model are lower than from correlated model. Opposite to NF_{min} and R_n, Y_{opt} from two models are close to each other with R_b. With R_b, the magnitudes of $\Re(Y_{opt})$ from both two models decrease, as well as $\Im(Y_{opt})$. Noisy R_b further decreases the magnitudes of $\Re(Y_{opt})$ and $\Im(Y_{opt})$.

4.4 Conclusions

Analytical expressions of noise correlation matrices for various noise representations are derived and used to successfully explain simulation and measurement results. Relative importance of individual noise sources is examined for all elements of the noise correlation matrices of the Y, Z and chain representations. The base resistances are identified to be the dominant extrinsic transistor equivalent circuit elements that determine the propagation of the intrinsic terminal current noises towards the extrinsic terminals. Further insight is then obtained into how correlated intrinsic current noises and base resistances affect transistor noise parameters. For the first time, we show that the reduction of NF_{min} by noise correlation is a strong function of R_b, and for zero R_b, noise correlation would have no impact on NF_{min}. As far as the impact on transistor NF_{min} is concerned, base resistance thermal noise as a noise source is actually not that important. Instead, R_b as a circuit element, modifies the transfer of intrinsic noise currents towards extrinsic terminals, and such modification causes significant *increase* of NF_{min}, particularly at higher frequency, regardless of whether the intrinsic terminal noise currents are correlated or not. The reduction of transistor NF_{min} by correlation is shown to be a strong function of R_b.

Chapter 5

Impact on Low Noise Amplifier Design

Low noise amplifier (LNA), usually the first stage of the receiver, must be able to amplify low noise as low as -100 dBm, while maintaining sufficient signal-to-noise-ratio and adding sufficient low noise to the circuit. The main contributor to the LNA noise figure is the RF noise of the transistor. In the previous chapter,we have discussed the noise physics and presented noise model on the transistor level. Adding correlation of terminal noise base and collector current has successfully improved the accuracy of the noise modeling results. On the circuit level, however, additional question remains.

An important RF property of bipolar transistor derived in [50] is that simultaneous noise and impedance match can be achieved through transistor sizing and the use of two inductors placed the emitter and base. At a given J_C, real part of noise matching is achieved by adjusting transistor size such that R_{opt} = 50 Ω, in a 50 Ω system. An emitter inductor L_e provides an input resistance R_{in} =50 Ω. A base inductor L_b cancels out the input reactance and at the same time transforms the source noise matching reactance of the LNA to 0 Ω. This important property that highly simplifies RF LNA design, however, was derived using the SPICE noise model that does not consider the frequency dependent correlation, together with additional approximations. A logical question is how frequency dependent correlation affects simultaneous noise and (input) impedance matching.

5.1 Analytical derivation of LNA noise figure

Assuming that the RF operating frequency is far above f_β (where the ac β begins to decrease mainly due to C_{be}), and that Miller effect is negligible, the equivalent circuit of an simple LNA consisting one single transistor can be shown as in Fig. 5.1.

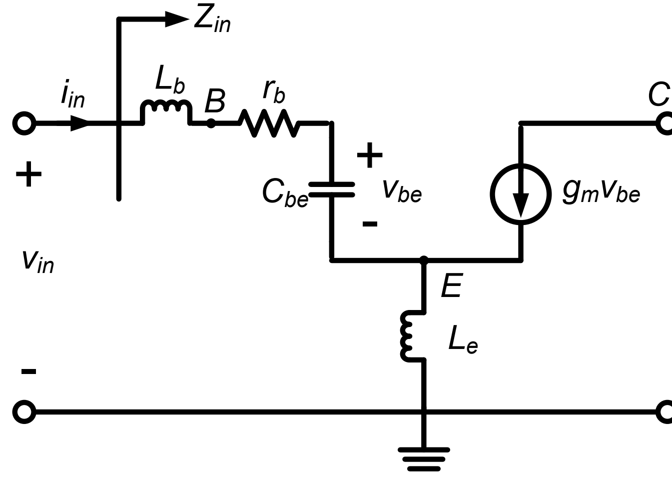

Figure 5.1: Simplified equivalent circuit for a transistor with an emitter inductor L_e and a base inductor L_b.

Next we consider the noise of the LNA. As illustrated in Fig. 5.2, the transistor has noise sources including the terminal noise current i_c and i_b and the thermal noise v_b of base resistance R_b. Power Source has a noise source v_s. We now derive the noise figure of the transistor with L_e and L_b. The noise figure of LNA is defined as

$$NF = 1 + \frac{\textit{Noise output due to LNA}}{\textit{Noise output due to source}}. \tag{5.1}$$

Using the very same method of single transistor noise figure derivation in Chapter 4, the analytical expression of LNA's noise parameters can be obtained as,

$$X_{opt,LNA} = \frac{\frac{1}{\omega C_{be}}\left(S_{i_c i_c^*} + B_u \frac{\omega_T}{\omega}\right)}{S_{i_c i_c^*} + S_{i_b i_b^*}\left(\frac{\omega_T}{\omega}\right)^2 + 2B_u \frac{\omega_T}{\omega}} + \omega\left(L_e + L_b\right). \tag{5.2}$$

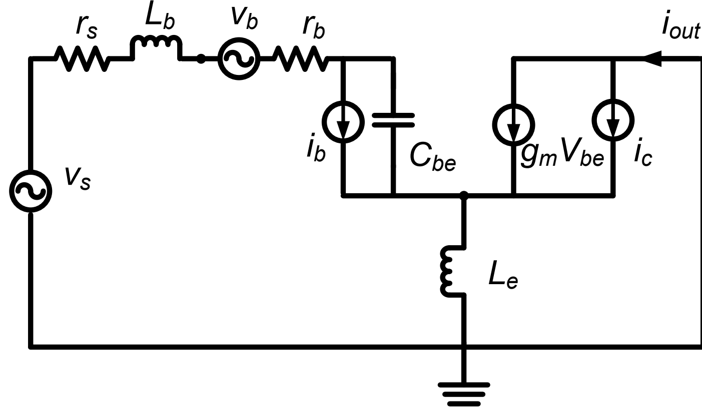

Figure 5.2: Simplified equivalent circuit for a "noisy" transistor with an emitter inductor L_e and a base inductor L_b. The transistor has noise sources including the terminal noise current i_c and i_b and the thermal noise v_b of base resistance R_b. Power Source has a noise source v_s.

$$R_{opt,LNA}^2 = \frac{4KTR_b\left(\frac{\omega_T}{\omega}\right)^2}{S_{i_c i_c^*} + S_{i_b i_b^*}\left(\frac{\omega_T}{\omega}\right)^2 + 2B_u\frac{\omega_T}{\omega}} + R_b^2 + \frac{\left(\frac{1}{\omega C_{be}}\right)^2\left(S_{i_c i_c^*} - 2G_u R_b g_m\right)}{S_{i_c i_c^*} + S_{i_b i_b^*}\left(\frac{\omega_T}{\omega}\right)^2 + 2B_u\frac{\omega_T}{\omega}} - \frac{\left(\frac{1}{\omega C_{be}}\right)^2\left(S_{i_c i_c^*} + B_u\frac{\omega_T}{\omega}\right)^2}{\left(S_{i_c i_c^*} + S_{i_b i_b^*}\left(\frac{\omega_T}{\omega}\right)^2 + 2B_u\left(\frac{\omega_T}{\omega}\right)\right)^2} \tag{5.3}$$

$$F_{min,LNA} = 1 + \frac{R_b}{R_{opt}} + \frac{1}{2KT}\left(\frac{\omega}{\omega_T}\right)^2\left(R_{opt} + R_b\right)\cdot\left(S_{i_c i_c^*} + S_{i_b i_b^*}\left(\frac{\omega_T}{\omega}\right)^2 + 2B_u\frac{\omega_T}{\omega}\right). \tag{5.4}$$

Compared with (4.60) (4.62) and (4.64), the noise parameters of LNA can be related to the noise parameters of the transistor alone as

$$X_{opt,LNA} = X_{opt} + \omega\left(L_e + L_b\right) \tag{5.5}$$

$$R_{opt,LNA} = R_{opt} \tag{5.6}$$

$$NF_{min,LNA} = NF_{min} \tag{5.7}$$

Adding L_e and L_b does not impact on R_{opt} and NF_{min} but impacts on X_{opt}. The above conclusion was previous obtained based on derivation with uncorrelated intrinsic terminal current noise, and adding the correlation of i_b and i_c does not vitiate it.

5.2 Simultaneous noise and impedance matching

Next we inspect whether the simultaneous noise and impedance matching is still valid. As shown in Fig. 5.1, the input impedance looking into the circuit before L_b is given by

$$Z_{in} = \frac{v_{in}}{i_{in}}, \tag{5.8}$$

where

$$i_{in} = v_{be} \cdot j\omega C_{be}, \tag{5.9}$$

and

$$v_{in} = (j\omega L_b + R_b) \cdot i_{in} + v_{be} + j\omega L_e (i_{in} + g_m v_{be}). \tag{5.10}$$

Substituting (5.9) and (5.10) into (5.8),

$$Z_{in} = j\omega L_b + j\omega L_e + R_b + \frac{1}{j\omega C_{be}} + \omega_T L_e, \tag{5.11}$$

as

$$\omega_T = \frac{g_m}{C_{be}}. \tag{5.12}$$

The ac β is also defined as

$$\beta_{RF} = \frac{g_m}{j\omega C_{be}} = \frac{\omega_T}{j\omega}. \tag{5.13}$$

A resistive component $\omega_T L_e$ is produced by using the emitter inductor. The value of L_e and L_b is needed to match the RF source impedance, meaning

$$\Re(Z_{in}) = R_b + \omega_T L_e = R_S, \tag{5.14}$$

and

$$\Im(Z_{in}) = \omega L_b + \omega L_e - \frac{1}{\omega C_{be}} = 0. \tag{5.15}$$

For simultaneous impedance and noise matching, the values of L_e and L_b required for the source impedance matching should be identical to the values required for $R_{opt} = R_S$ and $X_{opt} = 0\Omega$. Thus

$$X_{opt,LNA} = \frac{\frac{1}{\omega C_{be}}\left(S_{i_c i_c^*} + B_u \frac{\omega_T}{\omega}\right)}{S_{i_c i_c^*} + S_{i_b i_b^*}\left(\frac{\omega_T}{\omega}\right)^2 + 2B_u \frac{\omega_T}{\omega}} + \omega\left(L_e + L_b\right) = 0. \tag{5.16}$$

$$R_{opt,LNA}^2 = R_S^2 = \frac{4KTR_b\left(\frac{\omega_T}{\omega}\right)^2}{S_{i_c i_c^*} + S_{i_b i_b^*}\left(\frac{\omega_T}{\omega}\right)^2 + 2B_u \frac{\omega_T}{\omega}} + R_b^2 + \frac{\left(\frac{1}{\omega C_{be}}\right)^2\left(S_{i_c i_c^*} - 2G_u R_b g_m\right)}{S_{i_c i_c^*} + S_{i_b i_b^*}\left(\frac{\omega_T}{\omega}\right)^2 + 2B_u \frac{\omega_T}{\omega}} - \frac{\left(\frac{1}{\omega C_{be}}\right)^2\left(S_{i_c i_c^*} + B_u \frac{\omega_T}{\omega}\right)^2}{\left(S_{i_c i_c^*} + S_{i_b i_b^*}\left(\frac{\omega_T}{\omega}\right)^2 + 2B_u\left(\frac{\omega_T}{\omega}\right)\right)^2} \tag{5.17}$$

The value of $R_{opt,LNA}$ can be obtained though sizing the transistor. $X_{opt} = 0$ requires

$$\frac{\frac{1}{\omega C_{be}}\left(S_{i_c i_c^*} + B_u \frac{\omega_T}{\omega}\right)}{S_{i_c i_c^*} + S_{i_b i_b^*}\left(\frac{\omega_T}{\omega}\right)^2 + 2B_u \frac{\omega_T}{\omega}} = \frac{1}{\omega C_{be}}. \tag{5.18}$$

This condition can be automatically satisfied when we have

$$f = \sqrt{\frac{f_T}{\beta \tau_c}}, \tag{5.19}$$

β is the DC current gain. τ_c is proportional to τ_f. Even we assuming τ_c and β is constant before high injection, strict simultaneous noise and impedance matching can be only achieved by carefully choosing frequency at a certain bias, as f_T is bias dependent.

5.3 Simulation Results based on a Cascade LNA

Simulations are based on the SiGe HBT with 36 GHz peak f_T. The design kit provided by IBM uses the HICUM model for HBTs. The CB SCR noise model is used. The collector transit time parameter was extracted by fitting measured noise parameters. Other compact model parameters were extracted by fitting dc I-V curves and y-parameters.

Fig. 5.3 shows the modeled and measured noise parameters versus current density (J_C) at V_{CE} = 3.3 V and f = 5 GHz, including the minimum noise figure (NF_{min}), noise resistance (R_n),

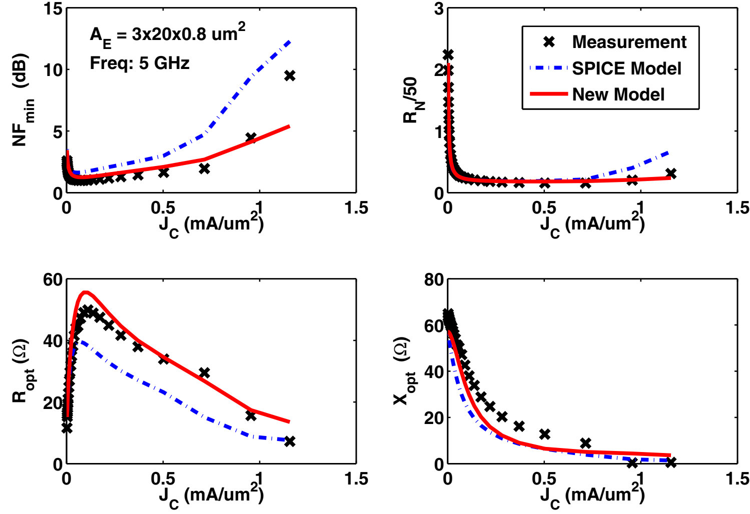

Figure 5.3: Modeled and measured noise parameters versus J_C at 5 GHz.

real and imaginary part of noise matching source impedance (R_{opt} and X_{opt}). The SiGe HBT used has an emitter area of 0.8×20×3 μm^2 and a peak f_T of 36 GHz. Noise measurements were made using an ATN system, and noises of the probing pads and interconnects leading from the pads to HBT terminals are de-embedded with open-short method. The CB SCR model produces much more accurate noise parameters than the SPICE noise model as expected. Observe that the noise matching source resistance R_{opt} from measurement and new model are higher than from the SPICE model. Consequently, at a given current density J_C (or V_{BE}), for noise matching through transistor sizing, one needs to use a larger size than given by the SPICE model, as detailed below.

A cascode topology shown in Fig. 5.4 is chosen for its better reverse isolation and excellent frequency stability [51]. C_b is for DC blocking, and L_{bias} is for AC blocking. Here we choose to use the same size for Q_1 and Q_2. Size adjustment is made by changing emitter length (L_E). We also optimize the output matching network for output impedance matching. R_c is fixed during optimization but can be optimized as well.

Fig. 5.5 shows the noise matching source impedance designs using new correlated model versus J_C at 5 GHz and 10 GHz. Real part noise matching is achieved using the size calculated from R_{opt} per emitter length (L_E), without optimization. $X_{opt,LNA}$ is generally close to 0 Ω. At

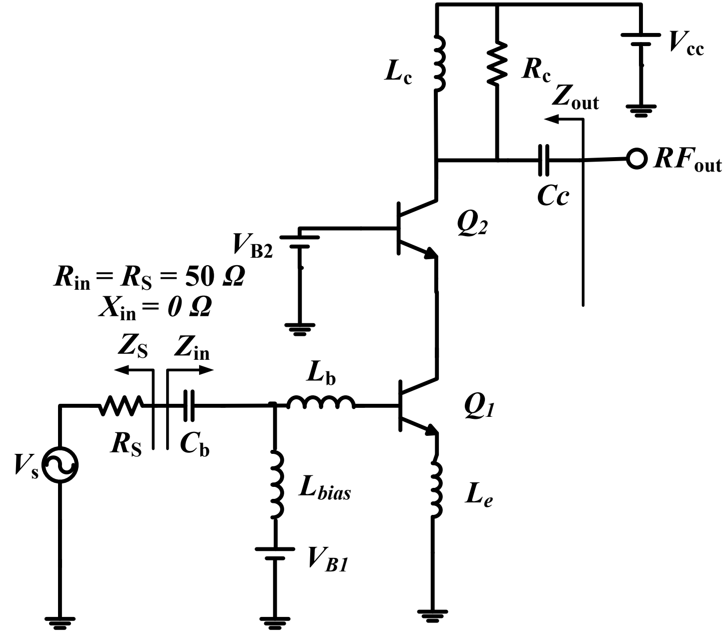

Figure 5.4: Schematic of the SiGe HBT cascode LNA used.

both 5 GHz and 10 GHz, $X_{opt,LNA}$ decreases with J_C increasing. $X_{opt,LNA} = 0\Omega$ happens at smaller J_C at 5 GHz than at 10 GHz. This can be explained by (5.19), as f_T increases with J_C before high injection and a smaller f_T is required at 5 GHz than at 10 GHz and thus smaller J_C to achieve simultaneous noise and impedance matching.

Fig. 5.6 shows L_E and I_C of cascode LNAs designed by using SPICE and new noise model versus J_C at 5 GHz. For the J_C, a larger emitter length is required for source resistance noise match, i.e. $R_{opt} = 50\Omega$, in all the new correlated noise model LNA designs. This directly translates into a higher I_C and thus higher power consumption at simultaneous noise and input impedance matching. The root cause of this can be found from transistor R_{opt} difference between two models. for the same transistor size, the new model R_{opt} is higher than SPICE model R_{opt}. Compared to measurements and the new model, the SPICE noise model underestimates R_{opt}, and consequently requires a smaller emitter length for adjusting R_{opt} to 50 Ω.

Fig. 5.7 shows NF_{LNA} and $NF_{min,LNA}$, gain and IIP3 of versus J_C at 5 GHz. For designs made using both models, NF_{LNA} is nearly identical to $NF_{min,LNA}$. Given that noise matching is done for

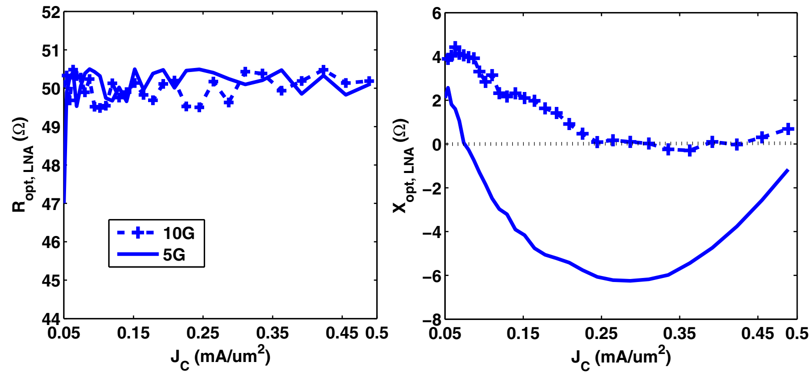

Figure 5.5: The noise matching source impedance of design using the correlated noise model versus J_c at 5 GHz and 10 GHz.

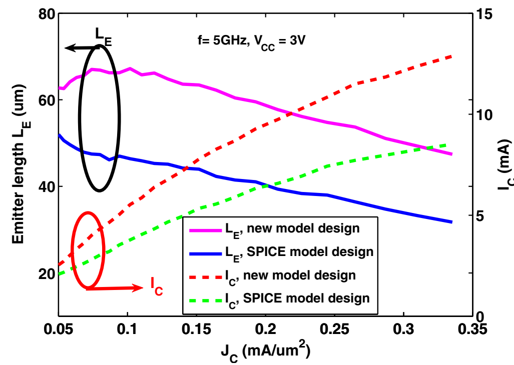

Figure 5.6: Emitter length (L_E) for R_{opt}=50 Ω and I_C versus J_C at 5 GHz.

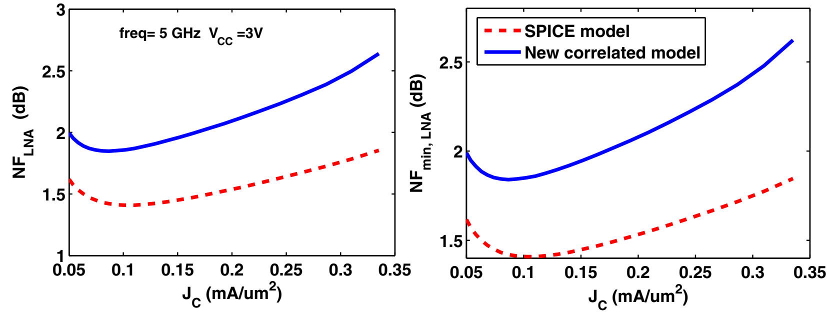

Figure 5.7: NF_{LNA} and $NF_{min,LNA}$ of designs using SPICE and new noise models versus J_C at 5 GHz.

both model designs, NF_{LNA} follows NF_{min}, which is higher for the SPICE model, as we expect from transistor level modeling shown earlier in Fig. 5.3.

However, experiment of re-simulating the SPICE model designed LNAs using our new correlated noise model shows that the SPICE model designs is fairly close to the noise figure of the new model designs, despite the clear inaccuracy of the SPICE noise model used in the design [52]. The reason is that the noise conductance G_n remains small enough such that the resulting $F - F_{min}$ is small compared to F_{min}. As a result, NF_{LNA} is still dominated by $NF_{min,LNA}$.

5.4 Conclusion

We have examined the impact of high frequency noise correlation on LNA design and performance. Analytical derivation shows that simultaneous noise and input impedance matching conditionally holds in presence of high frequency noise correlation. Noise matching, however, requires a considerably larger transistor and power consumption.

Bibliography

[1] J. D. Cressler, "SiGe HBT BiCMOS technology for extreme environment applications," in *JPL Extreme Environment Workshop*, 2005.

[2] J. S. Dunn, D. C. Ahlgren, and et al, "Foundation of rf CMOS and SiGe BiCMOS technologies," *IBM Journal of Research and Development*, vol. 47, no. 2, pp. 101–138, 2003.

[3] J. D. Cressler, *The Silicon Heterostructure Handbook: Materials, Fabrication, Devices, Circuits, and Applications of SiGe and Si Strained-Layer Epitaxy*. Cambridge University Press, 2010.

[4] P. Sakalas, J. Herricht, M. Ramonas, and M. Schroter, "Noise modeling of advanced technology high speed SiGe HBTs," in *Dig. of IEEE BCTM*, pp. 169–172, 2010.

[5] K. Xia, *Improved RF Noise Modeling for Silicon-Germanium Heterojunction Bipolar Transistor*. Auburn University, 2006.

[6] J. D. Cressler, "SiGe HBT Technology: A New Contender for Si-Baed RF and Microwave Circuit Applications," *IEEE Transactions on Microwave Theory and Techniques*, vol. 46, no. 5, pp. 572–589, 1998.

[7] J. D. Cressler and G. Niu, *Silicon-Germanium Heterojunction Bipolar Transistors*. Artech House, 2003.

[8] http://www.dotfive.eu.

[9] F. Bonani and G. Ghione, *Noise in Semi-conductor Devices: Modeling and Simulation*. Springer, 2001.

[10] W. Shockley, J. Copeland, and R. James, "The impedance field method of noise calculation in active semiconductor devices," *Quantum theory of atoms, molecules, and the solid-state.*, vol. 46, no. 5, pp. 537–563, 1966.

[11] M. Reisch, *High-Frequency Bipolar Transistors*. Springer, 2003.

[12] A. van der Ziel, *Noise in Solid State Devices and Circuit*. Wiley, New York, 1986.

[13] J. B. Johnson, "Thermal Agitation of Electricity in Conductors," *Phys. Rev.*, vol. 32, no. 1, pp. 97–109, 1928.

[14] H. Nyquist, "Thermal Agitation of Electric Charge in Conductors," *Phys. Rev.*, vol. 32, no. 1, pp. 110–113, 1928.

[15] G. Niu, “Noise in SiGe HBT RF Technology: Physics, Modeling, and Circuit Implications,” in *Proceedings of the IEEE*, pp. 1583–1597, 2005.

[16] G. Niu, J. D. Cressler, S. Zhang, W. E. Ansley, C. Webster, and D. L. Harame, “A Unified Approach to RF and Microwave Noise Parameter Modeling in Bipolar Transistors,” *IEEE Transactions on Electron Devices*, vol. 48, no. 11, pp. 2568–2573, 2001.

[17] M. Rudolph, R. Doerner, L. Klapproth, and P. Heymann, “An HBT noise model valid up to transit frequency,” *IEEE Electron Device Letters*, vol. 20, no. 1, pp. 24–26, 1999.

[18] H. Haus, W. Atkinson, G. Branch, W. Davenport, W. Fonger, W. Harris, S. Harrison, W. McLeod, E. Stodola, and T. Talpey, “Representation of noise in linear twoports,” in *Proceedings of the IRE*, pp. 69–74, 1960.

[19] L. Escotte, R. Plana, and J. Graffeuil, “Evaluation of Noise Parameter Extraction Methods,” *IEEE Transactions on Microwave Theory and Techniques*, vol. 41, no. 3, pp. 382–387, 1993.

[20] C. T. Stelzried, *Noise Temperature and Noise Figure Concepts: DC to Light*. TDA Mission Support Office, 1981.

[21] P. Chevalier, F. Pourchon, T. Lacave, G. Avenier, Y. Campidelli, L. Depoyan, G. Troillard, M. Buczko, D. Gloria, D. Celi, C. Gaquiere, , and A. Chantre, “Compact modeling of collector base junction space charge region transit time effect on noise in SiGe HBTs,” in *Dig. of IEEE BCTM*, pp. 1–4, 2009.

[22] IBM, *SiGe BiCMOS 5PAe: Advanced Through-Silicon Via Technology for RF Power Applications*. https://www-01.ibm.com.

[23] K. M. van Vliet, “General Transport Theory of Noise in PN Junction-like Devices-I. Three-dimensional Green’s Function Formulstion,” *Solid State Electron*, vol. 15, pp. 1033–1053, 1972.

[24] J. te Winkel, “Extended Charge-Control Model For Bipolar Transistors,” *IEEE Transactions on Electron Devices*, vol. 20, no. 4, pp. 389–394, 1973.

[25] K. Xia and G. Niu, “Discussions and Extension of van Vliet’s Noise Model for High Speed Bipolar Transistors,” *Solid State Electronics*, vol. 53, no. 3, pp. 349–354, 2009.

[26] K. Xia and G. Niu, “Impact of Collector-Base Space Charge Region on RF Noise in Bipolar Transitors,” in *Dig. of IEEE BCTM*, pp. 166–169, 2006.

[27] K. Xia and G. Niu, “Modeling the input non-quasi-static effect in small signal equivalent circuit based on charge partitioning for bipolar transistors and its impact on RF noise modeling,” *Solid State Electronics*, vol. 54, no. 12, pp. 1566–1571, 2010.

[28] J. C. J. Paasschens, R. J. Havens, and L. Tiemeijer, “Modeling the Correlation in the High-Frequency Noise of (Hetero-junction) Bipolar Transistors using Charge-Partitioning,” in *Dig. of IEEE BCTM*, pp. 221–224, 2003.

[29] P. Sakalas, J. Herricht, A. Chakravorty, and M. Schroter, “Compact Modeling of High Frequency Correlated Noise in HBTs,” in *Dig. of IEEE BCTM*, pp. 279–282, 2006.

[30] H. Klose and P. Russer, “The Transient Integral Charge Control Relation-A Novel Formulation of the Currents in a Bipolar Transistor,” *IEEE Trans. on Electron Devices*, vol. 34, pp. 1090–1099, 1987.

[31] G. Hurkx, “A new approach to A.C. characterization of bipolar transistors,” *Solid-State Electronics*, vol. 31, pp. 1269–1275, 1988.

[32] M. Rudolph, , F. Korndorfer, P. Heymann, and W. Heinrich, “Compact Large-Signal Shot-Noise Model for HBTs,” *IEEE Transactions on Microwave Theory and Techniques*, vol. 56, no. 1, pp. 7–14, 2008.

[33] C. Jungemann, B. Neinhus, B. Meinerzhagen, and R. W. Dutton, “Investigation of Compact Models for RF Noise in SiGe HBTs by Hydrodynamic Device Simulation,” *IEEE Transactions on Electron Devices*, vol. 51, no. 6, pp. 956–961, 2004.

[34] Z. Xu, G. Niu, and R. M. Malladi, “Compact modeling of collector base junction space charge region transit time effect on noise in SiGe HBTs,” in *IEEE Topical Meeting on SiRF Dig.*, pp. 180–183, 2010.

[35] K. Xia, G. Niu, and Z. Xu, “A New Approach to Implementing High-Frequency Correlated Noise for Bipolar Transistor Compact Modeling,” *IEEE Transactions on Electron Devices*, vol. 59, no. 2, pp. 302–308, 2012.

[36] C. C. McAndrew, J. A. Seitchik, and et al, “VBIC95, the vertical bipolar inter-company model,” *IEEE Journal of Solid-State Circuits*, vol. 31, no. 10, pp. 1476–1483, 1996.

[37] R. L. Pritchard, *Electrical Characteristics of Transistors*. McGraw-Hill, New York, 1967.

[38] C. C. McAndrew, G. Coram, A. Blaum, and O. Pilloud, “Correlated Noise Modeling and Simulation,” *WCM*, pp. 40–45, 2005.

[39] IBM, *SiGe BiCMOS 5PAe: Advanced Through-Silicon Via Technology for RF Power Applications*. https://www-01.ibm.com., 2007.

[40] G. Niu, K. J. Xia, D. Sheridan, and D. L. Harame, “Experimental extraction and model evaluation of base and collector RF noise in SiGe HBTs,” in *Proc. of IEEE RFIC*, pp. 615–618, 2004.

[41] Q. Liang, J. D. Cressler, G. Niu, Y. Lu, G. Freeman, D. C. Ahlgren, R. M. Malladi, K. Newton, and D. L. Harame, “A simple four-port parasitic deembedding methodology for high-frequency scattering parameter and noise characterization of bSiGe HBTs,” *IEEE Transactions on Microwave Theory and Techniques*, vol. 51, no. 11, pp. 2165–2174, 2003.

[42] K. Chen, H. Chen, G. Huang, W. Liao, and C. Chang, “RF noise modeling of SiGe HBTs using four-port de-embedding method,” in *Dig. of APMC*, pp. 1–4, 2008.

[43] H. Hillbrand and P. Russer, "An efficient method for computer aided noise analysis of linear networks," *IEEE Trans. Circuits and System*, vol. 23, pp. 235–238, 1976.

[44] *Verilog-AMS Language Reference Manual, Ver. 2.2*. http://www.eda.org/verilog-ams.

[45] Agilent, *Advanced Design System (ADS)*. http://www.agilent.com.

[46] IBM, *SiGe BiCMOS 7WL*. https://www-01.ibm.com.

[47] K. Xia, G. Niu, D. C. Sheridan, and S. L. Sweeney, "Frequency and Bias-Dependent Modeling of Correlated Base and Collector Current RF Noise in SiGe HBTs Using Quasi-Static Equivalent Circuit," *IEEE Transactions on Electron Devices*, vol. 53, no. 3, pp. 515–552, 2006.

[48] K. H. K. Yau and S. P. Voinigescu, "Modeling and extraction of SiGe HBT noise parameters from measured Y-parameters and accounting for noise correlation," in *IEEE Topical Meeting on SiRF Dig.*, pp. 226–229, 2006.

[49] Z. Xu and G. Niu, "Compact Modeling Based Extraction of RF Noise in SiGe HBT Terminal Currents," in *IEEE Topical Meeting on SiRF Dig.*, pp. 137–140, 2012.

[50] S. P. Voinigescu, M. C. Maliepaard, J. L. Showell, G. E. Babcock, D. Marchesan, M. Schroter, P. Schvan, and D. L. Harame, "A scalable high-frequency noise model for bipolar transistors with application to optimal transistor sizing for low-noise amplifier design," *IEEE Solid State Circuits*, vol. 32, no. 9, pp. 1430–1439, 1997.

[51] D. K. Shaeffer and T. H. Lee, "A 1.5-v 1.5ghz CMOS low noise amplifier," *IEEE Solid State Circuits*, vol. 32, no. 5, pp. 745–759, 1997.

[52] P. Shen, G. Niu, Z. Xu, and W. Zhang, " Impact of high frequency correlated noise on SiGe HBT low noise amplifier design ," in *IEEE Topical Meeting on SiRF Dig.*, pp. 125–128, 2012.

[53] Y. Cui, *High Frequency Noise Modeling and Microscopic Noise Simulation for SiGe HBT and RF CMOS*. Auburn University, 2005.

Appendices

Appendix A

Noise Representation Transformation

The transformation equations are copied from [53].

ABCD $\leftrightarrow$ Y

$$\begin{pmatrix} I_1 - i_a \\ I_2 \end{pmatrix} = \begin{bmatrix} Y_{11} & Y_{12} \\ Y_{21} & Y_{22} \end{bmatrix} \cdot \begin{pmatrix} V_1 - v_a \\ V_2 \end{pmatrix},$$

$$\begin{pmatrix} I_1 - i_1 \\ I_2 - i_2 \end{pmatrix} = \begin{bmatrix} Y_{11} & Y_{12} \\ Y_{21} & Y_{22} \end{bmatrix} \cdot \begin{pmatrix} V_1 \\ V_2 \end{pmatrix}.$$

$$i_1 = i_a - Y_{11} v_a,$$

$$i_2 = -Y_{21} v_a,$$

$$v_a = -\frac{1}{Y_{21}} i_2,$$

$$i_a = i_1 - \frac{Y_{11}}{Y_{21}} i_2,$$

$$S_{i_1,i_1^*} = S_{i_a,i_a^*} + |Y_{11}|^2 S_{v_a,v_a^*} - 2\Re(Y_{11}^* S_{i_a,v_a^*}),$$

$$S_{i_2,i_2^*} = |Y_{21}|^2 S_{v_a,v_a^*},$$

$$S_{i_2,i_1^*} = Y_{21} Y_{11}^* S_{v_a,v_a^*} - Y_{21} S_{i_a,v_a^*}^*.$$

$$S_{v_a,v_a^*} = \frac{1}{|Y_{21}|^2} S_{i_2,i_2^*},$$

$$S_{i_a,i_a^*} = S_{i_1,i_1^*} + \left| \frac{Y_{11}}{Y_{21}} \right|^2 S_{i_2,i_2^*} - 2\Re\left(\frac{Y_{11}}{Y_{21}} S_{i_2,i_1^*} \right),$$

$$S_{i_a,v_a^*} = \frac{Y_{11}}{|Y_{21}|^2} S_{i_2,i_2^*} - \frac{1}{Y_{21}^*} S_{i_2,i_1^*}^*.$$

ABCD $\leftrightarrow$ Z

$$\begin{pmatrix} I_1 - i_a \\ I_2 \end{pmatrix} = \begin{bmatrix} Y_{11} & Y_{12} \\ Y_{21} & Y_{22} \end{bmatrix} \cdot \begin{pmatrix} V_1 - v_a \\ V_2 \end{pmatrix},$$

$$\begin{pmatrix} I_1 \\ I_2 \end{pmatrix} = \begin{bmatrix} Y_{11} & Y_{12} \\ Y_{21} & Y_{22} \end{bmatrix} \cdot \begin{pmatrix} V_1 - v_1 \\ V_2 - v_2 \end{pmatrix}.$$

$$v_1 = v_a - \frac{Y_{22}}{Y_{11}Y_{22} - Y_{12}Y_{21}} i_a,$$

$$v_2 = \frac{Y_{21}}{Y_{11}Y_{22} - Y_{12}Y_{21}} i_a,$$

$$v_a = v_1 + \frac{Y_{22}}{Y_{21}} v_2,$$

$$i_a = \frac{Y_{11}Y_{22} - Y_{12}Y_{21}}{Y_{21}} v_2.$$

$$S_{v_1,v_1^*} = S_{v_a,v_a^*} + \left| \frac{Y_{22}}{Y_{11}Y_{22} - Y_{12}Y_{21}} \right|^2 S_{i_a,i_a^*} - 2\Re \left(\frac{Y_{22}}{Y_{11}Y_{22} - Y_{12}Y_{21}} S_{i_a,v_a^*} \right),$$

$$S_{v_2,v_2^*} = \left| \frac{Y_{21}}{Y_{11}Y_{22} - Y_{12}Y_{21}} \right|^2 S_{i_a,i_a^*},$$

$$S_{v_1,v_2^*} = \frac{Y_{21}^*}{Y_{11}^*Y_{22}^* - Y_{12}^*Y_{21}^*} S_{i_a,v_a^*}^* - \frac{Y_{22}Y_{21}^*}{|Y_{11}Y_{22} - Y_{12}Y_{21}|^2} S_{i_a,i_a^*}.$$

$$S_{v_a,v_a^*} = S_{v_1,v_1^*} + \left| \frac{Y_{22}}{Y_{21}} \right|^2 S_{v_2,v_2^*} + 2\Re \left(\frac{Y_{22}^*}{Y_{21}^*} S_{v_1,v_2^*} \right),$$

$$S_{i_a,i_a^*} = \left| \frac{Y_{11}Y_{22} - Y_{12}Y_{21}}{Y_{21}} \right|^2 S_{v_2,v_2^*},$$

$$S_{i_a,v_a^*} = \frac{Y_{22}^*(Y_{11}Y_{22} - Y_{12}Y_{21})}{|Y_{21}|^2} S_{v_2,v_2^*} + \frac{Y_{11}Y_{22} - Y_{12}Y_{21}}{Y_{21}} S_{v_1,v_2^*}^*.$$

ABCD $\leftrightarrow$ H

$$\begin{pmatrix} I_1 - i_1 \\ I_2 - i_2 \end{pmatrix} = \begin{bmatrix} Y_{11} & Y_{12} \\ Y_{21} & Y_{22} \end{bmatrix} \cdot \begin{pmatrix} V_1 \\ V_2 \end{pmatrix},$$

$$\begin{pmatrix} I_1 \\ I_2 - i_h \end{pmatrix} = \begin{bmatrix} Y_{11} & Y_{12} \\ Y_{21} & Y_{22} \end{bmatrix} \cdot \begin{pmatrix} V_1 - v_h \\ V_2 \end{pmatrix}.$$

$$v_h = -\frac{1}{Y_{11}} i_1$$

$$i_h = i_2 - \frac{Y_{21}}{Y_{11}} i_1.$$

$$i_1 = -Y_{11} v_h$$

$$i_2 = i_h - Y_{21} v_h,$$

$$S_{i_1,i_1^*} = |Y_{11}|^2 S_{v_h,v_h^*},$$

$$S_{i_2,i_2^*} = S_{i_h,i_h^*} + |Y_{21}|^2 S_{v_h,v_h^*} - 2\Re(Y_{21} S_{v_h,i_h^*}),$$

$$S_{i_1,i_2^*} = Y_{11} Y_{21}^* S_{v_h,v_h^*} - Y_{11} S_{v_h,i_h^*}.$$

$$S_{v_h,v_h^*} = \frac{1}{|Y_{11}|^2} S_{i_1,i_1^*},$$

$$S_{i_h,i_h^*} = S_{i_2,i_2^*} + \left| \frac{Y_{21}}{Y_{11}} \right|^2 S_{i_1,i_1^*} - 2\Re(\frac{Y_{21}}{Y_{11}} S_{i_1,i_2^*}),$$

$$S_{v_h,i_h^*} = \frac{Y_{21}^*}{|Y_{11}|^2} - \frac{1}{Y_{11}} S_{i_1,i_2^*}.$$

Appendix B
Derivation of Noise Parameters

Z_i denotes the input impedance of the two port. Z_S denotes the source impedance ($Z_S = 1/Y_S = 1/(G_S + jB_S)$) . The noise current delivered by the source to the noise free two port is

$$i_n = -i_s \frac{Z_s}{Z_i + Z_S}, \tag{B.1}$$

and

$$N_i =< i_n, i_n^* > \Re(Z_i) = 4KTG_s \frac{|Z_S|^2}{|Z_i + Z_S|^2} \Re(Z_i) \triangle f. \tag{B.2}$$

The noise current delivered to the noise free two port by the correlated noise voltage v_a and noise current i_a is

$$i_n^{'} = -v_a \frac{1}{Z_i + Z_S} - i_a \frac{Z_S}{Z_i + Z_S}, \tag{B.3}$$

and

$$N_i^{'} =< i_n^{'}, i_n^{'*} > \Re(Z_i) = \left(S_{v_a v_a^*} + S_{i_a i_a^*} |Z + S|^2 + 2\Re\left(S_{i_a v_a^*} Z_S \right) \right) \frac{1}{|Z_i + Z_S|^2} \Re(Z_i) \triangle f. \tag{B.4}$$

$$F = 1 + \frac{S_{v_a v_a^*} |Y_S|^2 + S_{i_a i_a^*} + 2\Re\left(S_{i_a v_a^*} Y_S^* \right)}{4KTG_S} \tag{B.5}$$

To find out B_{opt}, $\frac{\delta F}{\delta B_S} = 0$, we then get

$$B_{opt} = -\frac{\Im\left(S_{i_a v_a^*} \right)}{S_{v_a v_a^*}}. \tag{B.6}$$

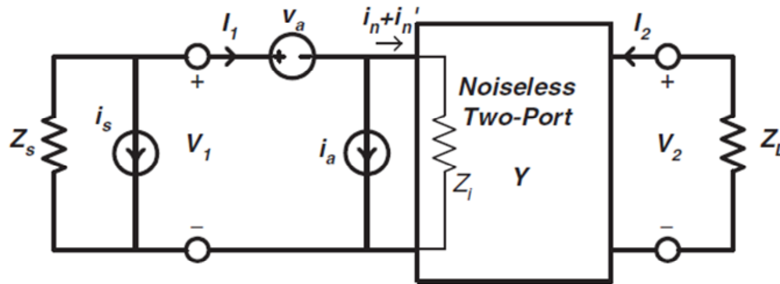

To find out G_{opt}, $\frac{\delta F}{\delta G_S} = 0$. Substituting $B_S = B_{opt}$,

$$G_{opt} = \sqrt{\frac{S_{i_a i_a^*}}{S_{v_a v_a^*}} - \frac{\Im\left(S_{i_a v_a^*}\right)^2}{{S_{v_a v_a^*}}^2}}. \tag{B.7}$$

Then we obtain F_{min},

$$F_{min} = 1 + \frac{\sqrt{S_{v_a v_a^*} S_{i_a i_a^*} - \Re\left(S_{v_a v_a^*}\right)^2} + \Re\left(S_{v_a v_a^*}\right)}{2KT}. \tag{B.8}$$

Appendix C
Matlab Code for Intrinsic Noise Extraction

```
function NoisePara_Extraction_5PAE
color = {'k','b','g','y','m','r','r--','r-o'};
%path = 'H:\Noise5PAE\Meas_XiaoyunSimu';
%myPath = 'Y:\public\ziyan\Noise7WL\Data\7WL_HPp48x20x1\';
myPath = 'D:\Noise7WL\Data\7WL_HPp48x20x1\';
FigNum=1;
Ltext={'open-short'};
AE = 0.48*20*1;


fopen1 = 'NpHp_p48x20_Open3';
fshort = 'NpHp_p48x20_Short4';
[freq_OS,Sopen,Topen]=read_SP_Fswp([myPath,fopen1],'21','MA','GHz');
[ftemp,Sshort,Tshort]=read_SP_Fswp([myPath,fshort],'21','MA','GHz');

% ====================================================================
if 1% frequency sweep de-embedding
    NPBiasx = {'Ic3p97_FDEL','Ic7p68_FDEL'};
    SPBiasx = {'Ic3p97_SP','Ic7p68_SP'};

    F_name = 'NpHp_p48x20_Vc2_';

    for BiaNo = 1;

        File_F_NP{BiaNo} = [F_name,NPBiasx{BiaNo}];
        File_F_SP{BiaNo} = [F_name,SPBiasx{BiaNo}];

        switch BiaNo
            case 1, SBias_Fswp = [0.841,2,32.0850e-6,3.9745e-3];
            case 2, SBias_Fswp = [0.859,2,64.7950e-6,7.6410e-3];
        end

        [fdut_Fswp,Sdut_Fswp,TdutSP_Fswp]=..
        read_SP_Fswp([myPath,File_F_SP{BiaNo}],'21','MA','GHz');
        [NPdut_Fswp,TdutNP_Fswp]=read_NP_Fswp([myPath,File_F_NP{BiaNo}],'MA','GHz');

        %------------%   NFmin before deem
```

```
freq_swp = NPdut_Fswp(:,1)*1e-9;
NFmin_b4os = NPdut_Fswp(:,2);
Fmin_b4os=10.^(NFmin_b4os/10);


Xtext = 'frequency (GHz)';
X = fdut_Fswp*1e-9;

% In case, open short frequency setup is different from dut
Fswp_index = find_list(freq_OS,fdut_Fswp);
Sopen_Fswp = Sopen(Fswp_index,:);
Sshort_Fswp = Sshort(Fswp_index,:);
Freq = fdut_Fswp;
[YINT_Fswp,CY_INT_Fswp,PNoise_INT_Fswp]= ...
DeemNP_OS_ziyan(fdut_Fswp,Sdut_Fswp,Sopen_Fswp,Sshort_Fswp,NPdut_Fswp);

%%%%%%%%%%%%%Ypara%%%%%%%%%%%%%%%%%%%
figure(9);%'21'
subplot(4,2,1);hold on;
plot(Freq*1e-9,real(YINT_Fswp(:,1)),'b-*');
ylabel('real(Y11) (S)');
subplot(4,2,2);hold on;
plot(Freq*1e-9,imag(YINT_Fswp(:,1)),'b-*');
ylabel('imag(Y11) (S)');
subplot(4,2,3);hold on;
plot(Freq*1e-9,real(YINT_Fswp(:,3)),'b-*');
ylabel('real(Y12) (S)');
subplot(4,2,4);hold on;
plot(Freq*1e-9,imag(YINT_Fswp(:,3)),'b-*');
ylabel('imag(Y12) (S)');
subplot(4,2,5);hold on;
plot(Freq*1e-9,real(YINT_Fswp(:,2)),'b-*');
ylabel('real(Y21) (S)');
subplot(4,2,6);hold on;
plot(Freq*1e-9,imag(YINT_Fswp(:,2)),'b-*');
ylabel('imag(Y21) (S)');
subplot(4,2,7);hold on;
plot(Freq*1e-9,real(YINT_Fswp(:,4)),'b-*');
ylabel('real(Y22) (S)');xlabel('Freq(GHz)');
subplot(4,2,8);hold on;
plot(Freq*1e-9,imag(YINT_Fswp(:,4)),'b-*');
ylabel('imag(Y22) (S)');xlabel('Freq(GHz)');

%*******************%   NFmin after deem
NFmin_os = PNoise_INT_Fswp(:,2)
```

```
Gopt_os = PNoise_INT_Fswp(:,3);
RN_os = PNoise_INT_Fswp(:,4)
Yopt_os=PNoise_INT_Fswp(:,5)
Fmin_os=10.^(NFmin_os/10);

Si1 = CY_INT_Fswp(:,1);  %CY_os11
Si21 = CY_INT_Fswp(:,2);  %CY_os21
Si12 = CY_INT_Fswp(:,3);  %CY_os12
Si2 = CY_INT_Fswp(:,4);  %CY_os22


mfigure(11);
subplot(4,2,7);hold on;
plot(freq_swp,real(Si1),'b-*');
xlabel('freq (GHz)');ylabel('real Sibib* (A^2/Hz)');
subplot(4,2,8);hold on;
plot(freq_swp,imag(Si1),'b-*');
xlabel('freq (GHz)');ylabel('imag Sibib* (A^2/Hz)');
subplot(4,2,1);hold on;
plot(freq_swp,real(Si2),'b-*');
xlabel('freq (GHz)');ylabel('real Sicic*(A^2/Hz)');
subplot(4,2,2);hold on;
plot(freq_swp,imag(Si2),'b-*');
xlabel('freq (GHz)');ylabel('imag Sicic*(A^2/Hz)');
subplot(4,2,5);hold on;
plot(freq_swp,real(Si12),'b-*');
xlabel('freq (GHz)');ylabel('real Sibic*(A^2/Hz)');
subplot(4,2,6);hold on;
plot(freq_swp,imag(Si12),'b-*');
xlabel('freq (GHz)');ylabel('imag Sibic*(A^2/Hz)');
subplot(4,2,3);hold on;
plot(freq_swp,real(Si21),'b-*');
xlabel('freq (GHz)');ylabel('real Sicib*(A^2/Hz)');
subplot(4,2,4);hold on;
plot(freq_swp,imag(Si21),'b-*');
xlabel('freq (GHz)');ylabel('imag Sicib*(A^2/Hz)');

datapath = 'D:\Noise7WL\Ads7WL_p48x20_g2_prj\Trans0621\';

NT_ibi =  sprintf('%sNT_ibi_Vc2Ic3p97.txt', datapath);
NT_ici =  sprintf('%sNT_ici_Vc2Ic3p97.txt', datapath);

[RNT_Ibx_ibi] = textread(NT_ibi,'',25,...
'delimiter',' ','headerlines',1);
freq = RNT_Ibx_ibi(:,1)*1e-9;
```

```
RNT_Ibx_Ibi = RNT_Ibx_ibi(:,2);
[INT_Ibx_ibi] = textread(NT_ibi,'',25,...
'delimiter',' ','headerlines',29);
INT_Ibx_Ibi = INT_Ibx_ibi(:,2);
[RNT_Icx_ibi] = textread(NT_ibi,'',25,...
'delimiter',' ','headerlines',57);
RNT_Icx_Ibi = RNT_Icx_ibi(:,2);
[INT_Icx_ibi] = textread(NT_ibi,'',25,...
'delimiter',' ','headerlines',85);
INT_Icx_Ibi = INT_Icx_ibi(:,2);

[RNT_Ibx_ici] = textread(NT_ici,'',25,...
'delimiter',' ','headerlines',1);
freq = RNT_Ibx_ibi(:,1)*1e-9;
RNT_Ibx_Ici = RNT_Ibx_ici(:,2);
[INT_Ibx_ici] = textread(NT_ici,'',25,...
'delimiter',' ','headerlines',29);
INT_Ibx_Ici = INT_Ibx_ici(:,2);
[RNT_Icx_ici] = textread(NT_ici,'',25,...
'delimiter',' ','headerlines',57);
RNT_Icx_Ici = RNT_Icx_ici(:,2);
[INT_Icx_ici] = textread(NT_ici,'',25,...
'delimiter',' ','headerlines',85);
INT_Icx_Ici = INT_Icx_ici(:,2);

format long;
NTIcx_Ibi = RNT_Icx_Ibi+INT_Icx_Ibi*j
NTIcx_Ici = RNT_Icx_Ici+INT_Icx_Ici*j
NTIbx_Ibi = RNT_Ibx_Ibi+INT_Ibx_Ibi*j
NTIbx_Ici = RNT_Ibx_Ici+INT_Ibx_Ici*j
NTI = [NTIcx_Ici,NTIcx_Ibi,NTIbx_Ici,NTIbx_Ibi];


NTIcx_Ibi_conj = RNT_Icx_Ibi-INT_Icx_Ibi*j;
NTIcx_Ici_conj = RNT_Icx_Ici-INT_Icx_Ici*j;
NTIbx_Ibi_conj = RNT_Ibx_Ibi-INT_Ibx_Ibi*j;
NTIbx_Ici_conj = RNT_Ibx_Ici-INT_Ibx_Ici*j;
NTI_conj =[NTIcx_Ici_conj,NTIbx_Ici_conj,NTIcx_Ibi_conj,NTIbx_Ibi_conj];

det_NTI = 1./(NTIcx_Ici.*NTIbx_Ibi-NTIcx_Ibi.*NTIbx_Ici);
NTI_inv = [NTIbx_Ibi.*det_NTI,...
 -NTIcx_Ibi.*det_NTI, -NTIbx_Ici.*det_NTI, NTIcx_Ici.*det_NTI];
NTI_conj_inv11 = real(NTI_inv(:,1))-j*imag(NTI_inv(:,1));
NTI_conj_inv12 = real(NTI_inv(:,3))-j*imag(NTI_inv(:,3));
NTI_conj_inv21 = real(NTI_inv(:,2))-j*imag(NTI_inv(:,2));
```

```
NTI_conj_inv22 = real(NTI_inv(:,4))-j*imag(NTI_inv(:,4));
NTI_conj_inv = [NTI_conj_inv11,NTI_conj_inv12,NTI_conj_inv21,NTI_conj_inv22];

%datapathR = 'D:\NoiseTransfer\Ndata_new\';
%SNTR =  sprintf('%sSNTR_new_correction.txt', datapathR);
SNTR =  sprintf('%sSNTR_Vc2Ic3p97_ex.txt', datapath);
[NTRI] = textread(SNTR,'','delimiter',' ','headerlines',0);
NTRI1 = NTRI(:,1)+j*NTRI(:,2);
NTRI2 = NTRI(:,3)+j*NTRI(:,4);
NTRI3 = NTRI(:,5)+j*NTRI(:,6);
NTRI4 = NTRI(:,7)+j*NTRI(:,8);

IX_os = [Si2-NTRI1,Si21-NTRI2,Si12-NTRI3,Si1-NTRI4];  %Ic, Icib, Ibic,Ib

%Si_int= multiple(NTI_inv,IX_os,NTI_conj_inv) %ic, icb, ibc, ic;
Si_int_pre1 = NTI_inv(:,1).*IX_os(:,1)+ NTI_inv(:,2).*IX_os(:,3);
Si_int_pre2 = NTI_inv(:,1).*IX_os(:,2)+ NTI_inv(:,2).*IX_os(:,4);
Si_int_pre3 = NTI_inv(:,3).*IX_os(:,1)+ NTI_inv(:,4).*IX_os(:,3);
Si_int_pre4 = NTI_inv(:,3).*IX_os(:,2)+ NTI_inv(:,4).*IX_os(:,4);
Si_int1  = Si_int_pre1.*NTI_conj_inv(:,1)+ Si_int_pre2.*NTI_conj_inv(:,3)
Si_int2  = Si_int_pre1.*NTI_conj_inv(:,2)+ Si_int_pre2.*NTI_conj_inv(:,4);
Si_int3  = Si_int_pre3.*NTI_conj_inv(:,1)+ Si_int_pre4.*NTI_conj_inv(:,3);
Si_int4  = Si_int_pre3.*NTI_conj_inv(:,2)+ Si_int_pre4.*NTI_conj_inv(:,4);


mfigure(2);
subplot(4,2,1);hold on;
%plot(freq_swp,real(Si_int(:,1)),'b');
plot(freq_swp,real(Si_int1),'k-o');
xlabel('freq (GHz)');ylabel('real Sicic*');
subplot(4,2,2);hold on;
%plot(freq_swp,imag(Si_int(:,1)),'b');
plot(freq_swp,imag(Si_int1),'k-o');
xlabel('freq (GHz)');ylabel('imag Sicic* ');
subplot(4,2,3);hold on;
%plot(freq_swp,real(Si_int(:,2)),'b');
plot(freq_swp,real(Si_int2),'k-o');
xlabel('freq (GHz)');ylabel('real Sicib*');
subplot(4,2,4);hold on;
%plot(freq_swp,imag(Si_int(:,2)),'b');
plot(freq_swp,imag(Si_int2),'k-o');
xlabel('freq (GHz)');ylabel('imag Sicib*');
subplot(4,2,5);hold on;
%plot(freq_swp,real(Si_int(:,3)),'b');
plot(freq_swp,real(Si_int3),'k-o');
```

```
xlabel('freq (GHz)');ylabel('real Sibic*');
subplot(4,2,6);hold on;
%plot(freq_swp,imag(Si_int(:,3)),'b');
plot(freq_swp,imag(Si_int3),'k-o');
xlabel('freq (GHz)');ylabel('imag Sibic*');
subplot(4,2,7);hold on;
%plot(freq_swp,real(Si_int(:,4)),'b');
plot(freq_swp,real(Si_int4),'k-o');
xlabel('freq (GHz)');ylabel('real Sibib*');
subplot(4,2,8);hold on;
%plot(freq_swp,imag(Si_int(:,4)),'b');
plot(freq_swp,imag(Si_int4),'k-o');
xlabel('freq (GHz)');ylabel('imag Sibib*');


if 0
    Si_out_pre1 = NTI(:,1).*Si_int1+NTI(:,2).*Si_int3;
    Si_out_pre2 = NTI(:,1).*Si_int2+NTI(:,2).*Si_int4;
    Si_out_pre3 = NTI(:,3).*Si_int1+NTI(:,4).*Si_int3;
    Si_out_pre4 = NTI(:,3).*Si_int2+NTI(:,4).*Si_int4;
    Si_out1 = Si_out_pre1.*NTI_conj(:,1)+Si_out_pre2.*NTI_conj(:,3)+NTRI1;
    Si_out2 = Si_out_pre1.*NTI_conj(:,2)+Si_out_pre2.*NTI_conj(:,4)+NTRI2;
    Si_out3 = Si_out_pre3.*NTI_conj(:,1)+Si_out_pre4.*NTI_conj(:,3)+NTRI3;
    Si_out4 = Si_out_pre3.*NTI_conj(:,2)+Si_out_pre4.*NTI_conj(:,4)+NTRI4;



    mfigure(10006);
    subplot(4,2,1);hold on;
    plot(freq_swp,real(Si2),'b');
    plot(freq_swp,real(Si_out1),'r');
    xlabel('freq (GHz)');ylabel('real Sicic*');
    subplot(4,2,2);hold on;
    plot(freq_swp,imag(Si2),'b');
    plot(freq_swp,imag(Si_out1),'r');
    xlabel('freq (GHz)');ylabel('imag Sicic* ');
    subplot(4,2,3);hold on;
    plot(freq_swp,real(Si21),'b');
    plot(freq_swp,real(Si_out2),'r');
    xlabel('freq (GHz)');ylabel('real Sicib*');
    subplot(4,2,4);hold on;
    plot(freq_swp,imag(Si21),'b');
    plot(freq_swp,imag(Si_out2),'r');
    xlabel('freq (GHz)');ylabel('imag Sicib*');
    subplot(4,2,5);hold on;
```

```
            plot(freq_swp,real(Si12),'b');
            plot(freq_swp,real(Si_out3),'r');
            xlabel('freq (GHz)');ylabel('real Sibic*');
            subplot(4,2,6);hold on;
            plot(freq_swp,imag(Si12),'b');
            plot(freq_swp,imag(Si_out3),'r');
            xlabel('freq (GHz)');ylabel('imag Sibic*');
            subplot(4,2,7);hold on;
            plot(freq_swp,real(Si1),'b');
            plot(freq_swp,real(Si_out4),'r');
            xlabel('freq (GHz)');ylabel('real Sibib*');
            subplot(4,2,8);hold on;
            plot(freq_swp,imag(Si1),'b');
            plot(freq_swp,imag(Si_out4),'r');
            xlabel('freq (GHz)');ylabel('imag Sibib*');
        end


    end

end

% =========================================================

return
```

Appendix D
Verilog-A Code for Compact Noise Model Implementation

```
electrical  na, nb; //added
branch            (na)       b_na;
branch            (nb)       b_nb;
real sic, sib;
real gn1, gn2, gn3, gn4; //added
twoq    = 2.0 * `P_Q;
sic = twoq*abs(it);
sib = twoq*abs(ibei);

I(b_na) <+ white_noise(1);
I(b_nb) <+ white_noise(1);
I(b_na) <+ V(b_na);
I(b_nb) <+ V(b_nb);

gn1  = sqrt(sic);
gn2  = -sqrt(sic)*Tf*fg1*((1.00/3.00)*Tf*fg1
     + (1.00/3.0+ eta*(1.00/9.00))*fg2*Tf)/((Tf*fg1
     + (1.00/3.0+ eta*(1.00/9.00))*fg2*Tf));
gn3  = sqrt(sic)*(Tf*fg1 + (1.00/3.0+ eta*(1.00/9.00))*fg2*Tf);   //optional
gn4  = sqrt(sic)*fg2*Tf*sqrt((1.00/3.00+eta*(4.00/45.00))
     -pow((1.00/3.00+eta*(1.00/9.00)),2));

I(bi,ei) <+ white_noise(sib, "shot")+gn3*ddt(V(b_na)) +gn4*ddt(V(b_nb));
I(ci,ei) <+ gn1*(V(b_na))+ gn2*ddt(V(b_na));
```

Appendix E
Derivation of relation between T_Y^{int} and T_Y

$I - V$ relation of T_Y is

$$I_1 = Y_{11}V_1 + Y_{12}V_2, \tag{E.1}$$
$$I_2 = Y_{21}V_1 + Y_{22}V_2. \tag{E.2}$$

$I - V$ relation of T_Y^{int} is

$$I_1 = Y_{11}^{int}(V_1 - I_1 r_b) + Y_{12}^{int}V_2, \tag{E.3}$$
$$I_2 = Y_{21}^{int}(V_1 - I_1 r_b) + Y_{22}^{int}V_2. \tag{E.4}$$

Then we have

$$Y_{11}V_1 + Y_{12}V_2 = Y_{11}^{int}(V_1 - I_1 r_b) + Y_{12}^{int}V_2, \tag{E.5}$$
$$Y_{21}V_1 + Y_{22}V_2 = Y_{21}^{int}(V_1 - I_1 r_b) + Y_{22}^{int}V_2. \tag{E.6}$$

Therefore

$$Y_{11}V_1 + Y_{12}V_2 = Y_{11}^{int}(V_1 - I_1 r_b) + Y_{12}^{int}V_2, \tag{E.7}$$
$$Y_{21}V_1 + Y_{22}V_2 = Y_{21}^{int}(V_1 - I_1 r_b) + Y_{22}^{int}V_2. \tag{E.8}$$

Replace I_1 in (E.8) with (E.2),

$$Y_{11}V_1 + Y_{12}V_2 = Y_{11}^{int}(V_1 - (Y_{11}V_1 + Y_{12}V_2)\, r_b) + Y_{12}^{int}V_2, \tag{E.9}$$
$$Y_{21}V_1 + Y_{22}V_2 = Y_{21}^{int}(V_1 - (Y_{11}V_1 + Y_{12}V_2)\, r_b) + Y_{22}^{int}V_2. \tag{E.10}$$

(E.10) should be independed of V_1 and V_2. Therefore

$$Y_{11}V_1 = Y_{11}^{int}V_1 - Y_{11}^{int}Y_{11}r_bV_1, \tag{E.11}$$
$$Y_{12}V_2 = Y_{12}^{int}V_2 - Y_{11}^{int}Y_{12}r_bV_2, \tag{E.12}$$
$$Y_{21}V_1 = Y_{21}^{int}V_1 - Y_{11}^{int}Y_{21}r_bV_1, \tag{E.13}$$
$$Y_{22}V_2 = Y_{22}^{int}V_2 - Y_{21}^{int}Y_{12}r_bV_1, \tag{E.14}$$

We are then able to obtain the relation between T_Y and T_Y^{int}.